Zoological Journal of the Linnean Society, 2026, **206**(**4**), zlaf135
https://doi.org/10.1093/zoolinnean/zlaf135

OXFORD

Original Article

The axial skeleton of the tuatara (Rhynchocephalia: *Sphenodon*): insights on intraspecific variability, ontogeny, sexual dimorphism, and remarks on fossil taxa

Victor Beccari[1,2,*], Marc E.H. Jones[3,4,5], Andrea Villa[6], Roberta Martino[7], Sophie Regnault[8], Frank Glaw[9,10], Oliver W.M. Rauhut[1,2,10]

[1]Bayerische Staatssammlung für Paläontologie und Geologie, Richard-Wagner-Straße 10, Munich, 80333, Germany
[2]Department of Earth and Environmental Sciences, Ludwig-Maximilians-Universität, Luisenstraße 37, Munich, 80333, Germany
[3]Science Group, Natural History Museum, London SW7 5BD, UK
[4]Research Department of Cell and Developmental Biology, Anatomy Building, UCL, University College London, London WCIE 6BT, UK
[5]School of Biological Sciences, University of Adelaide, Adelaide, South Australia, 5005, Australia
[6]Institut Català de Paleontologia Miquel Crusafont (ICP-CERCA), Edifici ICTA-ICP, Barcelona 08193, Spain
[7]GEOBIOTEC, Department of Earth Sciences, NOVA School of Science and Technology, Universidade Nova de Lisboa, Caparica P-2829 516, Portugal
[8]Aberystwyth School of Veterinary Science, Aberystwyth SY23 3FL, United Kingdom
[9]Zoologische Staatssammlung München, Münchhausenstraße 21, Munich, 81247, Germany
[10]GeoBioCenter, Ludwig-Maximilians-Universität, Luisenstraße 37, Munich, 80333, Germany

*Corresponding author. SNSB-Bayerische Staatssammlung für Paläontologie und Geologie, Munich, Germany. E-mail: victor.beccari@gmail.com

ABSTRACT

As the sole living rhynchocephalian, the tuatara (*Sphenodon punctatus*) provides important comparative information for fossil rhynchocephalians and lepidosaurs in general regarding expected intraspecific variability, ontogeny, and sexual dimorphism. The axial skeleton of *Sphenodon punctatus* is described here in detail, using Computed Tomography (CT)-scans and a comprehensive sample ($N = 33$) of different ontogenetic stages and sexes. The new description adds to already existing literature, and confirms some consistent morphological characters, such as number of vertebrae, position of accessory processes, and ossification patterns. We conducted 3D geometric morphometrics analyses to better understand regionalization of the axial skeleton, ontogenetic changes, and sexual dimorphism in *Sphenodon*. The morphology of presacral vertebrae is influenced by size and shows negative allometry, with increasing relative height of the neural spine, but decreasing relative vertebral width and length in larger individuals. We compare the morphology and ontogenetic implications of *Sphenodon* with Mesozoic fossil relatives. Some taxa, especially those from the Jurassic of Europe, show substantial differences in number, proportions, and morphology of vertebrae, including shifts in ossification timing, loss of vertebral intercentra, and changes in rib morphology. We highlight osteological features, such as ossification timing and morphology, that may correlate with taxonomy, systematics, and ecomorphology of Mesozoic rhynchocephalians.

Keywords: Lepidosauria; New Zealand; Anatomy; Geometric morphometrics

INTRODUCTION

The tuatara, *Sphenodon punctatus* (Gray, 1842), is the only living member of the clade Rhynchocephalia Günther, 1867. Important advancements in our knowledge of this endemic species from New Zealand have been made in the past decades, including studies on conservation (Hay *et al.* 2010, Cree 2014, Lamar *et al.* 2021), diet and feeding mechanics (Jones 2008, 2009, Jones *et al.* 2009a, Jones and Lappin 2009, Herrel *et al.* 2010, Lamar *et al.* 2022), osteology (Evans 2008, Russell and Bauer 2008, Jones *et al.* 2011), and systematics (Herrera-Flores *et al.* 2017, Gemmell *et al.* 2020, Simões *et al.* 2020). Aligned to these studies, important contributions on ecomorphology, systematics, and taxonomy of fossil rhynchocephalians have been made recently (e.g. Chambi-Trowell *et al.* 2019, 2021, Sues and Schoch 2021, 2024, Villa *et al.* 2021, DeMar *et al.* 2022, Herrera-Flores *et al.* 2022, Simões *et al.* 2022, Beccari *et al.* 2025a, b).

Received 23 May 2025; revised 15 July 2025; accepted 14 August 2025

Rhynchocephalians were abundant during the Mesozoic (e.g. Rauhut *et al.* 2017, Chambi-Trowell *et al.* 2019, 2021, Simões *et al.* 2020, 2022, Brownstein *et al.* 2022, DeMar *et al.* 2022). Although both the living and fossil taxa have been known for almost two centuries, much of the research on this group revolves around their skull anatomy, with a special focus on their unique dentition (e.g. Jones 2009, Rauhut *et al.* 2012, Chambi-Trowell *et al.* 2020). This includes ecomorphological works (e.g. Jones 2008, Jones *et al.* 2009a, Jones and Lappin 2009, Herrel *et al.* 2010, Rauhut *et al.* 2012), taxonomy, i.e. most of the diagnostic features of fossil taxa encompassing cranial characters, even when complete specimens are available (e.g. Cocude-Michel 1963, Fabre 1981), and phylogeny, with most recent phylogenetic analyses having over two-thirds of all morphological characters being cranial, half of which are exclusively jaw and dentition characters (Bever and Norell 2017, Simões *et al.* 2020, Chambi-Trowell *et al.* 2021, DeMar *et al.* 2022). Thus, the postcranial anatomy of rhynchocephalians is still underrepresented in the literature, although some studies have described the post-cranial anatomy of different taxa in depth (e.g. Howes and Swinnerton 1901, Hoffstetter and Gasc 1969, Evans 1981, Fraser and Walkden 1984, O'Brien *et al.* 2018, Villa *et al.* 2021, DeMar *et al.* 2022, Beccari *et al.* 2025a, b). Aspects of the postcranial anatomy, e.g. ossification timings, limb anatomy, body size, and some anatomical features have been shown to hold important information for ecomorphology, systematics, and taxonomy (e.g. Lee *et al.* 2016, O'Brien *et al.* 2018, Villa *et al.* 2021, DeMar *et al.* 2022, Gutarra *et al.* 2023, Beccari *et al.* 2025a, b).

Being the sole extant rhynchocephalian, understanding the anatomy of *Sphenodon* is key in resolving many lingering taxonomic and systematic issues that have plagued rhynchocephalian studies so far (see Villa *et al.* 2021, Simões *et al.* 2022, Beccari *et al.* 2025a, b). The postcranial anatomy of *Sphenodon* Gray, 1831, has been described in some detail before (e.g. Günther 1867, Howes and Swinnerton 1901, Romer 1956, Hoffstetter and Gasc 1969, Russell and Bauer 2008). However, these previous studies have used only a small number of individuals (e.g. Günther 1867, Fürbringer 1900, Schauinsland 1900, Howes and Swinnerton 1901, von Wettstein 1931, Romer 1956, Robb 1977), and almost no systematic survey of ontogeny (but see Reynoso 2000), sexual dimorphism, or intraspecific variability attempted. A previous survey of sesamoid bones among 19 individuals of different ages is a rare exception (Regnault *et al.* 2017).

The goal of the current study is to comprehensively describe the axial skeleton anatomy of *Sphenodon punctatus*, in light of recent studies of fossil rhynchocephalians. Specimens of different ontogenetic stages and sexes were CT-scanned and segmented to evaluate sexual dimorphism, ontogeny, and intraspecific variation. The digital specimens were used for 3D geometric morphometric analysis to understand regionalization in the axial skeleton and the influence of ontogeny, sex, and size across our sample. We also compared the morphology of *Sphenodon* with known fossil rhynchocephalians to highlight important morphological features that may be used for taxonomy and systematics.

MATERIAL AND METHODS

Specimens used in this study

We used a total of 33 wet-preserved specimens of *Sphenodon punctatus* (Fig. 1). These specimens have been CT-scanned, segmented, imaged, and measured for analyses. These specimens are housed in different collections (see Supporting Information, Data S1). To facilitate description and ontogenetic analysis, we divided these specimens into four ontogenetic categories (Table 1): hatchling (two specimens), juvenile (four specimens), subadult (11 specimens), and adult (16 specimens). However, these categories have been regarded as ambiguous and it has been previously recommended that 'skeletally immature' or 'skeletally mature' should be used instead (i.e. Griffin *et al.* 2020).

As shown by sesamoid anatomy, skeletal maturity involves a number of steps that do not always take place in the same order (Regnault *et al.* 2017). Nevertheless, we thus follow schemes similar to those that have been used previously for *Sphenodon* (i.e. Jones 2008, Jones *et al.* 2009b, 2011, Simões *et al.* 2022, Beccari *et al.* 2024, Beccari *et al.* 2025b), which usually divide the post-hatchling ontogenetic stages into juvenile, subadult, and adult. As no formal definition to these ontogenetic stages has been given for *Sphenodon* (usually regarding any non-adult specimens as those whose skeletal elements are less ossified or fused), we provide here a new definition, based on a combination of specimen size and osteological maturity. To show the sequence of maturity in our sample, as well as to visualize different ontogenetic stages, we coded ontogenetically variable characters (such as fusion and ossification of bones) into an ontogram, following the methodology of Ezcurra and Butler (2015). The ontogram aids in visualizing the sequence of changes during skeletal maturity of individuals through a characters list, similar to those of phylogenetic analyses, but focussing on incremental steps in ossification and fusion of elements, using a specimen-based dataset (Brochu 1992, Ezcurra and Butler 2015). The resulting dataset for the ontogram analysis includes 69 discrete ontogenetic characters (Supporting Information, Data S2): eight cranial characters derived from the observations of *Sphenodon* skull development in Jones *et al.* (2011) and 61 postcranial characters, including axial and appendicular elements, derived from our observations of the 33 specimens included in this work. All multistate characters (i.e. characters with at least three states: 0, 1, and 2), except for character 31 (fusion of the ribs in the first lumbar vertebra, as this feature does not seem to be related to ontogeny alone; see 'Presacral vertebrae 3 to 25' section below), were ordered, with the hatchling condition set to 0, whereas the latest ossification step was set to the highest character state. The smallest hatchling (SNSB-ZSM 20/1959, presacral vertebrae total length = 18.4 mm) was used as the outgroup in our analysis. A second set of ontogenetic analyses was done, this time including fossil rhynchocephalians from the Solnhofen Archipelago, as multiple specimens of different ontogenetic stages are known (Cocude-Michel 1963, Fabre 1981, Beccari *et al.* 2025b). The dataset for this set of analyses was simplified, as some characters (e.g. those related to cartilaginous or poorly ossified elements) cannot be consistently observed in the fossils. This resulted in a dataset with 32 discrete characters (Supporting Information, Data S2). Each taxon or taxonomic group, e.g. pleurosaurids, and the *Kallimodon–Leptosaurus* complex (*sensu* Rauhut and López-Arbarello 2016) was scored separately within the *Sphenodon* sample, to better visualize their ontogenetic timings. The ontogenetic analyses were done in the software TNT v.1.6 (Goloboff and Morales 2023) using traditional search, 1000 replications, and 20 saved trees per replication.

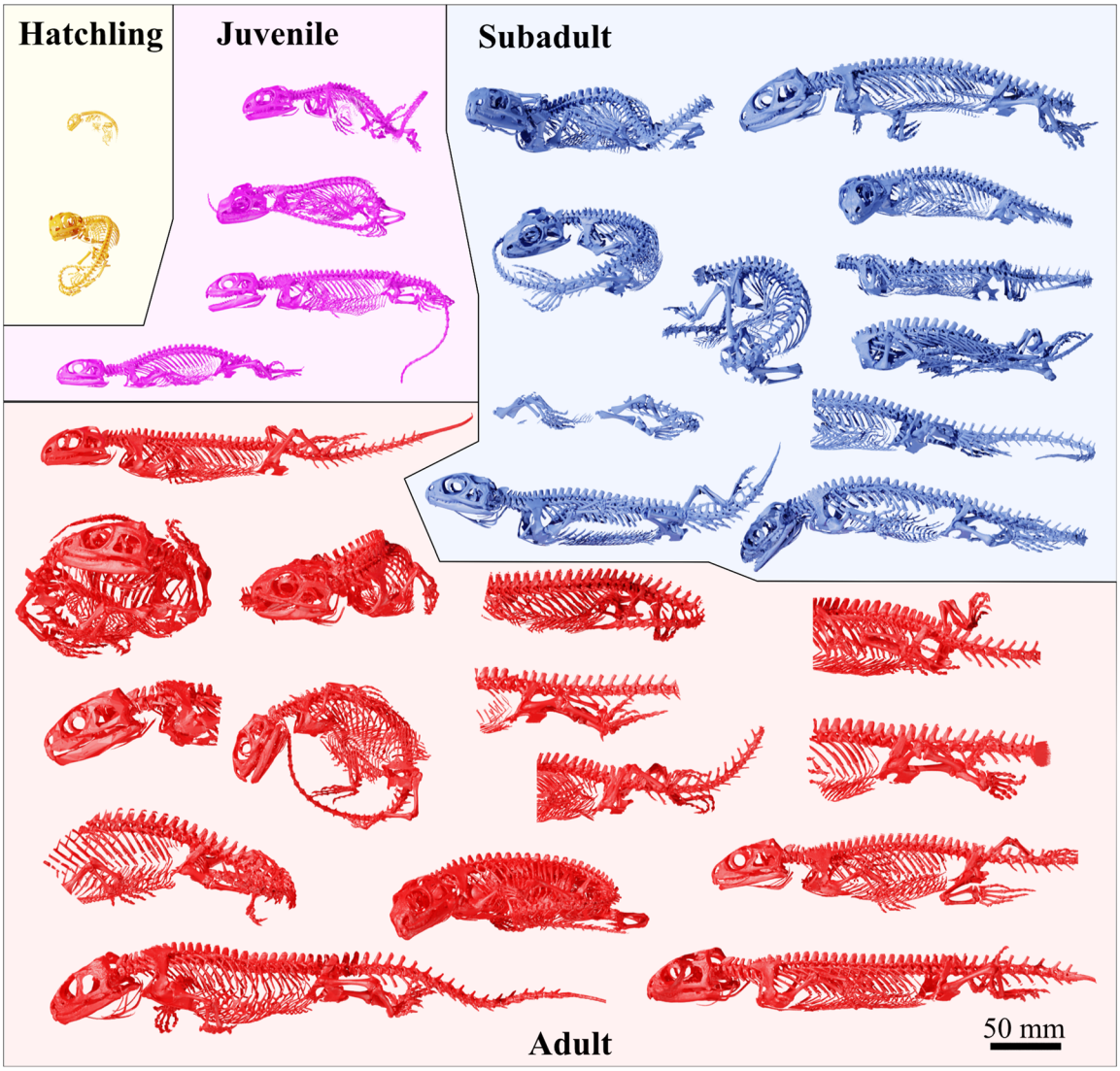

Figure 1. 3D representation of the skeleton of all *Sphenodon punctatus* specimens used in this study, grouped by ontogenetic stages (hatchling, juvenile, subadult, and adult).

Most specimens in this study have no precise information of locality and sex. Thus, although geographic origin (e.g. latitude and island provenance) might have an impact on the skeletal variation, we are unable to examine it in our analyses. Nevertheless, we do consider it as a possibility throughout our discussion. Although the sex was not indicated for most specimens by labels or other documentation (cf. Wainwright *et al.* 2024), we were able to identify the sex of some specimens through external morphology. *Sphenodon* is a dimorphic species, with one main external difference between adult males and females comprising the presence of enlarged, tightly packed nuchal and dorsal spikes in the dorsal crest of males (e.g. Jones and Cree 2012, Cree 2014, Lamar *et al.* 2021). Therefore, adult and subadult specimens whose dorsal crest could be visualized in the CT-scans could be classified as either males or females. Additionally, two specimens in this study (I-MEHJ S1 and UF.Herp 14110) have eggs inside their body cavity. In total, our study includes four females and 18 males that could be confidently sexed.

Osteological description

Each bone is described using a mature (adult) condition and subsequently compared to the different ontogenetic categories. When possible, we compared the postcranial anatomy of *Sphenodon* with formerly described and published fossil rhynchocephalians, but a complete and detailed comparison to these taxa falls outside the scope of this manuscript. The description of *Sphenodon* postcranial anatomy has been standardized using the proposed nomenclature and orientation of Hoffstetter and Gasc (1969) for most of the axial skeleton, and Russell and Bauer (2008) for the sternum. The CT-scan allowed for a detailed observation of many ridges in the vertebrae of *Sphenodon*. We adopt the laminae nomenclature of Tschopp (2016) to describe these ridges, when possible.

CT-scanning, image segmentation, and 3D mesh manipulation

The specimens were CT-scanned in different institutions, using different parameters (see Supporting Information, Data S1). Some

Table 1. *Sphenodon* specimens in this study, listing ontogenetic category and sex, as well as completeness of the body within the available CT-scan volume

Specimen	Ontogenetic category	Sex	Body represented in CT-scan volume
IDHRN NH 84.19	Adult	Male	All
I-MEHJ S1	Adult	Female[a,b]	All
ZMB 10607	Adult	Female	Alle
ZMB 13837	Adult	Male	All
ZMB 14023	Adult	?	All
NHMUK LS 1935.12.6.1	Adult	Male	Posterior half
NHMUK LS 1969.2204	Adult	?	Posterior half
NHMUK LS 1935.5.14.3	Adult	Male[b]	Anterior half
UMZC R2595	Adult	Male	Complete
UMZC R2604	Adult	Female	Complete
UMZC R2605	Adult	Male	Complete
UMZC R2607	Adult	Male	Posterior half
UMZC R2608	Adult	Male	Posterior half
UMZC R2609	Adult	Male	Posterior half
UMZC R2615	Adult	Male	Posterior half
UMZC R2616	Adult	Male	Posterior half
IDHRN NH 3-116	Subadult	Male	Posterior half
ZMB 9804	Subadult	?	Posterior half
MZH MS 1853	Subadult	?	Complete
UF.Herp 14110	Subadult	Female[a,b]	Complete
UMZC R2598	Subadult	?	Posterior half
SNSB-ZSM 1318-2006	Subadult	Male[b]	Complete
SAMA Herpetology 70524	Subadult	Male	Complete
UMMZ.Herp.406 51	Subadult	Male	Complete
UMZC R2596	Subadult	Male	Complete
UMZC R2602	Subadult	Male	Limbs and caudal series
UMZC R2603	Subadult	Male	Posterior half
NHMUK LS 1855.10.163	Juvenile	?	Complete
LDKCL X 11	Juvenile	?	Complete
NHMUK LS 1972.2050	Juvenile	?	Complete
QMUL QMBC 0614	Juvenile	?	Complete
NHMUK LS 19.5.14.6.10.b	Hatchling	?	Complete
SNSB-ZSM 20/1959	Hatchling	?	Complete

[a]Specimens with preserved eggs.
[b]Specimens with recorded sex information.

specimens were not scanned completely (Table 1) due to the original reason for scanning (i.e. studies focusing on the skull morphology or sesamoid bones; Jones *et al.* 2011, Regnault *et al.* 2016, 2017) and the limited maximum dimensions of scanners. All CT-scan data is available publicly online, i.e. UF.Herp 14110 is part of the oVert project (ark:/87602/m4/M11065; Blackburn *et al.* 2024), and the other *Sphenodon* specimens have been made available through previous studies (i.e. https://osf.io/bds35; Regnault *et al.* 2017), and in MorphoSource (see Supporting Information, Data S1 for complete list of specimens and links).

All scans were imported into Avizo v.9.2 (Thermo Fisher Scientific, MA, USA) for image segmentation. For the segmentation, the skeleton was initially isolated using the Threshold tool and the bones were selected using the Magic Wand tool when possible, or segmented slice-by-slice using the brush tool to separate the elements in different materials. The Generate Surface tool was used to export the 3D meshes from Avizo into Wavefront (.obj) files. The surfaces were generated using the 'Compactify' option (which reduces the number of faces on the meshes) and 'Smoothing' set to 'none'.

The 3D meshes were imported into the software Blender v.4.1 (Blender Foundation, Amsterdam, Netherlands) for cleaning up and measuring. The meshes straight from Avizo contain multiple islands (floating geometry) inside the objects, as well as faces that are normally poorly calculated (inside facing geometry). For the cleaning of the meshes to improve quality during rendering and decrease the number of faces, a workflow derived from Clark *et al.* (2023) was used. The internal islands were removed to reduce the total face-count and speed the rendering process. The inside facing geometry creates lighting artefacts when rendering. Therefore, we fixed this geometry using the 'Recalculate Normals' function in Blender. After cleaning up the meshes, they were smoothed for rendering using the 'Smooth modifier' option with the parameters 'factor = 1', and 'repeat = 5 to 10', depending on the quality of the scans. The renders were saved in Portable Network Graphic (.png) file format, with 15% compression.

3D geometric morphometrics

Presacral and sacral vertebrae shapes were analysed using a landmark-based 3D Geometric Morphometrics (GMM) approach

(Adams *et al.* 2004, Lawing and Polly 2010). On each presacral vertebra used (i.e. PSV4, 6, 8–11, 13, 16, 18, 20, 22, and 24), and sacral vertebrae 1 and 2, we digitized 16 landmarks (Fig. 2) using the free software 3D Slicer (Kikinis *et al.* 2014) and the 'SlicerMorph' module (Rolfe *et al.* 2021). Following the methodology established by Rohlf and Slice (1990), a generalized Procrustes analysis (GPA) was used to translate, rotate, and scale the configurations of landmarks, standardizing them to a unit centroid size (CS), which is calculated as the square root of the total of the squared distances from the centroid (Bookstein 1991). A principal components analysis (PCA) was conducted on the covariance matrix of Procrustes scores to enhance the visualization and the study of orthogonal axes which represent the morphological variation. Both GPA and PCA were performed in 3D Slicer. All the data were then imported into the RStudio environment (v.4.2.1© RStudio; R Core Team 2020) to further test the results of the 3D GMM analysis. To better visualize the changes within the PC, we warped one specimen (PSV11 of I-MEHJ S1) to the values of shape related to PC1+, PC1–, PC2+, and PC2– of adult presacral vertebrae analysis, using the Thin Plate Splines (TPS) principles. The warping process was carried out using the package 'Rvcg' and the function tps3d included in the package 'Morpho' (Schlager 2017). Packages 'devtools', 'vegan', and 'pairwiseAdonis' were employed to conduct permutational analyses of variance (PERMANOVA) and test whether the ontogenetic stages and the different sexes analysed in this study affected the results of the shape variation (Oksanen *et al.* 2013, Harrell and Harrell 2019, Martinez Arbizu 2020, Wickham *et al.* 2022). A *P*-value below 0.05 suggests that the factor under investigation (sex or ontogeny) significantly influences all scores derived from the Principal Component Analysis (PCA). The R2 value quantify how much the analysed factor accounts for the shape variation (e.g. R2 = 0.5, 50% of the shape variation).

The CS of all the scaled specimens was used to also evaluate the possible allometric trends in our sample and the contribution of the size on all the PCA scores. PERMANOVA analyses with 9999 permutations using all the PCA scores and different factors such as CS-sex (SV All, adults PSV4, adults PSV11, adults PSV24) and CS-ontogenetic stages (All PSV4, All PSV11, All PSV24, All PSV All) were run to test the possible influence of CS, sex, and combined CS-sex on the PCA results. A significant *P*-value ($p < 0.05$) means that the analysed factor (sex, ontogeny, or both factors) affects the PCA scores. The R2 value quantify how much the analysed factor influences the shape variation. The previous analysis was performed on the Euclidean distance between the PCA scores implementing a Holm correction using the package 'pairwiseAdonis' (Martinez Arbizu 2020). The Pearson correlation test implemented in the package 'Hmisc' was used to test the influence of size on the PC1 scores. The reported results include the t-value (magnitude and direction of the correlation), d.f. (degrees of freedom), F-value (ratio of mean squares for between and within groups), *P*-value (statistical significance), and cor (correlation coefficient) (see Supporting Information, Data S3) (Harrell and Harrell 2019). A negative cor indicates a negative correlation between PC1 and CS, whereas a positive cor indicates a positive correlation between PC1 and CS. A higher absolute t-value suggests a stronger correlation between PC1 and CS. The *P*-value indicates whether the correlation is statistically significant ($p < 0.05$). A statistically significant *P*-value, along with a positive correlation and a high positive absolute t-value, suggests the presence of positive allometry in the first principal component (PC1). However, if these values are negative, a negative allometry affects the PC1 values. The r2CS value indicates how much of the variation in one variable (PC1) is explained by the other variable (CS). A low value suggests that CS does not explain the PC1 variation, whereas a higher value indicates a strong correlation. A plot correlating the CS and the PC1 values is also reported in the Supporting Information, Data S3. For ontogenetic size-shape covariation between the different specimens in our sample (All PSV4, All PSV11, All PSV24), we performed linear regressions of shape coordinates onto the natural logarithm of the centroid size using the procD.lm function implemented in 'geomorph' (Adams and Otárola-Castillo 2013). A statistically significant *P*-value of the Ordinary Least Squares (OLS) analysis indicates that the regression score is affected by the CS. The plot resulting from the linear regression was investigated to understand how the regression score of the ontogenetically different specimens varies with size increase, providing insights into the allometry of the studied species (see Supporting Information, Data S3). The results of all the aforementioned analyses were plotted using the package 'ggplot2' for a better visualization (Wickham *et al.* 2016).

Photographs and figures

Photographs of fossil rhynchocephalian specimens used in this study were taken with a mirrorless camera OM-System OM1 (OM Digital Solutions Corporation, Shinjuku, Tokyo, Japan), equipped with the M.Zuiko Digital ED 60 mm Macro lens. UV-light photography was carried out using the Alonefire SV003 10 W UV-lamp - 365 nm (Shenzhen Shiwang Technology Co., Guangdong, China) and no filters. All figures were made in the software Affinity Designer 2 (Serif Ltd, West Bridgford, United Kingdom).

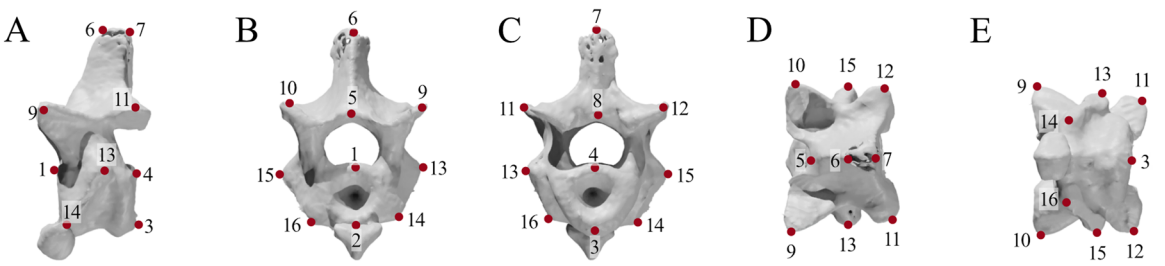

Figure 2. 3D representation of presacral vertebra 4 (PSV 4) of *Sphenodon* (I-MEHJ S1), with 16 landmarks used on the 3D geometric morphometric analysis. 3D renders of PSV 4 in: (A) lateral view; (B) anterior view; (C) posterior view; (D) dorsal view; (E) ventral view.

Phylogenetic analysis

To test the influence of morphological characters of the axial skeleton (following the new axial characters of Beccari *et al.* 2025a), two phylogenetic analyses were conducted: (A1) a maximum parsimony analysis using the dataset of Beccari *et al.* (2025a), including 34 characters of the axial skeleton; (A2) a maximum parsimony analysis using the updated dataset of Simões *et al.* [(2022); updated by Beccari *et al.* (2025a)], with 18 characters of the axial skeleton. Both analyses were run in the software TNT v.1.6 (Goloboff and Morales 2023) using New Technology Search (50 hits).

Institutional abbreviations

NHMUK LS, Natural History Museum UK, Collection Specimen, London, England, UK; IDHRN NH, Horniman Museum and Gardens, Natural History Collection, London, England, UK; I-MEHJ, University College London, UK, Laboratory of Susan E. Evans, London, England; LDKCL, The Museum of Life Sciences, King's College London, London, England, UK; MB.R., Museum für Naturkunde, Reptiles and Amphibians, Berlin, Germany; MZH MS, Luomus Finnish Museum of Natural History, Zoology Collections, University of Helsinki, Helsinki, Finland; QMUL QMBC, Queen Mary University of London, Queen Mary Biology Collection, London, England, UK; SAMA, South Australian Museum Australia provider for OZCAM (Online Zoological Collections of Australian Museums), Adelaide, Australia; SMF, Senckenberg Museum, Frankfurt a. M., Germany; SNSB-BSPG, Bayerische Staatssammlung für Paläontologie und Geologie, Munich, Germany; SNSB-ZSM, Zoologische Staatssammlung München, Munich, Germany; TM, Tylers Museum, Haarlem, Netherlands; UF.Herp, University of Florida, Herpetology Collection, Gainesville, FL, USA; UMMZ.Herp, University of Michigan Museum of Zoology, Herpetology Collection, Ann Arbor, MI, USA; UMZC R, University of Cambridge, Zoological Specimens, Cambridge, England, UK; ZMB, Museum für Naturkunde, Zoological Collection, Berlin, Germany.

RESULTS

Ontogenetic analysis

In this study, we arranged *Sphenodon* specimens into four ontogenetic categories (hatchling, juvenile, subadult, and adult), based on ontogenetically variable morphological traits, such as bone ossification and fusion. To test for clear patterns of skeletal maturity, these traits were scored to be used in an ontogram. This resulted in three most parsimonious trees (best score = 165), where the steps show stages of bone development. The strict consensus tree (Fig. 3) shows a sequence of steps from the smallest and least skeletally mature juvenile in our sample (NHMUK LS 1855.10.163) to the subadult and adult specimens. Aside from character 31 (lumbar vertebra 1, rib; see 'Presacral vertebrae 3 to 25' section below), all characters showed a clear pattern in ossification timing, with the lowest character score (0) marking the hatchling condition.

The hatchling skeleton was poorly ossified and most elements that fuse during ontogeny (e.g. neural arches, girdles, and limb bone epiphyses) were yet unfused. Therefore, 38 out of 69 characters (see Supporting Information, Data S4 for the complete list of character changes) marked the transition from hatchlings to the earliest juvenile specimen (NHMUK LS 1855.10.163). These characters regard the initial steps in bone ossification, with four characters (i.e. characters 2, 3, 4, and 9) showing the final stage of development already in post-hatchling specimens. Juvenile specimens are here defined as the earliest post-hatchlings with the lowest degree of skeletal maturity. These specimens were substantially smaller than adult and subadult specimens (Fig. 3F–G). The largest juvenile specimen in our sample had a presacral vertebrae length (PSVL) = 89.02 mm (NHMUK LS 1972.2050). During this stage, ossification of bones progressed gradually. In the axial skeleton, this stage marked the fusion of neural arch pedicels, and the closure of the notochordal canal. Ribs, cartilaginous ribs, and gastralia developed at this stage, and in one juvenile (NHMUK LS 1972.2050) reached the latest stage of ossification in these elements. The appendicular skeleton was poorly ossified and especially the epiphyses in limb bones were unfused and incipient.

Subadult specimens and adult specimens were similar in size (presacral vertebrae total length > 100 mm), adults being, on average, slightly larger (Fig. 3F–G). Subadults, however, were not fully skeletally mature, and showed a gradual increase of ossification and fusion of bones. Most elements in the axial skeleton were fully ossified at this stage, except for the fusion of the sacral intercentrum between sacral vertebrae 1 and 2 (see 'Sacral vertebrae' section below). Subadults showed a higher degree of fusion in the appendicular skeleton, compared to juveniles. In all subadults, the scapulocoracoid was a fused, well-ossified element. Some subadult specimens had fused proximal epiphyses of the radius, tibia, and fibula, and distal epiphyses of the humerus, and manual and pedal phalanges. The proximal epiphyses of the humerus, ulna, femur, and manual and pedal phalanges, as well as the distal epiphyses of the radius and femur were only fully fused in adult specimens. The radiale, pisiform, and ulnare were poorly ossified in subadult specimens. The astragalocalcaneum was already fused in subadults, but the lateral process (*sensu* Russell and Bauer 2008) was unfused at this ontogenetic stage. The pelvic girdle elements were only fused in adult specimens.

Osteological description

In the following sections, the four ontogenetic stages will be described in detail to what regards their axial anatomy. Each section is divided into (i) the general adult morphology of *Sphenodon*; (ii) ontogenetic and individual variation in *Sphenodon*; and (iii) remarks on fossil taxa.

Number and regionalization of vertebrae

General adult morphology

The presacral vertebra (PSV), i.e., the atlas, axis, cervical vertebrae (CV), anterior dorsal vertebrae (ADV), posterior dorsal vertebrae (PDV), and lumbar vertebrae (LV), count was usually 25 (Fig. 4), but some specimens in this study (i.e. ZMB 55044 and UF.Herp 14110) showed only 24 presacral vertebrae, and one specimen (QMUL QMBC 0615) showed 26. The sacrum typically consisted of two sacral vertebrae (SV). Some specimens, however, showed up to three sacral vertebrae (i.e. UMZC R2616 and ZMB

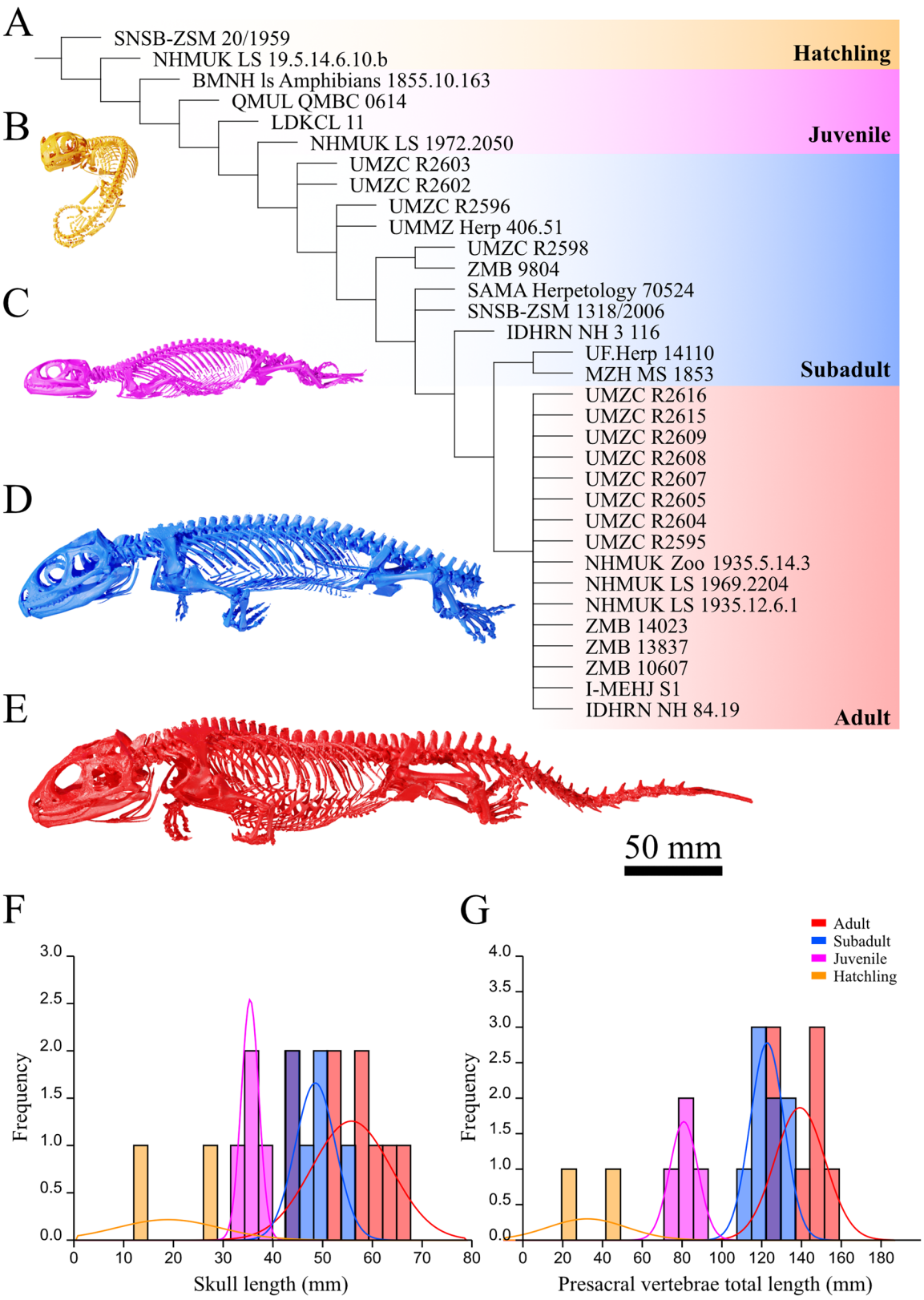

Figure 3. Ontogram showing the ossification sequence in *Sphenodon* specimens of different ontogenetic stages. A, strict consensus tree rooted in the smallest hatchling specimen in our sample (SNSB-ZSM 20/1959). B, 3D render of specimen NHMUK LS 19.5.14.6.10.b (hatchling). C, 3D render of specimen LDKCL X 11 (juvenile). D, 3D render of specimen SAMA Herpetology 70524 (subadult). E, 3D render of specimen ZMB 14023 (adult). F, histogram of the distribution of skull length of *Sphenodon* specimens in this study. G, histogram of the distribution of presacral vertebrae total length (body size) of *Sphenodon* specimens in this study.

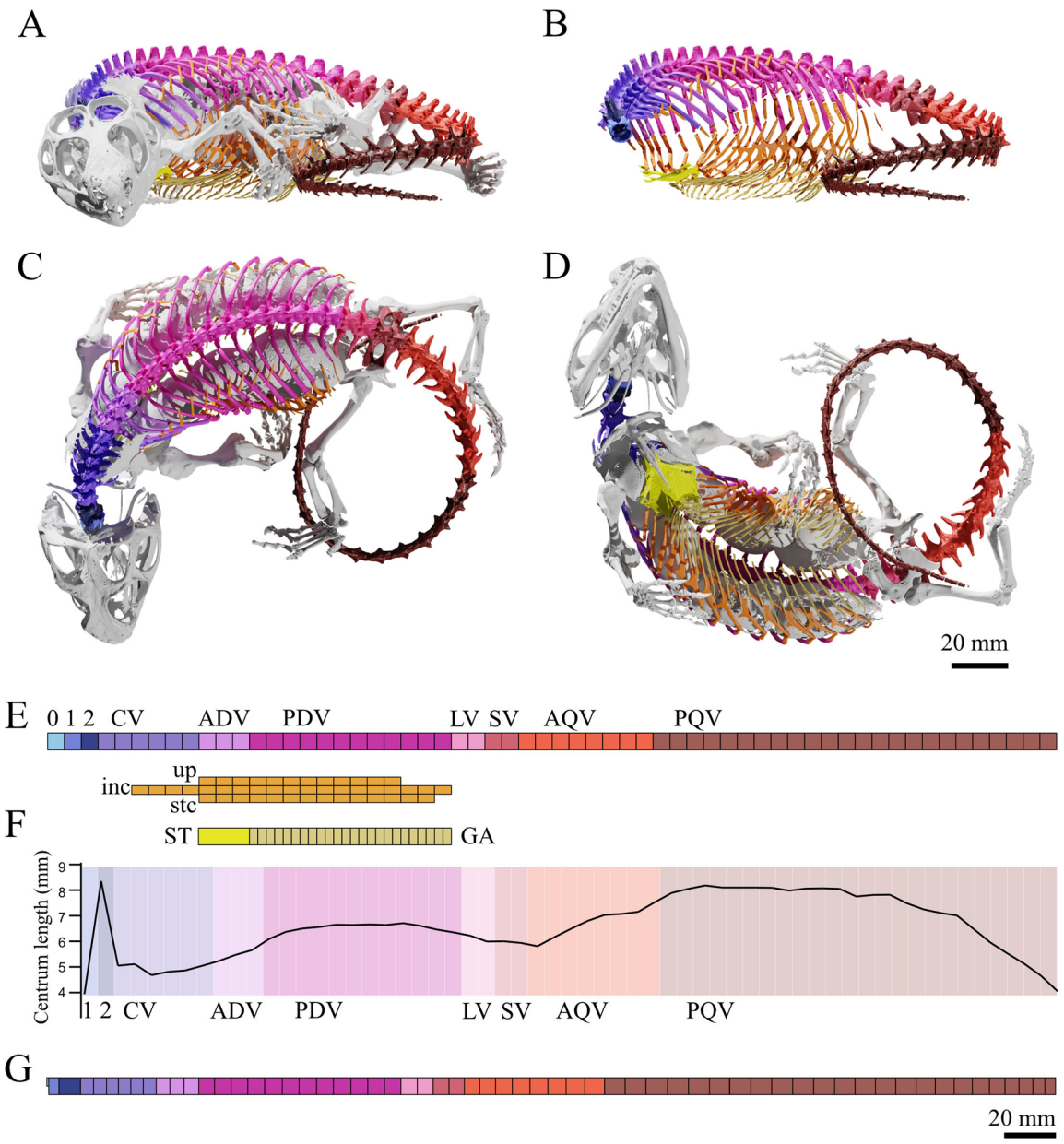

Figure 4. 3D representation of the skeleton of *Sphenodon* (I-MEHJ S1). A–D, 3D renders of specimen IMEHJ S1 in (A) lateral view; (B) axial skeleton only in lateral view; (C) dorsal view; (D) ventral view; (E) schematic representation of the axial series; (F) graph with absolute length of the vertebral centra of I-MEHJ S1; (G) schematic representation of the scaled axial series. The colours represent the different elements of the axial skeleton. Abbreviations: 0, proatlas; 1, atlas; 2, axis; ADV, anterior dorsal vertebrae; AQV, anterior caudal vertebrae; CV, postaxial cervical vertebrae; GA, gastralia; inc, intercostal ribs; LV, lumbar vertebrae; PDV, posterior dorsal vertebrae; PQV, posterior caudal vertebrae; ST, sternum; stc, sternocostal ribs; SV, sacral vertebrae; up, uncinate processes.

9804 in this study, and the 'Dublin Museum specimen' reported by Howes and Swinnerton (1901: fig. 6). The caudal vertebrae (QV) count can vary drastically across specimens, mostly because of tail autotomy: an autotomic septum is present in *Sphenodon*, and many specimens in this study show at least a partially regrown tail (see Supporting Information, Data S1 for the complete list of preserved and scanned bones). The maximum number of caudal vertebrae in our sample was 40 in a hatchling individual (NHMUK LS 19.5.14.6.10.b). The autotomic septum was usually present starting from QV8, but in five specimens (i.e. NHMUK LS 1935.12.6.1, NHMUK LS 1969.2204, UMZC R2605, UMZC R2608, and UMZC R2615), QV7 showed a complete autotomic plane, and in one specimen (UMZC R2609), the first autotomic plane was present in QV9.

Both the presacral and caudal series can be subdivided into subregions through anatomy and morphometry. The cervical vertebrae (CV) are here regarded as the anterior presacral vertebrae that do not contact the sternum through the articulating ribs (following Romer 1956, Hoffstetter and Gasc 1969), and include the atlas and axis. There are usually eight cervical vertebrae in *Sphenodon*, with a single exception in this study having seven cervical vertebrae (UMZC R2605). In all but this specimen, the dorsal vertebrae count started on PSV9. Subsequent presacral vertebrae were further subdivided into anterior dorsals (ADV), posterior

dorsals (PDV), and lumbar vertebrae (LV). The anterior dorsals are those that contact the sternum through assessorial cartilaginous ribs, i.e. intercostal and sternocostal ribs. These are usually the three anteriormost dorsal vertebrae (PSV9–11). Specimens with four anterior dorsals have also been reported (Howes and Swinnerton 1901, Hoffstetter and Gasc 1969). Among the specimens in this study, only UMZC R2605 showed this condition, having a 'dorsalized' last cervical vertebra. The posterior dorsals are those associated with both intercostal and sternocostal ribs, but do not contact the sternum (i.e. PSV12–23). A pair of gastralia are secondarily attached to each sternocostal rib pair through connective tissue (Hoffstetter and Gasc 1969). The lumbar vertebrae are the last two presacral vertebrae (PSV24–25), which are not associated with cartilaginous ribs and the gastralia. In all adult specimens, the last pair of ribs was ankylosed to the centrum of the last PSV. These ribs are here considered as pleurapophyses (*sensu* Hoffstetter and Gasc 1969) of the associated vertebra. In seven specimens (i.e. juveniles LDKCL X 11 and NHMUK LS 1972.2050; subadults UMZC R2603 and ZMB 9804; adults I-MEHJ S1, UMZC R2604, and 2605), the ribs of the second to last PSV were also ankylosed, but this was less consistent across our sample.

The regionalization of presacral vertebrae was also evident in the PCA (Fig. 5). A total of 48 variation axes were recovered, the two main axes (PC1 and PC2) explaining 63.3% of the variation, and 95% of the variation being explained by the combination of

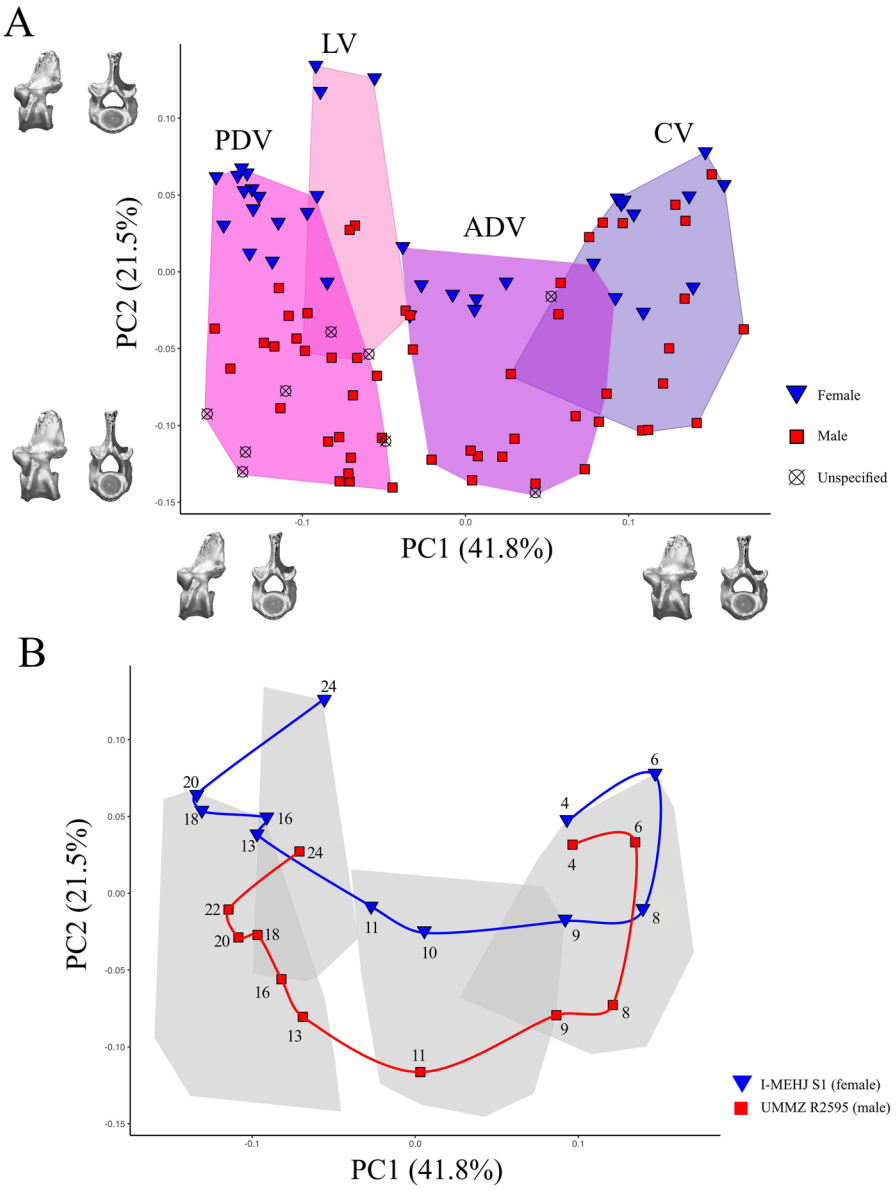

Figure 5. Combination of the main axes of the Principal Component Analysis (PCA) of the presacral vertebrae (PSV) of adult specimens of *Sphenodon*. A, combination of the main axes of variation (PC1 and PC2), and theoretical given in their respective axes (PC1 and PC2). B, combination of the main axes of variation (PC1 and PC2), highlighting the sequence of vertebrae in two specimens, I-MEHJ S1 (female, in blue), and UMMZ R2595 (male, in red). Abbreviations: ADV, anterior dorsal vertebrae (PSV 9–11); CV, cervical vertebrae (PSV 4, 6, and 8); LV, lumbar vertebrae (PSV 24); PDV, posterior dorsal vertebrae (PSV 13, 16, 18, 20, and 22).

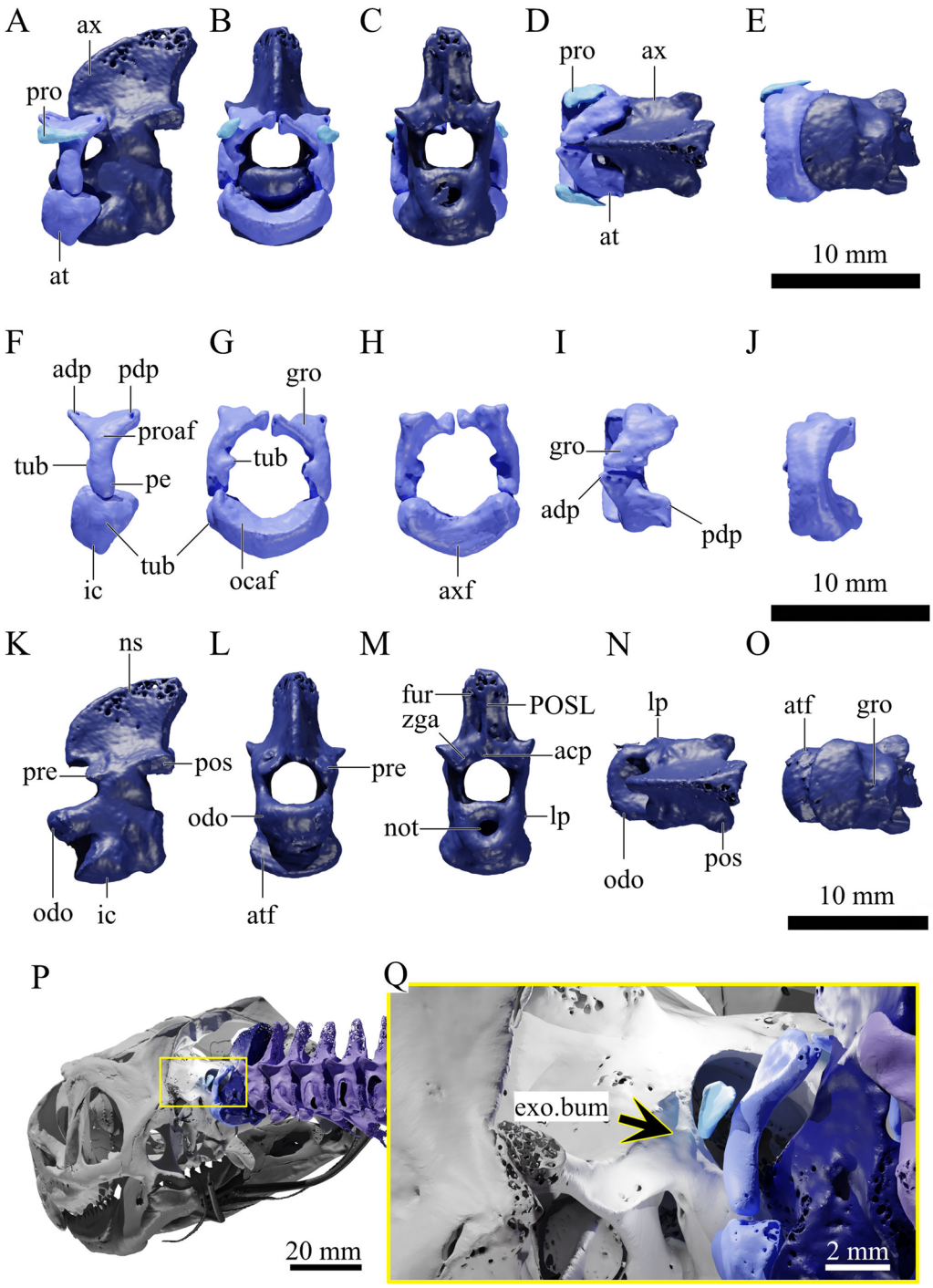

Figure 6. 3D representation of the proatlas, atlas, and axis of *Sphenodon* (I-MEHJ S1). A–E, 3D renders of the articulated proatlas, atlas, and axis. F–J, 3D renders of the atlas. K–O, 3D renders of the axis. A, F, K, left lateral view. B, G, L, anterior view. C, H, M, posterior view. D, I, N, dorsal view. E, J, O, ventral view. P, Q, 3D renders of the skull and anterior vertebrae of *Sphenodon* (NHMUK LS 1935.5.14.3); (P) posterolateral view of the skull and anterior vertebrae; (Q) posterolateral view of the braincase and anterior vertebrae, with arrow pointing to the articular facet for the proatlas in the exoccipital. Abbreviations: acp, accessory process; adp, anterodorsal process; at, atlas; atf, articular facet for the atlas; ax, axis; fur, furrow; exo.bum, exoccipital bump (articular facet for the proatlas); gro, groove; ic, intercentrum; lp, lateral protuberance; not, notochordal canal; ns, neural spine; ocaf, articular facet for the occipital condyle; odo, odontoid process; pdp, posterodorsal process; pe, pedicel; pos, postzygapophysis; POSL, postspinal lamina; pre, prezygapophysis; pro, proatlas; proaf, proatlas articular facet; tub, tubercle; zga, zygantrum.

the first 17 axes. The post-axial cervical vertebrae were slightly stouter, i.e. wider, shorter, and lower, than the dorsal vertebrae, especially the posterior dorsals (i.e. PSV12–23). The anterior dorsals showed intermediate proportions among the presacral vertebrae and gradually changed from the more robust cervical morphology to the more gracile posterior dorsal morphology. These latter vertebrae show relatively longer centra and taller neural spines than the other presacral vertebrae. The lumbar vertebrae (usually PSV24–25, albeit three specimens show different number of presacral vertebrae, as mentioned above) were slightly more robust than the rest of the posterior dorsals, but not to the same degree as the cervical and anterior dorsal vertebrae. These subdivisions were significantly different (PERMANOVA: CV x ADV: F-value = 13.6, p = 0.001; CV x PDV: F-value = 58.0, p = 0.001; CV x LV: F-value = 19.6, p = 0.001; ADP x PDV: F-value = 22.7, p = 0.001; ADP x LV: F-value = 14.1, p = 0.001; PDV x LV: F-value = 6.5, p = 0.002).

The caudal series is here divided into anterior and posterior caudals (AQV and PQV, respectively). The anterior caudals are those anterior to, but including, the first autotomic vertebra (i.e. QV1–8, in the most common configuration). These vertebrae were usually shorter than the posterior caudals (QV9 and posterior; Fig. 4F–G). QV1 to 8 showed fused ribs (pleurapophyses), whereas QV9 and posterior showed laterally expanded diapophyses (transverse processes). The length to height ratio of these caudals increased posteriorly, meaning that they got progressively longer, and their neural spines shorter. The space between left and right zygapophyses decreased throughout the posterior caudal series, resulting in single median pre- and postzygapophyseal surfaces in the posteriormost caudals.

Remarks on fossil taxa

The number of presacral vertebrae in fossil rhynchocephalians was usually close to that of *Sphenodon*, being 23 in *Vadasaurus herzogi* Bever & Norell, 2017, 24 in many taxa, e.g. *Homoeosaurus maximiliani* von Meyer, 1847, *Homoeosaurus parvipes* Cocude-Michel, 1963, *Kallimodon cerinensis* Cocude-Michel, 1963, and *Kallimodon pulchellus* (Zittel 1887–1890), and 25 presacral vertebrae in *Sphenofontis velserae* Villa *et al.*, 2021 (Cocude-Michel 1963, Fabre 1981, Bever and Norell 2017, Villa *et al.* 2021). In pleurosaurids (i.e. *Acrosaurus frischmanni* von Meyer, 1854, *Palaeopleurosaurus posidonae* Carroll, 1985, *Pleurosaurus ginsburgi* Fabre, 1974, and *Pleurosaurus goldfussi* von Meyer, 1831), the number of presacral vertebrae was greatly increased, ranging from 37 in *Palaeopleurosaurus* Carroll, 1985 to 57 in *Pleurosaurus ginsburgi* (Fabre 1974, Carroll 1985, Dupret 2004, Beccari *et al.* 2025b). In fossil rhynchocephalians, the number of cervicals may be closer to that of *Sphenodon*, with many taxa described with seven cervical vertebrae (e.g. *Homoeosaurus* von Meyer, 1847, *Kallimodon* Cocude-Michel, 1963, and *Sapheosaurus* von Meyer, 1850). However, clearly assessing the number of cervical vertebrae in these taxa is not straightforward, as even in specimens where soft tissue is preserved, the sternum and sternocostal ribs may be disarticulated and poorly preserved or obscured by other skeletal elements.

There were no fossil rhynchocephalians with more than two sacral vertebrae described so far. The number of caudal vertebrae can vary significantly across taxa, reaching a maximum of over 100 caudals in pleurosaurids (e.g. 118 QVs in *Pleurosaurus ginsburgi* SNSB-BSPG 1977 X 40; Beccari *et al.* 2025b).

Although regionalization in the axial skeleton of fossil rhynchocephalians may follow the same patterns of *Sphenodon*, until now no attempt at subdividing the dorsals and caudals has been made. Proper subdivision in fossil taxa is hampered by various factors, such as preservation of specimens, with many fossils being incomplete or taphonomically deformed (this is often the case with e.g. the Solnhofen Archipelago taxa; Munnecke *et al.* 2008, Rauhut and Röper 2013, Rauhut and López-Arbarello 2016, Rauhut *et al.* 2017, Villa *et al.* 2021) and lacking the important indicators mentioned above for *Sphenodon*. Missing information might include the number of vertebrae connected to the sternum (one of the main indicators for the anterior dorsals), or the position of the first autotomic septum (which cannot be observed in many specimens and is absent in pleurosaurids and *Kallimodon pulchellus*; Cocude-Michel 1963, Dupret 2004, Beccari *et al.* 2025a, b). The incompleteness and taphonomy of fossils also complicate geometric morphometric studies. Therefore, subdividing the axial skeleton of fossil rhynchocephalians should be done case by case and falls outside the scope of this current study. However, the main morphological aspects of fossil taxa will be noted throughout the description below.

Proatlas

General adult morphology

A proatlas (Fig. 6) was present in *Sphenodon*, loosely associated to the atlas (Osborn 1900, Howes and Swinnerton 1901, Jones *et al.* 2009a, Čerňanský and Stanley 2019). The proatlas consisted of paired arches anterior to the atlantal neural arch. In lateral view, the proatlas was triangular, with the apex pointing posteriorly. It was longer than tall, and both the anterior and dorsal margins were concave in lateral view, whereas the ventral margin was straight. The proatlas articulated with the atlas at the lateral surface of the atlantal neural arch, ventral to the anterodorsal process of the atlas. The posterior surface of the exoccipital was marked by a low bulbous articular facet for the proatlas (Fig. 6P–Q), possibly marking the occipital proatlas ligament (oc.proat.lig in Jones *et al.* 2009a: fig. 42).

Ontogenetic and individual variation

The proatlas was not visible in the CT-scan of hatchling specimens and was possibly unossified at this stage. It was visible and ossified in juveniles but was shorter than the subadult and adult proatlas (Fig. 7F–T). The proatlas was identical among subadult and adult specimens.

Remarks on fossil taxa

The proatlas has not been described yet for fossil taxa. Its size and location between skull bones (i.e. exoccipital, parietal, squamosal, and supraoccipital) and the atlas, likely makes recognizing the proatlas challenging. It has not been identified in specimens where the neighbouring elements (i.e. braincase and atlas) are well preserved and have been CT-scanned (O'Brien *et al.* 2018). Similarly, it remains unreported from complete and well-preserved specimens from the Solnhofen Archipelago. The proatlas has been proposed as a plesiomorphic structure in tetrapods (Baur 1886, Hoffstetter and Gasc 1969, Pardo and Anderson 2016) and may

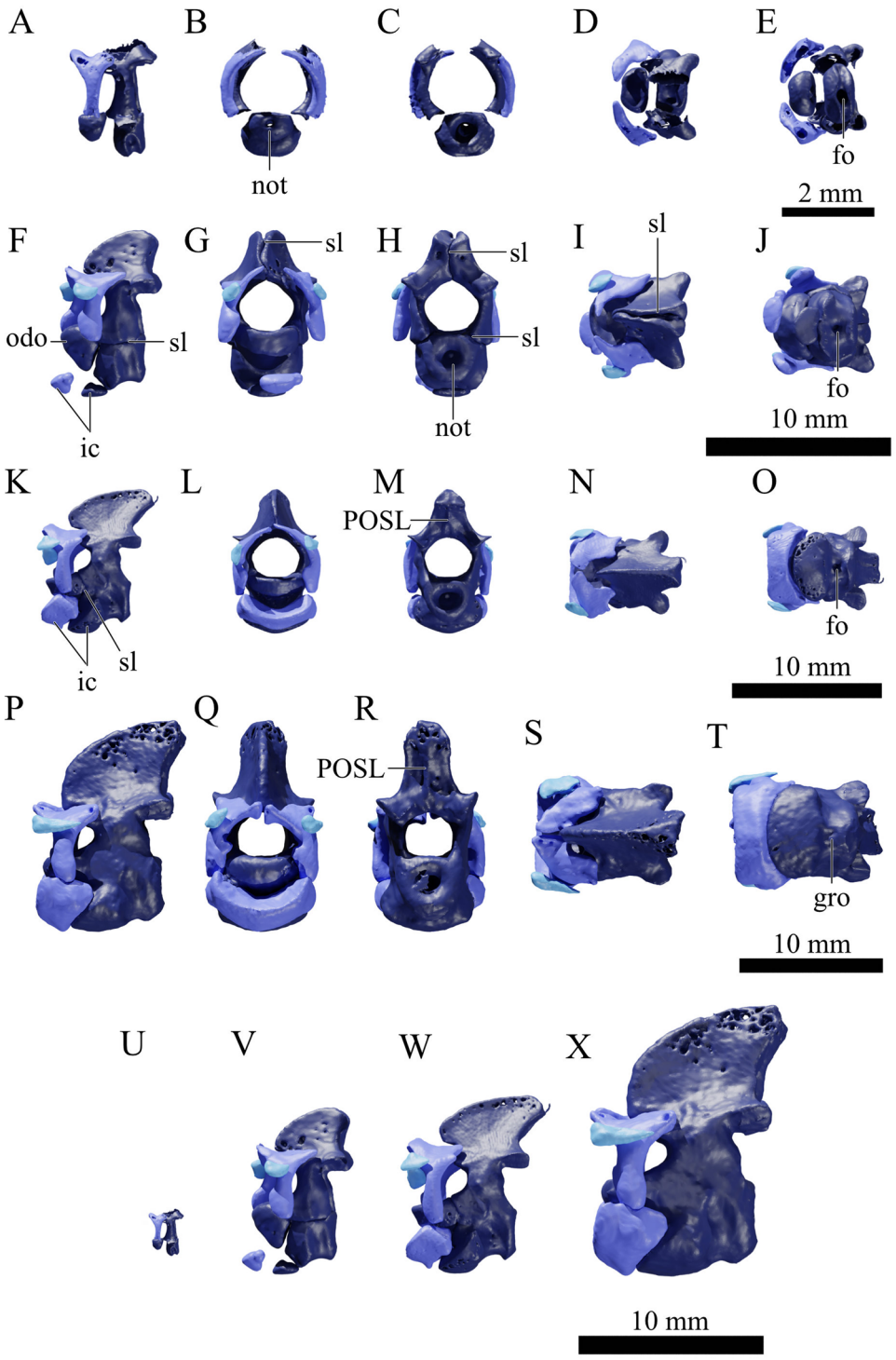

Figure 7. 3D representation of the proatlas, atlas, and axis of *Sphenodon* specimens of different ontogenetic stages. A–E, 3D renders of the articulated atlas, and axis of the hatchling SNSB-ZSM 20/1959. F–J, 3D renders of the articulated proatlas, atlas, and axis of the juvenile QMUL QMBC 0614. K–O, 3D renders of the articulated proatlas, atlas, and axis of the juvenile NHMUK LS 1972.2050. P–T, 3D renders of the articulated proatlas, atlas, and axis of the adult I-MEHJ S1. A, F, K, P, left lateral view. B, G, L, Q, anterior view. C, H, M, R, posterior view. D, I, N, S, dorsal view. E, J, O, T, ventral view. U–X, size comparison between the atlas-axis complex of (U) SNSB-ZSM 20/1959; (V) QMUL QMBC 0614; (W) NHMUK LS 1972.2050; and (X) I-MEHJ S1. Abbreviations: fo, foramen; gro, groove; ic, intercentrum; not, notochordal canal; odo, odontoid process; POSL, postspinal lamina; sl, suture line.

have been present in fossil rhynchocephalians. Nevertheless, it is possible that the proatlas has been lost in some clades of rhynchocephalians, given that it has been lost in squamates (Hoffstetter and Gasc 1969).

Atlas

General adult morphology

The atlas (Fig. 6A–J) was formed by the atlantal intercentrum and two neural arch pedicels. The atlantal centrum was fused to the axis, forming the odontoid process in the latter. The atlas was locked to the axis by the atlantal intercentrum and the axial odontoid process, but these vertebrae were never fused together (Fig. 6A–E). The atlas did not articulate with ribs.

Intercentrum

The atlantal intercentrum (Fig. 6F–J) was wedge shaped in lateral view, wider than long, and ventrally convex in anterior view. It was much wider than the other intercentra in the axial series. The articular facets for the occipital condyle anteriorly and axis posteriorly were deep and involved the full width of the element. The atlantal intercentrum was locked between the odontoid process and the axial intercentrum. A median ridge may be present on the ventral surface of the atlantal intercentrum, but was less marked than that of post-axial cervical intercentra. Each lateral surface of the atlantal intercentrum was marked by a rounded tubercle, also visible in anterior view (Fig. 6F–G), which has been inferred as the articular facet for an atlantal rib in fossil taxa (Evans 1981), albeit no fossil rhynchocephalian has been described with preserved atlantal ribs so far.

Neural arch

The paired atlantal neural arch pedicels were independent elements, unfused to the intercentrum and to each other (Fig. 6F–J). They met at the midline above the neural canal, but did not form a neural spine. Both pedicels were curved medially, and the neural canal opening was large and circular. The articular facet with the occipital condyle was marked on the anteroventromedial margin of the pedicels. The dorsal margin of this articulation formed a medially oriented tubercle in the atlantal pedicels (Fig. 6F–G). Posteromedial to the occipital articulation, the pedicels articulated with the odontoid process of the axis. The shallow articular facet for the proatlas was laid on the lateral surface of the pedicel, dorsal to the occipital articulation. The medial margin of the pedicel was pierced by a single nutrient foramen.

The dorsal half of the neural arch expanded anteroposteriorly, and formed the anterodorsal and posterodorsal processes (Fig. 6F). The dorsolateral surface between these processes was marked by a longitudinal shallow groove. The anterodorsal process expanded medially, forming a horizontal shelf. In some specimens, the pedicels contacted through this medial expansion of the anterodorsal process, but they always remain unfused. The posterodorsal process was shorter than the anterodorsal process and laid dorsolateral to the anterior end of the axis neural arch. The articular facet to the axis laid on the medial margin of this process and was flattened. This medial articulation differed from the ventrolateral postzygapophyseal articulation of other vertebrae. The articulation between atlas and axis has not been considered as zygapophyseal in some studies (e.g. Hoffstetter and Gasc 1969), but has been proposed as such in more recent works (e.g. Evans 1981, Jones *et al.* 2009a). We here regard this articulation as a true zygapophyseal articulation and the posterodorsal process of the atlas as an incipient postzygapophysis.

Ontogenetic and individual variation

Intercentrum

The atlantal intercentrum was not formed or poorly ossified in hatchlings and could not be clearly observed in the CT-scans. It was visible in juveniles but was poorly ossified at this stage, being fully ossified in subadult and adult specimens only (Fig. 7P–T). The lateral tubercles were only prominent in subadult and adult specimens.

Neural arch

The dorsal and ventral ends of the atlantal neural arch pedicels were poorly ossified in hatchlings, and the occipital articulation was incipient at this stage. In juveniles, the pedicels were already fully ossified, and the occipital articulation was developed. The dorsolateral groove between the anterodorsal and posterodorsal processes was less marked in juveniles (Fig. 7G, L, Q).

The medial nutrient foramen of the atlantal pedicels may be present in both left and right elements, or only in one (e.g. it is only present in the left pedicel of NHMUK LS 1935.5.14.3, adult). This foramen was larger (occupies relatively more of the medial surface of the pedicel) in juvenile specimens.

Remarks on fossil taxa

The atlas is known and has been described in detail in many fossil rhynchocephalians, e.g. *Clevosaurus hudsoni* Swinton, 1939 (O'Brien *et al.* 2018), *Gephyrosaurus bridensis* Evans, 1980 (described in Evans 1981), *Planocephalosaurus robinsonae* Fraser & Walkden, 1984, and *Sphenofontis velserae* Villa *et al.*, 2021. Even in the taxa at the end of early-branching lineages, such as *Gephyrosaurus* Evans, 1980 and *Planocephalosaurus* Fraser & Walkden, 1984, the general atlantal morphology is similar to that of *Sphenodon* (Evans 1981, Fraser and Walkden 1984). In these fossil taxa, the atlas is composed of a wedge-shaped atlantal intercentrum, and two unfused neural arch pedicels. In *Clevosaurus hudsoni* NHMUK PV R36832 (O'Brien *et al.* 2018), the atlantal intercentrum was described as a paired element, differing from the single one of *Sphenodon*. In the posterior dorsals and lumbar vertebrae of *Sphenodon*, the intercentrum was paired in juveniles and only fused into a wedge-like bone in subadults. It is unclear if the atlantal intercentrum of NHMUK PV R36832 is either broken, would fuse in later ontogenetic stages in *Clevosaurus hudsoni*, albeit this specimen pertaining to a subadult to adult (O'Brien *et al.* 2018), or a unique morphological feature of this taxon.

The occipital tubercle in the atlantal neural arch of *Sphenodon* was more pronounced anteromedially than in fossil taxa. In *Pleurosaurus goldfussi* (SNSB-BSPG 1925 I 18), the atlantal intercentrum was spherical rather than wedge shaped (Fig. 8A, B). The ventral surface of this intercentrum was marked by a longitudinal median ridge and two foramina lateral to this ridge. Only the feet of the neural arch pedicels were exposed in this specimen. A small

tubercle, possibly the diapophysis, laid at the posterolateral surface of the foot. However, no ribs were associated with this atlas.

Axis

General adult morphology

The axis (Fig. 6K–O) was the largest vertebra, being taller, wider, and slightly longer than all other presacral vertebrae. No ribs were associated with the axis.

Centrum and intercentrum

The axial centrum was robust due to its fused elements (Fig. 6K–O). Without the odontoid process, the axial centrum was about as long as wide. The odontoid process (fused atlantal pleurocentrum) extended anteriorly and held the atlantal intercentrum in place. This process was semi-circular in lateral view, with a straight dorsal margin, and a convex ventral margin (Fig. 6K). It was separated from the fused axial intercentrum by a deep transverse groove. The axial intercentrum was massive, expanding further laterally and ventrally than the axial centrum. The intercentrum was slightly tilted posteriorly, so that it was oriented obliquely to the axial centrum, with the anterior margin pointing slightly ventrally (Fig. 6K–L).

The axial centrum was marked by a deep median groove on its ventral surface, posterior to the axial intercentrum (Fig. 6O). This groove was formed by the closing of a large mesial subcentral foramen present in early ontogenetic stages (hatchling and juveniles; Fig. 7E, J). The lateral surface of the axial centrum showed a lateral protuberance, which could be best observed in anteroposterior and dorsal views (Fig. 6L–N; *sensu* Hoffstetter and Gasc 1969), which was an incipient diapophysis or transverse process (*sensu* Jones *et al.* 2009a). The closed notochord canal was marked at the centre of the posterior surface of the axial centrum (Fig. 6M).

Zygapophyses

The axial prezygapophyses were incipient and not laterally expanded as in the typical morphology in post-axial vertebrae. The prezygapophyseal articular facet was flattened and laid on the dorsolateral surface of the neural arch (Fig. 6K). The axial postzygapophyses were narrow in dorsal view (Fig. 6N) compared to those in PSV3–25 and sacral vertebrae. These zygapophyses were triangular in dorsal view and slightly twisted laterally, so that the articular facet for the prezygapophysis of PSV3 was visible in lateral view (Fig. 6K). Medially, a zygantrum was present for articulation with the zygosphene of PSV3 (Fig. 6M).

Neural arch and spine

The axial neural arch was tall and anteroposteriorly constricted at its base. In lateral view, the anterior margin was concave and the posterior margin convex (Fig. 6K). As in the atlas, the medial surface of the lateral walls of the neural arch may be pierced by a nutrient foramen.

The neural spine was massive compared to that of the post-axial vertebrae. The morphology of the neural spine varied among specimens regarding its height and length, but it was overall anteroposteriorly expanded, longer than tall, and blade like (Fig. 6K). The anterior margin of the neural spine was convex, and the dorsal and posterior margins were straight in lateral view. The spine widened posteriorly, being almost triangular in dorsal view. In posterior view, a marked dorsoventral ridge, the postspinal lamina (POSL), crossed the midline of the neural spine (Fig. 6M). On each side of this lamina, the posterior surface of the axial neural spine was excavated by a vertical furrow. Ventral to the POSL and the lateral furrows, the neural spine expanded slightly forming the accessory process (Fig. 6M; *sensu* Fraser 1988).

Ontogenetic and individual variation

The axis was already the largest presacral vertebra in hatchlings, but poorly ossified (Fig. 7A–E).

Centrum and intercentrum

The axial intercentrum was absent in hatchlings (Fig. 7A–E). It formed in juveniles and had started its fusion to the axial centrum at this stage already (Fig. 7F, O). The axial intercentrum was fully fused, with no visible suture lines, to the axial centrum in all but one subadult specimen (partially fused in UMMZ.Herp 406.51), and all adult specimens. In two adult specimens (i.e. IDHRN NH 84.19 and NHUMK LS 1935.5.14.3), the posterior margin of the axial intercentrum projected posteroventrally at the mesial margin, forming a 'spur' or process that covered the ventral midline groove of the axial pleurocentrum (Fig. 9).

The odontoid process was unfused to the pleurocentrum in hatchlings and pierced by the notochordal canal (Fig. 7B–C). The fusion of the odontoid process had begun in early juvenile specimens, but a suture line was still clearly visible at this stage (Fig. 7F, K). In some juvenile individuals (LDKCL X 11 and NHMUK LS 1972.2050), the axial intercentrum fused before the odontoid process. Only subadults and adults showed a completely fused odontoid process.

The axial centrum was anteroposteriorly narrow in hatchlings (Fig. 7A). The notochordal canal was fully open at this stage, and the centrum was pierced by two dorsal foramina, and a single subcentral foramen (Fig. 7E). This subcentral foramen had started to close in juveniles to form the ventral groove of the axis, being fully closed in subadults. The lateral protuberances (incipient diapophysis) of the axis were only prominent in subadult and adult specimens, being highly incipient in juveniles.

Zygapophyses

Half of the specimens had the prezygapophyseal articulation flush with the anterior margin of the neural arch, whereas the other half had an anteriorly expanding prezygapophysis (anteriorly expanding in Fig. 9A, and flush in Fig. 9C). There seemed to be no correlation with ontogeny or sexual dimorphism for the different morphologies of these zygapophyses (see Supporting Information, Data S1). The axial postzygapophyses were already fully formed in hatchlings. The lateral torsion of these zygapophyses occurred in juveniles (Fig. 7H, M). At this stage, the postzygapophyses were relatively wider compared to the adult condition (Fig. 7I, N, S).

Neural arch and spine

The axial neural arch was paired in hatchlings, and the pedicels were poorly ossified, being similar in morphology to the atlantal pedicels at this stage (Fig. 7A–E). The fusion of these pedicels had

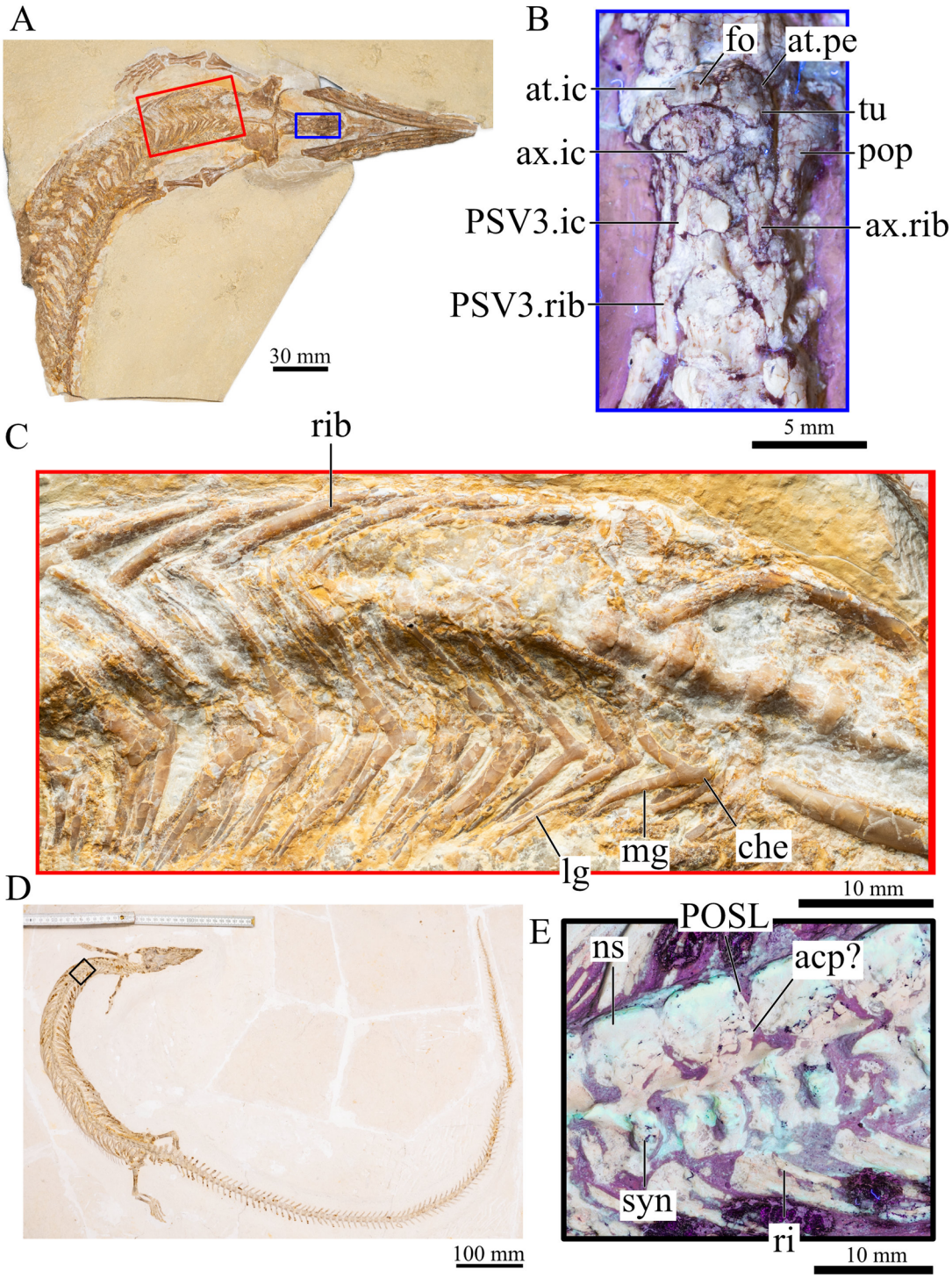

Figure 8. Presacral ribs and gastralia of *Pleurosaurus goldfussi* (SNSB-BSPG 1925 I 18) and *Pleurosaurus ginsburgi* (SNSB-BSPG 1977 X 40). A, photograph in standard light of the anterior part of the skeleton of SNSB-BSPG 1925 I 18, with highlighted areas of interest. B, photograph under UV-light of the cervical vertebrae of SNSB-BSPG 1925 I 18 in ventral view. C, photograph in standard light of the dorsal vertebrae and gastralia of SNSB-BSPG 1925 I 18 in ventral view. D, photograph in standard light of SNSB-BSPG 1977 X 40, with highlighted area of interest. E, photograph of the dorsal vertebrae of SNSB-BSPG 1977 X 40 in left lateral view. Abbreviations: acp?, possible accessory process of the neural spine; at, atlas; ax, axis; che, chevron; fo, foramen; ic, intercentrum; lg, lateral gastralium; mg, medial gastralium; ns, neural spine; pe, pedicel; pop, paroccipital process; POSL, postspinal lamina; PSV, presacral vertebra; ri, ridge; rib, rib; syn, synapophysis; tu, tubercle.

started in juveniles, firstly fusing to each other through the neural spine, and then to the axial centrum. The POSL formed by fusion of the neural arch pedicels sometime during the juvenile stage, but it was still incipient at this point. Only subadult and adults showed a well-developed POSL. In four specimens (i.e. subadults UMMZ Herp 406.51, and SAMA Herpetology 70524; and adults NHMUK LS 1935.5.14.3, and ZMB 14023), the accessory process of the neural spine was bifid (Fig. 9D).

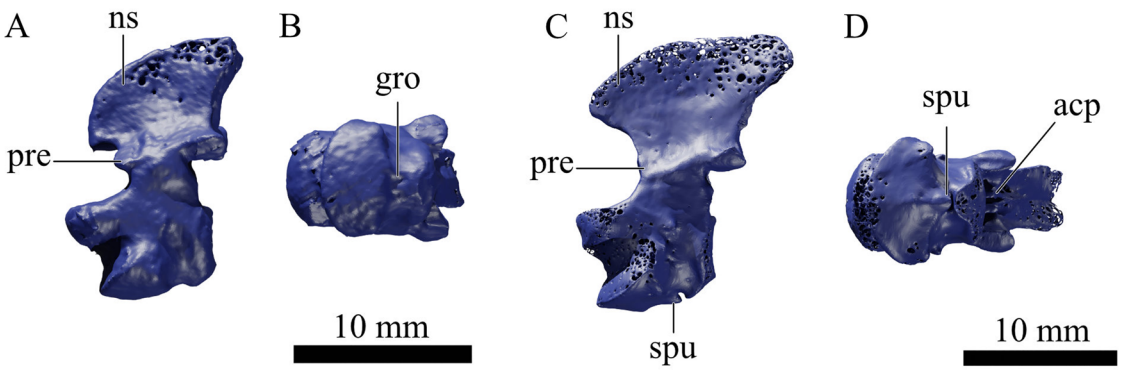

Figure 9. 3D representation of the axis of *Sphenodon*, highlighting interspecific variability. A–B, 3D renders of the axis of I-MEHJ S1. C–D, 3D renders of the axis of NHMUK LS 1935.5.14.3. A, C, in lateral view. B, D, in ventral view. Abbreviations: acp, accessory process; gro, groove; ns, neural spine; pre, prezygapophysis; spu, spur.

Remarks on fossil taxa

The axis morphology is variable among fossil rhynchocephalians. In early branching taxa (i.e. *Gephyrosaurus* and *Planocephalosaurus*), the axial intercentrum is not as wide and anteriorly pronounced as in *Sphenodon* (Evans 1981, Fraser and Walkden 1984). In *Clevosaurus hudsoni*, the odontoid fuses to the axial intercentrum, and those are not fused to the axial centrum even in a possibly adult specimen (NHMUK PV36832; O'Brien *et al.* 2018). This differs from *Gephyrosaurus*, *Opisthiamimus gregori* DeMar *et al.*, 2022, and *Sphenodon*, where the odontoid and axial intercentrum fuse independently to the axial centrum (Hoffstetter and Gasc 1969, Evans 1981, DeMar *et al.* 2022). The neural spine of *Planocephalosaurus* is triangular in lateral view (Fraser and Walkden 1984), rather than blade shape, and in *Opisthiamimus* DeMar *et al.*, 2022, the neural spine is shorter anteroposteriorly than in *Sphenodon* (DeMar *et al.* 2022). The POSL and accessory process of the neural spine are present at least in *Clevosaurus hudsoni* and *Opisthiamimus* (Fraser 1988, DeMar *et al.* 2022), and they seem to be present in *Pleurosaurus ginsburgi* SNSB-BSPG 1977 X 40 as well, but the preservation (axis taphonomically compressed in lateral view) of this specimen hampers the proper observation of these features (V.B., personal observations).

The fusion and ossification timings in fossil taxa may differ from that of *Sphenodon*. The axial intercentrum and neural arch can be unfused in some subadult and adult specimens, i.e. in specimens of *Kallimodon pulchellus* (unfused axial intercentrum in specimen SNSB-BSPG 1922 I 15, a possible subadult; V.B., personal observations), *Pleurosaurus ginsburgi* (unfused neural arch in SNSB-BSPG 1978 I 7, regarded as a subadult; Beccari *et al.* 2025b), *Pleurosaurus goldfussi* (Fig. 8A, B; unfused axial intercentrum in SNSB-BSPG 1925 I 18, regarded as an adult; Beccari *et al.* 2025b), and *Sphenofontis* (unfused axial intercentrum in specimen SNSB-BSPG 1993 XVIII 4, regarded as a subadult; Villa *et al.* 2021).

Presacral vertebrae 3 to 25

General adult morphology

Centrum

The presacral vertebrae centra were amphicoelous, longer than tall, and about as long as wide in the cervicals, anterior dorsals, and lumbars, and longer than wide in the posterior dorsals (Figs 10–12). The notochordal canal was closed but still marked as a deep depression at the anterior and posterior cotyles of the vertebrae (Fig. 10D–E, I–J, N–O). The ventral surface of the anteriormost presacral vertebrae (i.e. PSV3–6) showed a deep ventral median groove (present in at least some vertebrae of 14 specimens), similar to that of the axis (Fig. 10G, L). However, five specimens (one juvenile, three subadult, and one adult) showed a median ridge instead (Fig. 10Q), whereas three specimens (one juvenile, one subadults, and one adult) have a smoothed ventral surface. The median ridge can also be present in PSV7–11 (Fig. 11F), as was the case of six specimens (one subadult and five adults), but posterior dorsal vertebrae always showed a smooth ventral surface (Fig. 11K, P).

The first post-axial cervical (PSV3) showed posterolaterally oriented lateral protuberances (Fig. 10C–G), which were more developed than those of the axis. This lateral protuberance represented the diapophysis, but no ribs were associated with this vertebra. The parapophysis was absent in PSV3.

Presacral vertebrae 4 to 25 showed well-developed and oblique (posterodorsal to anteroventrally oriented) synapophyses (merged dia- and parapophyses). Especially in the cervical vertebrae PSV5–8 (Fig. 10M–Q) and the anterior dorsal vertebra PSV9 (Fig. 11B–F), the synapophyses were massive and expanded further laterally and ventrally than in any other presacral vertebra. In the cervical vertebrae, the ventral half of the diapophysis and the complete parapophysis laid on the centrum (Fig. 10H, M), whereas the dorsal half of the diapophysis was located on the neural arch. In the dorsals (Fig. 11B, G, L) and lumbars (Fig. 12A, F), the articulation was shifted more dorsally, with only the ventral portion of the parapophysis lying on the centrum. The articular facet for the ribs was always lateral, but slightly inclined ventrally in PSV4–9 (Fig. 10H, L, M, Q). A ridge was present posterior to the dorsal margin of the synapophysis, inclined posteroventrally (Fig. 10C, H, M). This ridge can be interpreted as the posterior centrosynapophyseal lamina (PCYL in Tschopp 2016). A deep and marked groove laid ventral to this lamina and posterior to the synapophysis. This post-synapophyseal groove was more pronounced in the cervical and anterior dorsal vertebrae but was still visible even in the posteriormost lumbar vertebrae (Fig. 12A, F).

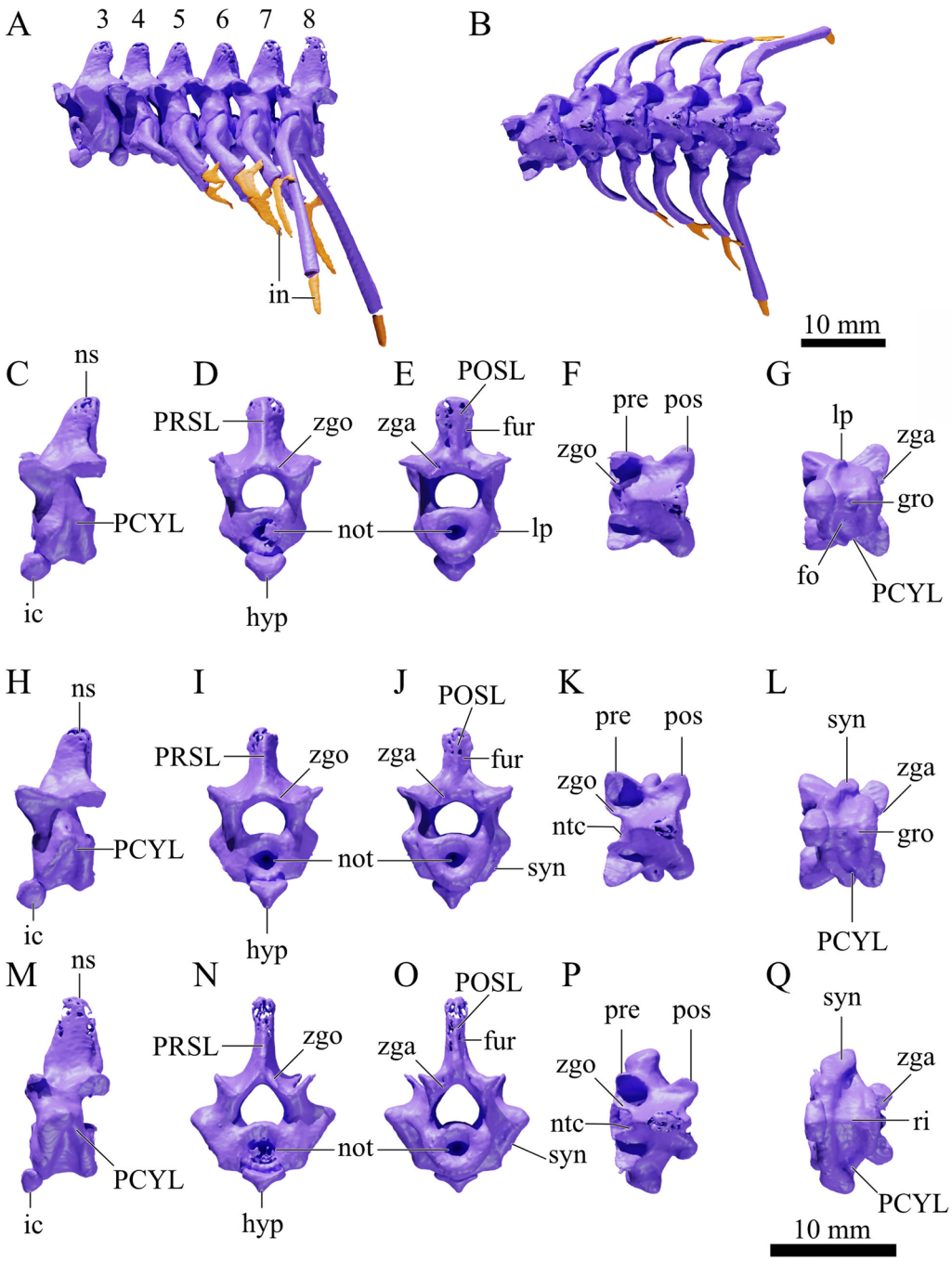

Figure 10. 3D representation of the post-axial cervical vertebrae of *Sphenodon* (I-MEHJ S1). A–B, 3D renders of the articulated post-axial cervical vertebrae in (A) lateral view; (B) dorsal view. C–G, 3D renders of cervical vertebra 3 (PSV 3). H–L, 3D renders of cervical vertebra 4 (PSV 4). M–Q, 3D renders of cervical vertebra 8 (PSV 8). C, H, M, left lateral view. D, I, N, anterior view. E, J, O, posterior view. F, K, P, dorsal view. G, L, Q, ventral view. Abbreviations: 3-8, cervical vertebrae 3-8; fo, foramen; fur, furrow; gro, groove; hyp, rudimentary hypapophysis; ic, intercentrum; in, intercostal cartilage; lp, lateral protuberance; not, notochordal canal; ns, neural spine; ntc, notch; PCYL, posterior centrosynapophyseal lamina; pos, postzygapophysis; POSL, postspinal lamina; pre, prezygapophysis; PRSL, prespinal lamina; ri, ridge; syn, synapophysis; zga, zygantrum; zgo, zygosphene.

Foramina

In some presacral vertebrae, but not all, subcentral foramina may be present, either on a single side or paired on both sides of the ventral surface of the centra (Fig. 10G). These foramina may be present throughout the presacral series (e.g. in adult UMZC R2608, present from the anteriormost scanned vertebrae, i.e. PSV12, to PSV21), or in different vertebra, with no apparent pattern (e.g. in adult ZMB 10607, which showed subcentral foramina in PSV8–10 and 18–20).

Intercentrum

Intercentra were present throughout the complete presacral series (Figs 10–12). These were usually wedge shaped, wider than long bones in front of the centra. The intercentra of the cervical

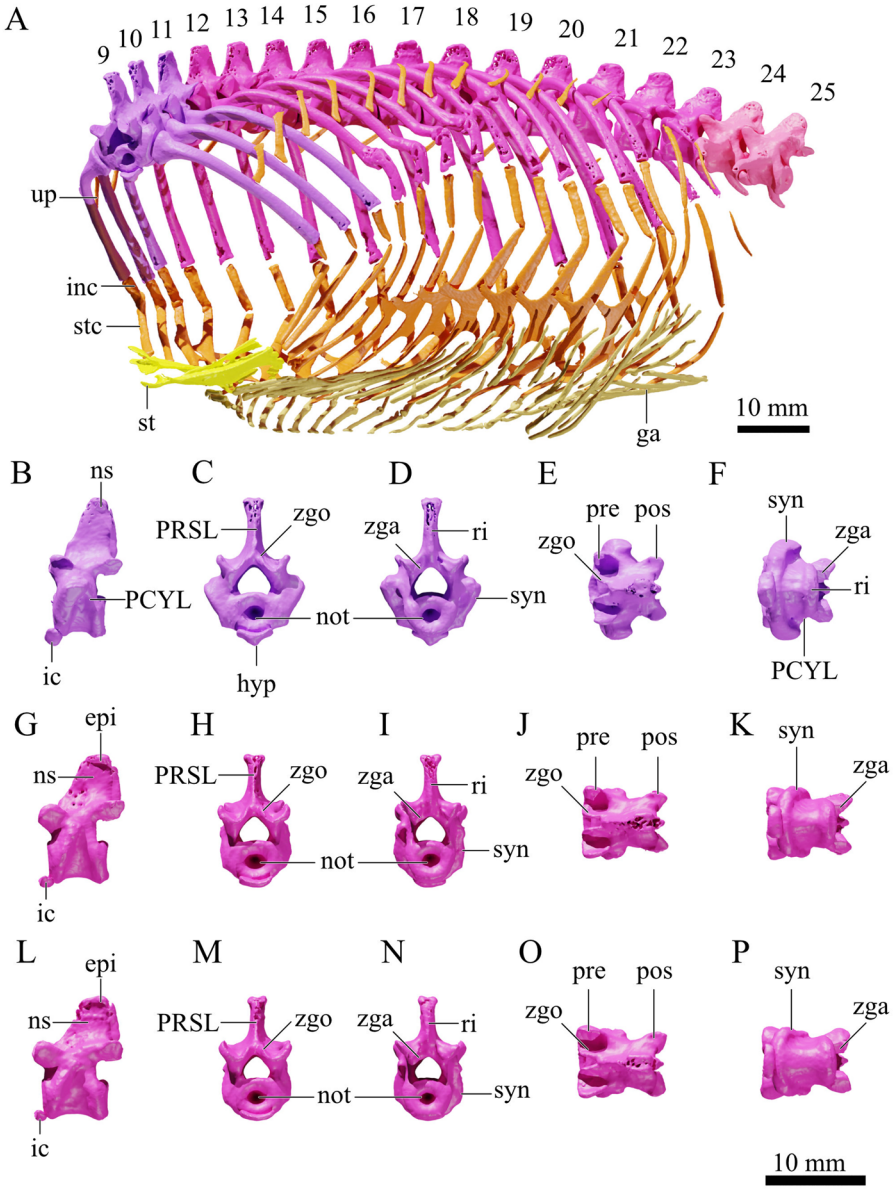

Figure 11. 3D representation of the anterior and posterior dorsal vertebrae, and lumbar vertebrae of *Sphenodon* (I-MEHJ S1). A, a 3D render of the articulated dorsal and lumbar vertebrae, sternum, and gastralia in lateral view. B–F, 3D renders of anterior dorsal vertebra 9. G–K, 3D renders of posterior dorsal vertebra 13. L–P, 3D renders of posterior dorsal vertebra 18. B, G, L, left lateral view. C, H, M, anterior view. D, I, N, posterior view. E, J, O, dorsal view. F, K, P, ventral view. Abbreviations: 9–25, dorsal vertebrae 9–25; epi, epiphysis; ga, gastralia; hyp, rudimentary hypapophysis; ic, intercentrum; inc, intercostal cartilage; not, notochordal canal; ns, neural spine; PCYL, posterior centrosynapophyseal lamina; pos, postzygapophysis; POSL, postspinal lamina; pre, prezygapophysis; PRSL, prespinal lamina; st, sternum; stc, sternocostal ribs; syn, synapophysis; up, uncinate process; zga, zygantrum; zgo, zygosphene.

vertebrae (Fig. 10C–Q) were more robust than those of the dorsal (Fig. 11B–P) and lumbar vertebrae (Fig. 12) and had an anteroposterior median keel (Fig. 10D, I, N). This keel was well-developed in the cervical vertebrae and the anteriormost anterior dorsal (PSV9) and has been interpreted as a rudimentary hypapophysis at least in fossil taxa (e.g. *Clevosaurus hudsoni*; O'Brien *et al.* 2018).

Neural arch and canal

The presacral vertebral neural arches were stout, being almost as long as tall. The neural canal was smaller in diameter than the centrum. The ventral margin of the neural canal was horizontal in anterior view. The medial surface of each lateral wall of the neural arch may be pierced by a nutrient foramen.

Zygapophyses

All post-axial presacral vertebrae had robust pre- and postzygapophyses. These extended away from the centrum and laterally, giving an 'X'-like shape to the vertebrae in dorsal view (Figs 10–12). The anterolateral and dorsoventral position of the prezygapophysis relative to the postzygapophysis changed throughout the presacral series. In dorsal view, the prezygapophyses of PSV3 were slightly narrower than the postzygapophyses (Fig. 10F). Throughout the presacral series, the prezygapophyses gradually

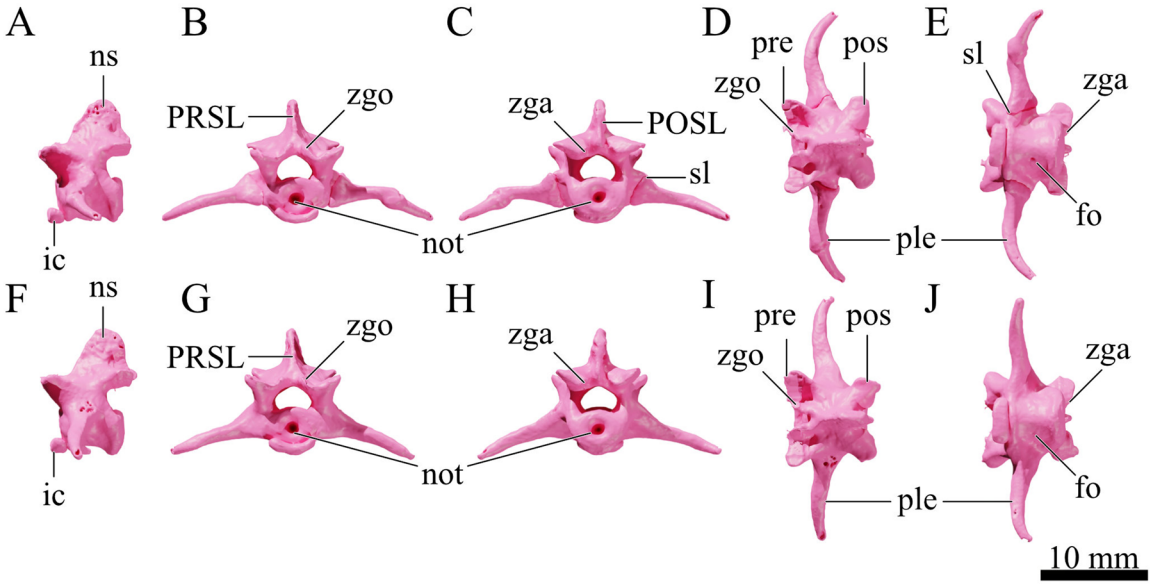

Figure 12. 3D representation of the lumbar vertebrae of *Sphenodon* (I-MEHJ S1). A–E, 3D renders of lumbar vertebra 1 (PSV 24). F–J, 3D renders of lumbar vertebra 2 (PSV 25). A, F, left lateral view. B, G, anterior view. C, H, posterior view. D, I, dorsal view. E, J, ventral view. Abbreviations: fo, subcentral foramen; ic, intercentrum; not, notochordal canal; ns, neural spine; ple, pleurapophysis; pos, postzygapophysis; POSL, postspinal lamina; pre, prezygapophysis; PRSL, prespinal lamina; sl, suture line; zga, zygantrum; zgo, zygosphene.

became wider than the postzygapophyses. This shift usually occurred by PSV7 or 8 (Fig. 10P). In lateral view, the cervical prezygapophyses expanded slightly more dorsally than the postzygapophyses (Fig. 10C, H, M), whereas the prezygapophyses of the posterior dorsal vertebrae laid slightly more ventral compared to the postzygapophyses (Fig. 11G, L). The prezygapophyses were tilted about 30 to 45° dorsally, with their articular facet facing dorsomedially. The postzygapophysis was slightly laterally twisted, articulating ventrolaterally with the prezygapophysis of the subsequent vertebra.

The medial margin of the prezygapophyses formed an incipient, dorsolaterally facing zygosphene (Figs 10D, I, N, 11C, H, M, 12B, G). The zygosphenal facets laid shallower than the articular facets of the prezygapophyses. A deep and wide notch was visible in dorsal view, between the zygosphenal facets (Fig. 10K, P). The neural spine started just posterior to this notch, generally being in contact with it. The zygantrum laid on the posterior margin of the neural arch, medial to the postzygapophyses. The zygantral facets were arranged in an oblique angle in posterior view. The zygosphene–zygantrum articular surfaces were straight and incipient, not forming a deep articular lock as in some lizards and snakes (Hoffstetter and Gasc 1969, Szyndlar and Georgalis 2023).

Neural spine

The neural spine morphology varied throughout the presacral series. The spines were usually tall midline crests that widened posteriorly. In most cases, the presacral neural spines fused with the paired vertebral epiphyses, having slight lateral protuberances at their apexes, which formed a longitudinal midline depression in the dorsal surface of the spine, in anterior and posterior views (Fig. 11C, H, M). The neural spines were mostly trapezoidal in lateral view (Figs 10–12), deflected slightly posterodorsally, and narrowing towards the dorsal end. In some individuals (i.e. SNSB-ZSM 1318/2006, UMZC R2608, and ZMB 14023), these spines were subrectangular but still slightly posterodorsally oriented. The anterior margin of the neural spine was always oblique in lateral view, and the posterior margin was subvertical, but slightly inclined anterodorsally in the same view (Figs 10M, 11B, G, L, 12A, F). The anterior margin of the presacral neural spine formed a sharp edge, the prespinal lamina (PRSL), and POSL were present throughout the presacral series. Only in the cervical vertebrae was the POSL flanked by a pair of vertical furrows, as in the axis (Fig. 10E, J, O). The accessory process of the neural spine, when present, was restricted to the cervical vertebrae.

Sexual dimorphism, ontogeny, and individual variation

The PCA including cervical, anterior dorsal, posterior dorsal, and lumbar vertebrae (Fig. 5) showed significant differences between male and female vertebrae (pairwise Adonis between male and females: d.f. = 1, F-value = 3.5, p = 0.015). All adult female specimens in our analyses showed slightly wider, longer, and lower vertebrae than adult male specimens (Fig. 13). However, for individual vertebrae (PSV4, 11, and 24) the significance between sexes varied. The cervical vertebra PSV4 (Fig. 13A) was not significantly different between males and females (d.f. = 1, F-value = 2.2, p = 0.057), whereas the anterior dorsal PSV11 (d.f. = 1, F-value = 3.4, p = 0.015) and lumbar vertebra PSV24 (d.f. = 1, F-value = 5.8, p = 0.024; Fig. 13F) were significantly different between sexes. Size played an important role in the morphology of the vertebrae. In PSV4 and 24, size significantly explained the morphology of the vertebrae (24.1%, p = 0.01, and 33.3%, p = 0.006, respectively), whereas sex did not significantly explain morphology in these vertebrae (24.8%, p = 0.16, and 24.1%, p = 0.11, respectively).

Ontogeny also influenced vertebral morphology (Fig. 14). The PCA comparing the cervical PSV4 in juvenile, subadult, and adult

specimens recovered 20 variation axes, the combination of PC1 and PC2 explaining 49.2% of the variation (Fig. 14A). The PCA of lumbar vertebra PSV24 between ontogenetic categories recovered 26 variation axes, the combination of PC 1 and PC2 explained 56% of the variation (Fig. 14G). *Sphenodon* showed negative allometry for the presacrals, as shown by the reversed relation between the centroid size (CS) and regression scores (Fig. 14B, H). This indicated that the shape of structures in the vertebrae (e.g. centrum, neural spine, or zygapophyses) changed relatively less as size increased. Although the neural spines of large adult specimens (e.g. male specimens) were proportionally taller than juveniles, the width and length of the vertebrae decreased considerably in regard to overall size. Therefore, juvenile specimens tended to have proportionally longer and wider centra, and lower neural spines than subadult and adult specimens (Fig. 14). This juvenile vertebral morphology was similar to that of subadult/adult female individuals. This similarly could also be observed by changing the groupings in the PCAs from ontogenetic stages to sexes for the older specimens (Fig. 15). In both PSV4 (Fig. 15A) and PSV24 (Fig. 15B), as well as the combination of all presacral vertebrae (Fig. 15C), the vertebrae of juvenile specimens were not significantly different from those of females ($p = 0.06$ in all analyses) but were significantly different from the much larger male vertebrae ($p = 0.001$). The subadult and adult vertebrae were not significantly different in these analyses, and PSV4 and 24 of these two ontogenetic stages occupied the same morphospace (Fig. 14).

Centrum

The ossification of the centrum followed the same pattern as in the axis, with the added development of the synapophysis (Fig. 16). The merging of the dia- and parapophysis began in the juvenile stage (Fig. 16F), being completely unfused in the earliest post-hatchling specimens (NHMUK LS 1855.10.163 and QMUL QMBC 0614) but fully developed in the anteriormost (cervical) vertebrae of LDKCL X 11 and NHMUK LS 1972.2050. Only in subadults were the synapophyses completely formed throughout the presacral series (Fig. 16P). The neurocentral suture split the diapophyses in the cervical vertebrae, and the parapophyses in the dorsal and lumbar vertebrae (Fig. 16F).

As mentioned above, the ventral surface of the centrum was highly variable, with some specimens having exclusively median ridges in the anterior presacral vertebrae (e.g. the juvenile NHMUK LS 1972.2050, the subadult SAMA Herpetology 70524, and the adult NHMUK LS 1935.5.14.3), and others having exclusively median grooves (e.g. the juvenile LDKCL X 11, the subadult MZH MS 1853, and the adult IDHRN NH 84.19), whereas the rest showed a combination of groove on the anteriormost presacral

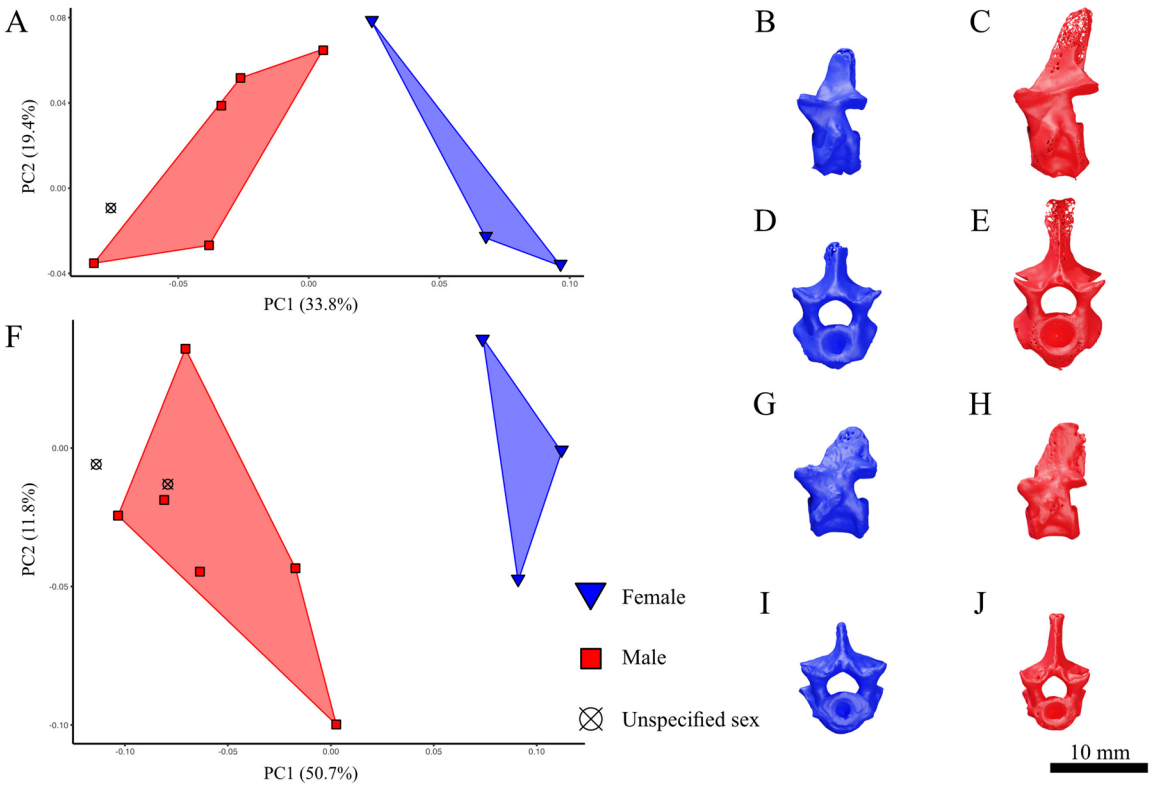

Figure 13. Combination of the main axes of the Principal Component Analysis (PCA) of the presacral vertebrae (PSV) of adult *Sphenodon*. A, combination of the two main axes of variation (PC1 and PC2) of PSV 4 of adult males and females. B–E, 3D renders of PSV 4 of the adult specimens I-MEHJ S1 (in blue) and NHMUK LS 1935.5.14.3 (in red) in (B–C) left lateral view; (D–E) anterior view. F, combination of the two main axes of variation (PC1 and PC2) of PSV 24 of adult males and females. G–J, 3D renders of PSV 24 of the adult specimens I-MEHJ S1 (in blue) and NHMUK LS 1935.5.14.3 (in red) in (G–H) left lateral view; (I–J) anterior view.

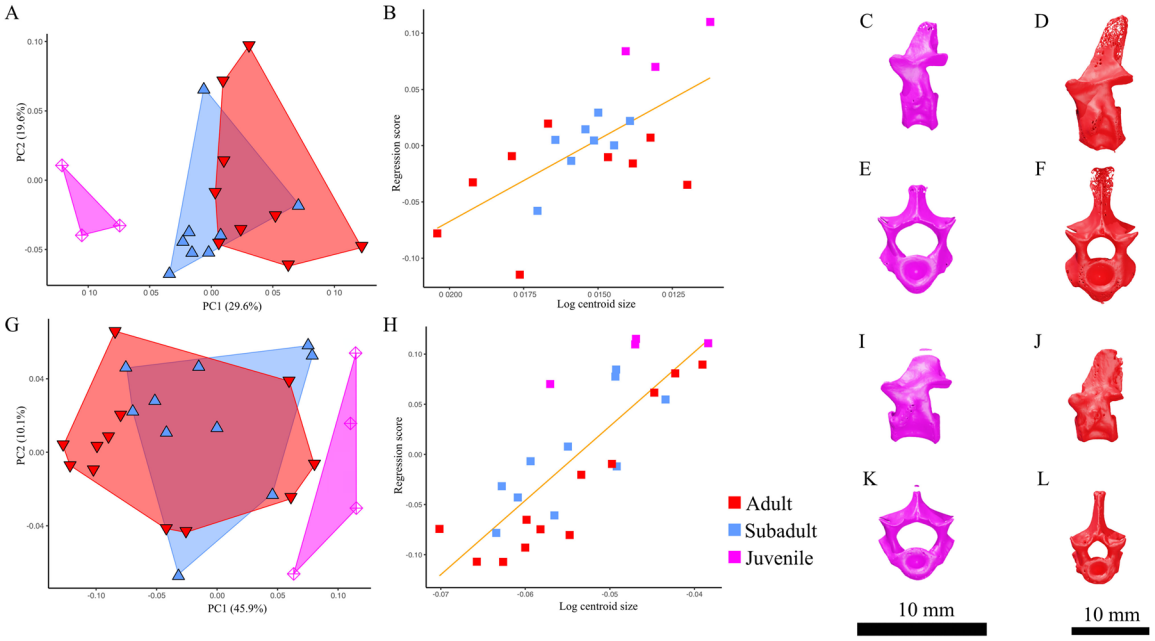

Figure 14. Combination of the main axes of the Principal Component Analysis (PCA) and allometry of the presacral vertebrae (PSV) of *Sphenodon* specimens of different ontogenetic stages. A, combination of the two main axes of variation (PC1 and PC2) of PSV 4 of juvenile, subadult, and adult specimens. B, regression curve of PSV 4. C–F, 3D renders of PSV 4 of the juvenile specimen NHMUK LS 1972.2050 (in pink) and the adult specimen NHMUK LS 1935.5.14.3 (in red) in (C–D) left lateral view; (E–F) anterior view. G, combination of the two main axes of variation (PC1 and PC2) of PSV 24 of juvenile, subadult, and adult specimens. H, regression curve of PSV 24. I–L, 3D renders of PSV 24 of the juvenile specimen NHMUK LS 1972.2050 (in pink) and the adult specimen NHMUK LS 1935.5.14.3 (in red) in (I–J) left lateral view; (K–L) anterior view.

vertebrae (PSV3–6), ridge on the mid presacral vertebrae (PSV7–13), and smooth posterior presacrals (e.g. the juvenile NHMUK LS 1855.10.163, and the adult ZMB 14023). This variability does not seem to be correlated to ontogeny or sex.

Foramina

The hatchling specimens and some juvenile specimens showed paired dorsal, lateral, and subcentral foramina in the centrum (Fig. 16 A, E), but except for the latter, these were always absent in subadult and adult specimens.

The presence of subcentral foramina was highly variable in the presacral series, even in adults. This varied between specimens, but also throughout the presacral series, e.g. NHMUK LS 1935.5.14.3, with some vertebrae showing paired foramina (PSV3, 7, 8, and 10 in this specimen), some a single foramen (PSV5 and 11 on the left side, and PSV6 on the right), and some lacking subcentral foramina completely (PSV4, 9, and 12).

Intercentrum

Most of the presacral intercentra were already present in juveniles, but they can be paired in the posterior dorsals in these specimens. Only in subadults and adults were all the intercentra completely formed. All specimens in this study showed the rudimentary hypapophysis in the cervical vertebrae, and simple wedge-shaped dorsal and lumbar intercentra. In some specimens (i.e. LDKCL X 11 and UMMZ.Herp 406.51), the eighth presacral lacked the rudimentary hypapophysis, and a single specimen (ZMB 14023) had a hypapophysis in PSV9.

Neural arch and canal

As in the axis, the neural arch was paired, and pedicels were poorly ossified in hatchlings (Fig. 16A–E). The fusion of pedicels started in the anterior vertebrae of the earliest juveniles. The pedicels fused firstly to each other, and then to the centrum, with the neural spines ossifying later. The neural arch was completely formed already in the juvenile stage. The neural canal was relatively much wider in hatchlings and juveniles than in adult specimens (Fig. 16B, G, L, Q). In the early ontogenetic stages, the neural canal was almost as wide as the centrum (excluding the parapophysis).

Zygapophyses

The development of the zygapophyses in the presacral vertebrae was similar to that of the axis. Lateral torsion of the postzygapophyses occurred in juveniles (Fig. 16F, H, K, M). The zygosphene-zygantrum articulation appeared in subadult and adult specimens (Fig. 16Q–R) but was absent or highly incipient in juveniles (Fig. 16G–H, L–M).

Neural spine

Similar to the neural arch, the neural spine started forming in the earliest juveniles (Fig. 16G–H). However, in all juveniles the neural spines were significantly lower than those of adults and

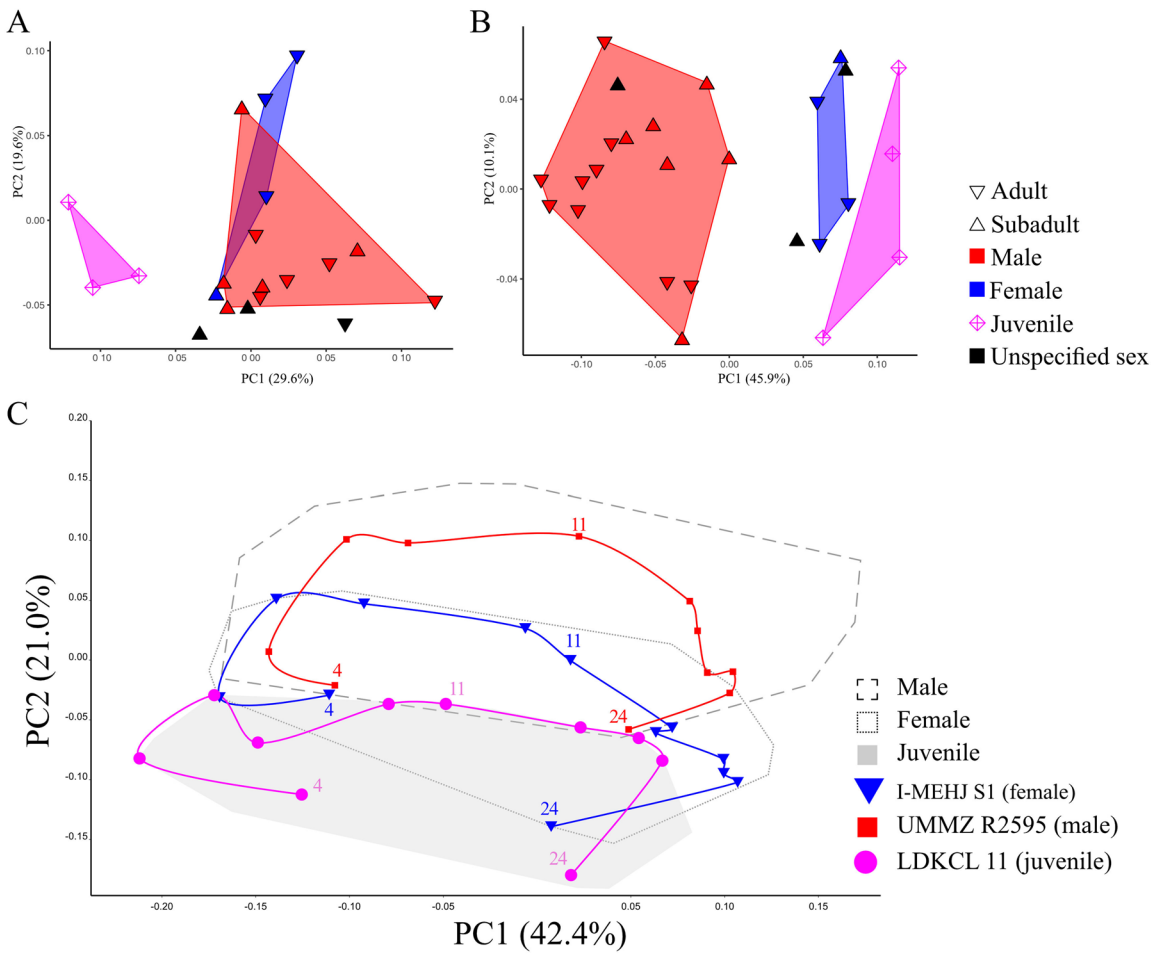

Figure 15. Combination of the main axes of the Principal Component Analysis (PCA) and allometry of the presacral vertebrae (PSV) of *Sphenodon* specimens of different ontogenetic stages. A, combination of the two main axes of variation (PC1 and PC2) of PSV 4 of juvenile specimens (not sexed), and sexed female and male subadult, and adult specimens. B, combination of the two main axes of variation (PC1 and PC2) of PSV 24 of juvenile specimens (not sexed), and sexed female and male subadult, and adult specimens. C, combination of the main axes of variation (PC1 and PC2) of presacral vertebrae of juvenile, adult male, and adult female specimens, highlighting the sequence of vertebrae in three specimens, LDKCL X 11 (juvenile, in pink), I-MEHJ S1 (female, in blue), and UMMZ R2595 (male, in red).

subadults (Fig. 16V–X), even though the spines were already completely developed in some juveniles (Fig. 16K–M).

Remarks on fossil taxa

The presacral centrum in most fossil rhynchocephalians was relatively similar to that of *Sphenodon*, i.e. it was amphicoelous and usually hourglass shaped, with laterally constricted margins. Some presacral vertebrae of *Gephyrosaurus* showed subcentral foramina (Evans 1981). Foramina seem to be absent in other fossil rhynchocephalians, e.g. *Homoeosaurus*, *Kallimodon*, *Pleurosaurus* von Meyer, 1831, and *Sphenofontis* (V.B., personal observations). Most taxa showed oblique synapophyses, similar to those of *Sphenodon*. However, pleurosaurids (i.e. *Palaeopleurosaurus* and *Pleurosaurus*) showed vertical synapophyses in the presacral vertebrae (Fig. 8E). These were elliptical and not as massive as in other rhynchocephalians. The articular facet for the ribs was usually on the lateral surface of the vertebrae in fossil rhynchocephalians, but in *Kallimodon*, the synapophysis was slightly bent posteriorly, and the ribs articulated posterolaterally in specimens assigned to this taxon (Fig. 17). An anteroventrally-oriented synapophyseal ridge (Fig. 17B) was present at the ventral margin of the parapophysis in *Kallimodon*, *Sapheosaurus*, and *Vadasaurus* Bever & Norell, 2017, but not in *Clevosaurus hudsoni*, *Gephyrosaurus*, *Homoeosaurus maximiliani*, *Planocephalosaurus*, *Pleurosaurus*, or *Sphenofontis* (V.B., personal observations). The PCYL was sharply marked in *Kallimodon pulchellus* (SNSB-BSPG 1887 VI 1 and SNSB-BSPG 1922 I 15), but it seemed absent in *Pleurosaurus ginsburgi* (SNSB-BSPG 1977 X 40).

The intercentra of fossil rhynchocephalians were usually wedge shaped, and in many taxa, e.g. *Clevosaurus hudsoni*, *Gephyrosaurus*, and *Kallimodon*, the anteriormost (cervical) intercentra showed a rudimentary hypapophysis (Cocude-Michel 1963, Evans 1981, O'Brien *et al.* 2018). Intercentra were present only in the cervical vertebrae of *Homoeosaurus maximiliani*, *Kallimodon pulchellus*, and *Sphenodraco scandentis* Beccari *et al.*, 2025a but were present throughout the presacral series in *Palaeopleurosaurus*, *Pleurosaurus*, and *Sphenofontis* (Cocude-Michel 1963, Fabre 1981, Carroll 1985, Villa *et al.* 2021, Beccari *et al.* 2025a).

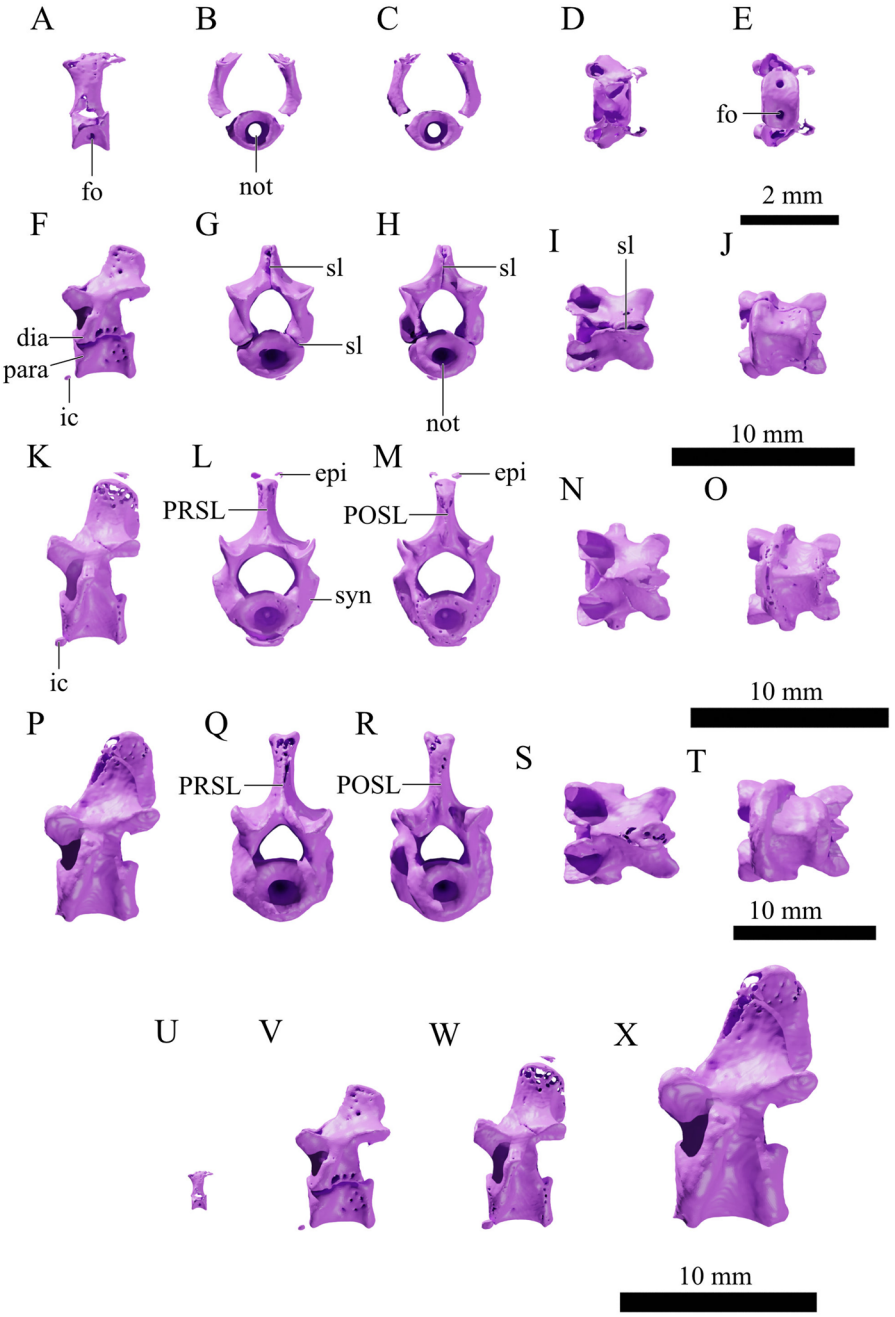

Figure 16. 3D representation of the anterior dorsal vertebra PSV 11 of *Sphenodon* specimens of different ontogenetic stages. A–E, 3D renders of PSV 11 of the hatchling SNSB-ZSM 20/1959. F–J, 3D renders of PSV 11 of the juvenile QMUL QMBC 0614. K–O, 3D renders of PSV 11 of the juvenile NHMUK LS 1972.2050. P–T, 3D renders of PSV 11 of the adult I-MEHJ S1. A, F, K, P, left lateral view. B, G, L, Q, anterior view. C, H, M, R, posterior view. D, I, N, S, dorsal view. E, J, O, T, ventral view. U–X, size comparison between the atlas–axis complex of (U) SNSB-ZSM 20/1959; (V) QMUL QMBC 0614; (W) NHMUK LS 1972.2050; and (X) I-MEHJ S1. Abbreviations: dia, diapophysis; epi, epiphysis; fo, foramen; ic, intercentrum; not, notochordal canal; para, parapophysis; POSL, postspinal lamina; PRSL, prespinal lamina; sl, suture line; syn, synapophysis.

In some fossil rhynchocephalians, the prezygapophysis was located more ventral in the cervical vertebrae than the postzygapophysis (e.g. *Clevosaurus cambrica* Keeble *et al.*, 2018, *Clevosaurus hudsoni*, *Gephyrosaurus*, and *Planocephalosaurus*; Evans 1981, Fraser and Walkden 1984, Fraser 1988, Keeble *et al.* 2018, O'Brien *et al.* 2018). The zygosphene-zygantrum complex was present in the early branching rhynchocephalian *Gephyrosaurus* (Evans 1981), but it seems to be lost in many rhynchocephalians, including another early branching genus, *Planocephalosaurus* (Fraser and Walkden 1984).

In *Gephyrosaurus* and *Planocephalosaurus*, as well as in clevosaurids (e.g. *Clevosaurus cambrica* and *Clevosaurus hudsoni*), the neural spines were low and trapezoidal in lateral view (Evans 1981, Fraser and Walkden 1984, O'Brien *et al.* 2018). In Solnhofen

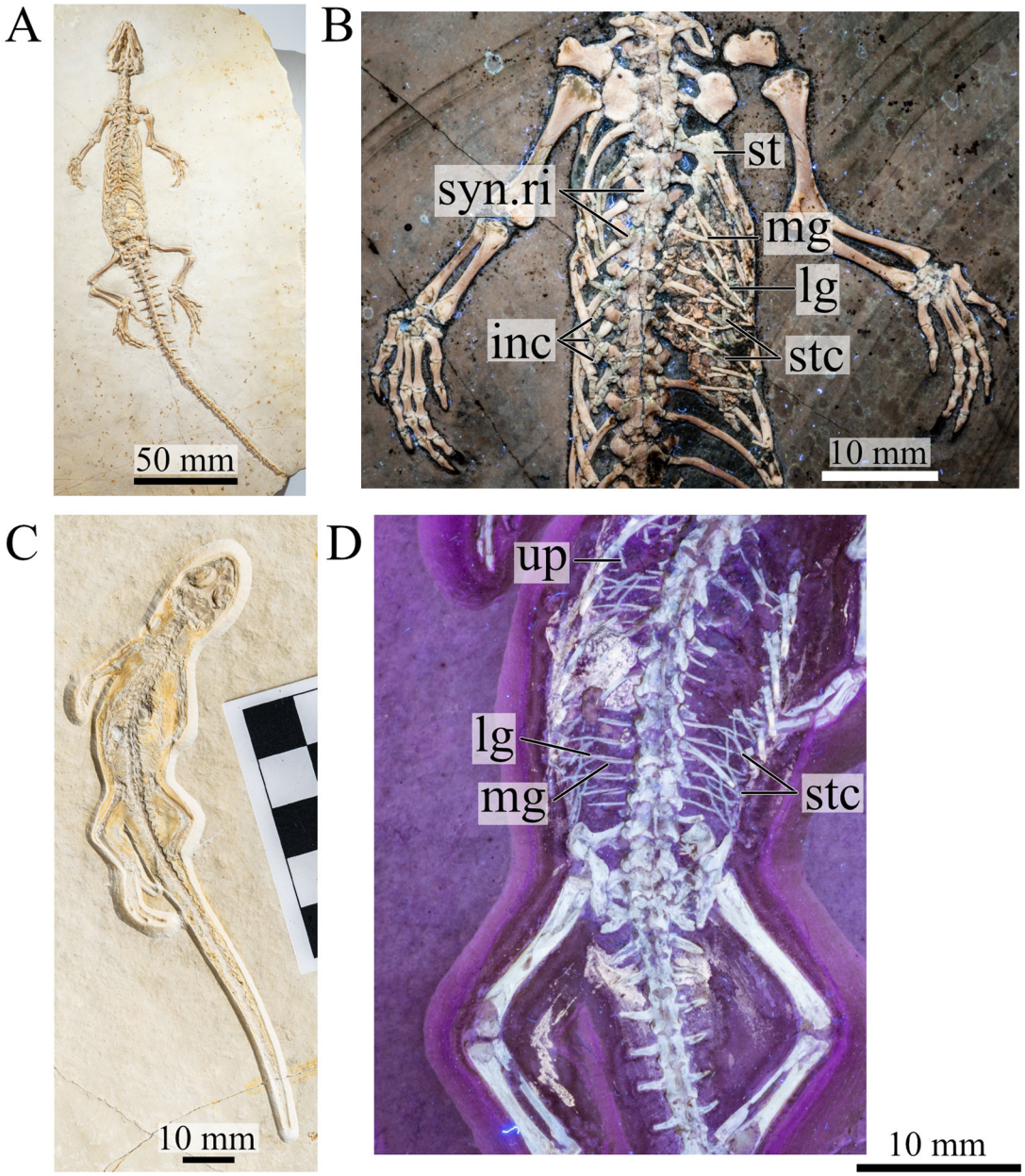

Figure 17. Presacral vertebrae, ribs, and gastralia of *Kallimodon pulchellus* (SNSB-BSPG 1887 VI 1) and *Homoeosaurus parvipes* (MB.R.1007). A, photograph in standard light of the SNSB-BSPG 1887 VI 1, with highlighted area of interest. B, photograph under UV-light of the dorsal vertebrae, ribs, and gastralia of SNSB-BSPG 1887 VI 1, in ventral view. C, photograph in standard light of the MB.R.1007, with highlighted area of interest. D, photograph under UV-light of the dorsal vertebrae, ribs, and gastralia of MB.R.1007, in dorsal view. Abbreviations: inc, intercostal rib; lg, lateral gastralium; mg, medial gastralium; st, sternum; stc, sternocostal rib; syn.ri, anteroventral synapophyseal ridge; up, uncinate process.

Archipelago rhynchocephalians, the spine was usually squared, i.e. about as long as tall, in lateral view, especially in *Pleurosaurus ginsburgi* (Fig. 8E), whereas in *Navajosphenodon sani* Simões *et al.*, 2022, *Opisthiamimus*, and *Priosphenodon avelasi* Apesteguía & Novas, 2003, the neural spines were subrectangular in lateral view, similar to that of *Sphenodon* (Apesteguía 2008, DeMar *et al.* 2022, Simões *et al.* 2022). The POSL and a putative accessory process were present throughout the presacral series of *Pleurosaurus ginsburgi* SNSB-BSPG 1977 X 40 (Fig. 8E).

As was the case for the axis, the ossification timing may also vary in some fossil taxa, especially the fusion of the neural arch to the pleurocentrum. In *Pleurosaurus* and possibly *Kallimodon*, subadult specimens still showed a marked neurocentral suture in the presacral vertebrae (Beccari *et al.* 2025b). The neural spines in subadult specimens were already ossified, as observed in *Sphenodon*, which means that the fusion of the neural arch to the pleurocentrum was much delayed in these extinct taxa.

Presacral ribs

General adult morphology

Paired ribs were present on presacral vertebrae 4 to 25 (Figs 10–11, 18), albeit being always fused to the centrum and therefore

being regarded as pleurapophyses (*sensu* Hoffstetter and Gasc 1969) in PSV25 (Fig. 12F–J).

The presacral ribs were sub-bicipital (*sensu* Hoffstetter and Gasc 1969), meaning that they have merged the tuberculum and capitulum but with some distinction between both (Fig. 18I). In six adult specimens (IDHRN NH 84.19, NHMUK LS 1935.5.14.3, UMZC R2595, UMZC R2605, ZMB 10607, and ZMB 13837), the first two pair of ribs were truly bicipital, i.e. the capitulum and tuberculum were unmerged and fully separated as distinct articular processes. The tuberculum was wider than the capitulum throughout the presacral series. The anterior margin of the tuberculum was marked by a longitudinal ridge (Fig. 18), which was pronounced in the anteriormost (cervical and anterior dorsal vertebrae), and less pronounced in the posterior dorsals and lumbars (Fig. 18I–J). The ribs contacted the synapophyses perpendicular to the centrum.

The ribs associated with PSV4 to 7 were short and posteroventrally oriented (Fig. 18A, D, H–K). These cervical ribs were anteroposteriorly flattened throughout their length, with the anterior surface marked by a deep longitudinal ridge between the enlarged tuberculum and the capitulum (Fig. 18I–K). In proximal view, the head of the cervical ribs was slightly elongated, with an anteroposterior constricted margin between the tuberculum and capitulum. These ribs were associated with short cartilaginous intercostal ribs. The pair of ribs of PSV8 shows an intermediate morphology between the cervical and dorsal ribs, with a flatter profile than the dorsals, but being almost as long as the rib of PSV9 (Fig. 18B, E, H–K). Ribs associated with PSV9 to 21 (Fig. 18C, F, H–K) were elongated, slender, and tubular. These ribs were twisted anteriorly at their distal half, with their dorsal margin taking a more anterior position (Fig. 18C). The rib head was bean shaped in the anterior dorsal ribs, and elliptical in the posterior

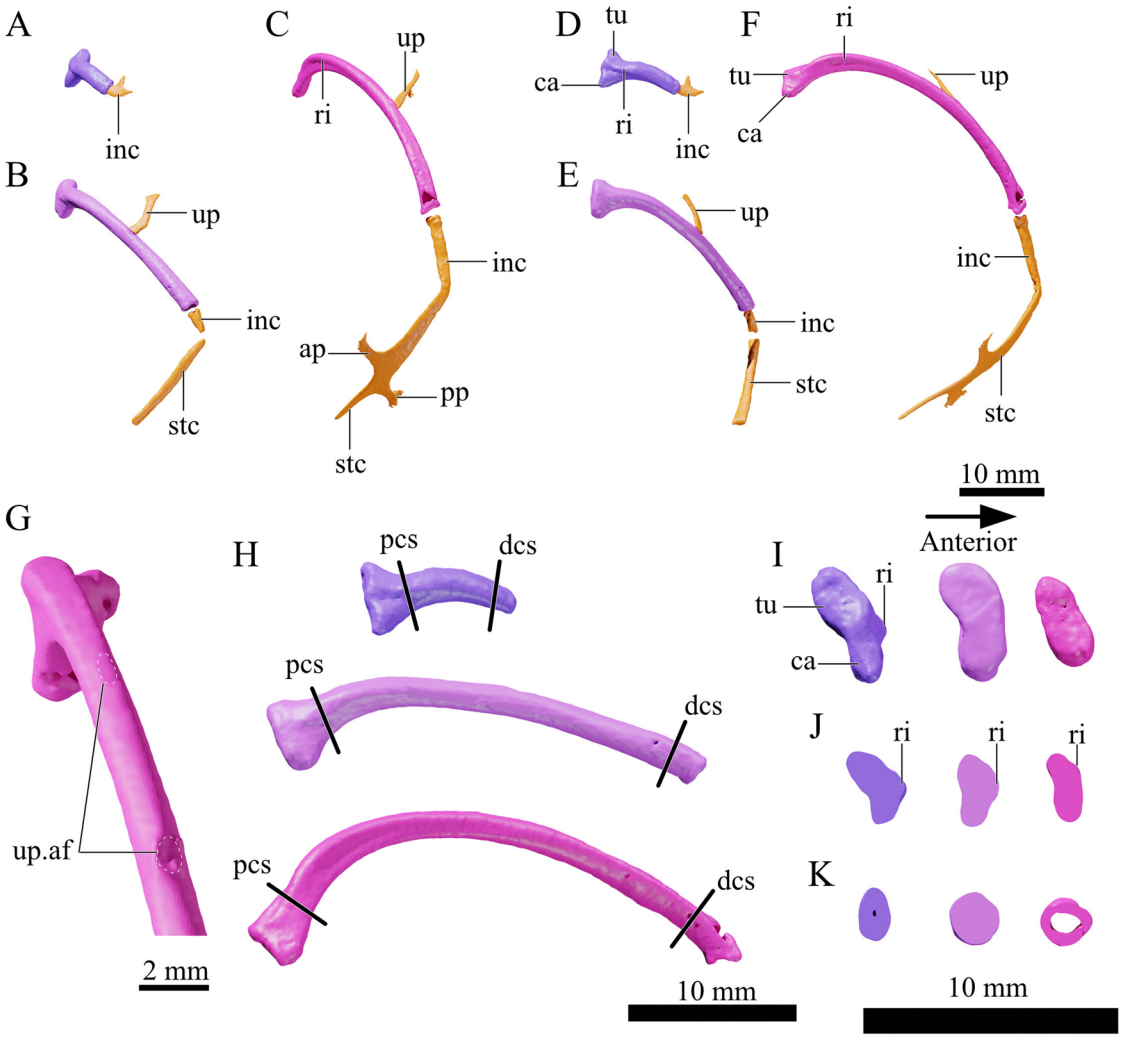

Figure 18. 3D representation of the presacral ribs of *Sphenodon* (I-MEHJ S1). A–F, 3D renders of articulated ribs and associated cartilaginous elements of (A, D) left cervical rib 4 (PSV 4); (B, E) left anterior dorsal rib 9 (PSV 9); (C, F) left posterior dorsal rib 18 (PSV 18) in (A–C) lateral view; (D–F) anterior view. G, 3D renders of posterior dorsal rib 16 (PSV 16) in posterolateral view. H, 3D renders of ribs 4, 9, and 18 in anterior view showing the location and orientation of cross-section cuts. I, proximal end of ribs 4, 9, and 18 in medial view. J, proximal cross-section of ribs 4, 9, and 18. K, distal cross-section of ribs 4, 9, and 18. Abbreviations: ap, anterior process; ca, capitulum; dcs, distal cross-section cut; inc, intercostal rib; pcs, proximal cross-section cut; pp, posterior process; ri, ridge; stc, sternocostal rib; tu, tuberculum; up, uncinate process; up.af, articular facets for the uncinate processes.

dorsal ribs (Fig. 18J–K). The proximal half of both anterior and posterior dorsal ribs was anteroposteriorly flattened, having an upside-down, shape in cross-section in the anterior dorsals, and a more elliptical cross-section in the posterior dorsals (Fig. 18J). Their distal ends were subcircular in cross-section. These ribs were associated with posterodorsally oriented, cartilaginous uncinate processes, and cartilaginous intercostal and sternocostal ribs. The posteriormost pairs of ribs (PSV22–25) were short and subcircular in cross-section (Fig. 12A, F). The pair of ribs of PSV22 and PSV23 were associated with intercostal ribs, but only the former was associated with sternocostal ribs. The ribs of PSV24 and 25 were free ribs, with no cartilaginous elements associated with them.

Ontogenetic and individual variation

In hatchlings, only the shaft of the ribs was ossified, with open ends and a cartilaginous, incipient tuberculum and capitulum. With growth, ossification continued towards the distal and proximal ends. In the juvenile stage, the ends of the ribs were already ossified, and the ribs were similar in morphology to those of subadults and adults.

The last pair of presacral ribs (associated to PSV25) was only fully ankylosed in adult specimens, and two subadults (SNSB-ZSM 1318-2006 and UMZC R2598). The penultimate pair of ribs (associated to PSV24) was ankylosed in some specimens (fully ankylosed in ZMB 9804 and UMZC R2604, and partially in I-MEHJ S1 and UMZC R2605).

Remarks on fossil taxa

The position of the first rib varied among fossil rhynchocephalians, with some taxa, e.g. *Homoeosaurus* and *Kallimodon* showing the first rib on PSV6 or 7. The axis lacked associated ribs in most rhynchocephalians. However, *Pleurosaurus ginsburgi* (SNSB-BSPG 1977 X 40) and *Pleurosaurus goldfussi* (SNSB-BSPG 1925 I 18) bore a pair of short axial ribs (Fig. 8B). A putative axial rib was also figured for one specimen of *Clevosaurus hudsoni*, NHMUK PV36832 (O'Brien *et al.* 2018: fig. 14). In these taxa, the axial ribs were much shorter than the post-axial ribs. In *Pleurosaurus goldfussi* (SNSB-BSPG 1925 I 18), the axial rib was bicipital (Fig. 8B).

The first rib pair in some fossil taxa, i.e. *Derasmosaurus pietraroiae* Barbera & Macuglia, 1988, *Gephyrosaurus*, *Kallimodon pulchellus*, *Pleurosaurus goldfussi*, and *Vadasaurus*, was bicipital (Evans 1981, Barbera and Macuglia 1988, Bever and Norell 2017; V.B., personal observations). At least in *Gephyrosaurus* and *Kallimodon pulchellus*, the capitulum was longer and extended further anteriorly than the tuberculum, compared to *Sphenodon* specimens that showed bicipital anteriormost ribs (Romer 1956, Hoffstetter and Gasc 1969, Evans 1981). The presacral ribs of *Gephyrosaurus*, *Homoeosaurus*, and *Kallimodon* lacked the anterior longitudinal ridge (Cocude-Michel 1963, Evans 1981), whereas this ridge was marked in the presacral ribs of *Pleurosaurus ginsburgi* (Fig. 8E). Even in adult specimens, the last pair of presacral ribs was unfused with the centrum in *Pleurosaurus*, but it was fused with the centrum in *Homoeosaurus maximiliani*, *Kallimodon*, and *Sapheosaurus* (Cocude-Michel 1963).

Compared to *Sphenodon*, the presacral ribs of *Palaeopleurosaurus* showed a slight increase in density [osteosclerosis *sensu* Houssaye 2009 (Klein and Scheyer 2017)], whereas those of *Ankylosphenodon pachyostosus* Reynoso, 2000 showed a substantial increase in both density and diameter [pachyostosis *sensu* Houssaye 2009 (Reynoso 2000)]. *Pleurosaurus* showed an intermediate rib robustness compared to *Ankylosphenodon* and *Palaeopleurosaurus*, and is, therefore, at least partially pachyostotic (Carroll and Wild 1994, Beccari *et al.* 2025b).

Cartilaginous ribs and gastralia

General adult morphology

Cartilaginous uncinate processes were present on ribs associated with PSV9 to 21. The processes were flattened cartilaginous strips that connected the ribs of subsequent vertebrae. At their base, they were slightly expanded to articulate with the rib. The articular facets for the uncinate processes on the rib laid on the posterolateral surface of the rib, the one articulating with the proximal end of the uncinate process forming a raised, oval lip, positioned at about the midlength of the rib, and the second, which marked the contact of the uncinate process of the anterior rib, being shallow and positioned at about the proximal third of the rib length (Fig. 18G).

The cervical intercostal ribs were short, mediolaterally flattened, and tapered distally to a point (Figs 10A, 18A, D). The dorsal vertebrae intercostal ribs were tubular (Fig. 18B, E) and grew in length posteriorly in the presacral series, until reaching the maximum length by PSV23 (Fig. 11A). The anterior sternocostal ribs (those associated with PSV9–11) were tubular and concur in bridging their corresponding vertebrae to the sternum, i.e., being the ribs associated with the sternum (Fig. 18B, E). The posterior sternocostal ribs (associated with PSV12–23) were aliform (*sensu* Hoffstetter and Gasc 1969), having an anterior process (or expansion in Klein and Scheyer 2017) at the proximal third of the length, and a posterior process at the distal third (Fig. 18C, F). This generated an asymmetrical X shape. These sternocostal ribs were always associated with the gastralia through connective tissue (Hoffstetter and Gasc 1969).

A total of 24 gastralia was present, located in the body portion going from the level of PSV12 to 23. Each PSV was associated with two gastralia. The gastralia were formed by a median gastralium and two unfused paired lateral gastralia (Fig. 19). The median gastralium was V-shaped, forming a chevron (*sensu* O'Brien *et al.* 2018), with a pointed and anteriorly directed median projection. The angle between the arms of the medial gastralium ranged from 90° to 120°. This angle was the lowest at the anterior- and posteriormost gastralia. The lateral elements were rod like and slightly bowed posteriorly at their distal ends. The contact between each lateral gastralia and each posterolateral arm of the medial gastralium covered about two-thirds of their length, extending from around the distal third of the former to the proximal third of the latter (Fig. 19).

Ontogenetic and individual variation

All cartilaginous elements (uncinate processes, and intercostal and sternocostal ribs) were present already in the smallest juvenile specimen (NHMUK LS 1855.10.163). The uncinate processes were

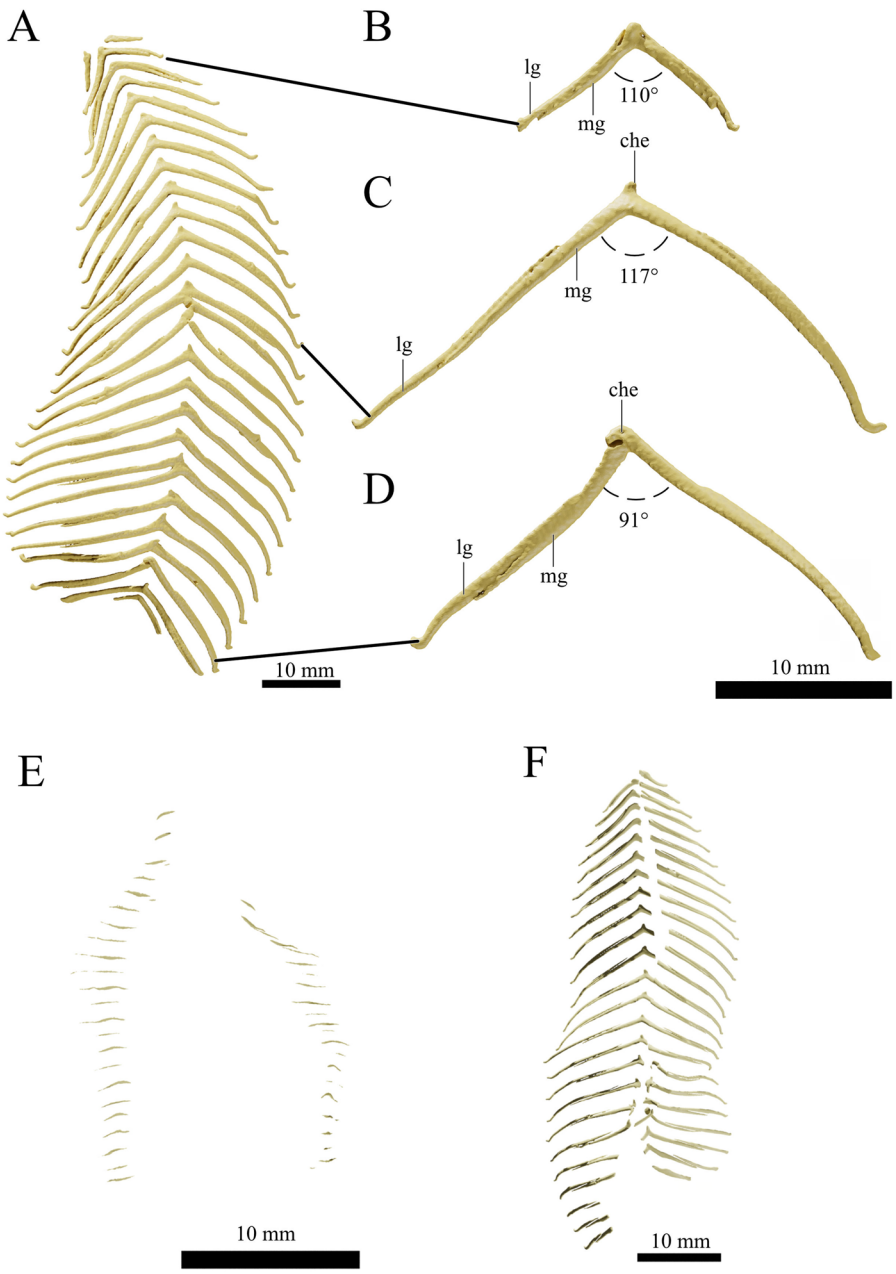

Figure 19. 3D representation of the gastralia of *Sphenodon*. A–D, UMZC R2605, adult. E, NHMUK LS 19.5.14.6.10.b, hatchling. F, NHMUK LS 1972.2050, juvenile. A, E, F, 3D renders of the articulated gastralia in ventral view. B–D, 3D renders of the isolated gastralium (B) anterior gastralium; (C) mid gastralium; (D) posterior gastralium. Abbreviations: che, chevron; lg, lateral gastralium; mg, medial gastralium. The angles of divergence between the gastralium rami are noted.

rod like at this stage and developed a strip morphology in subadults. Similarly, the sternocostal ribs were more slender and relatively longer in juveniles than in subadult and adult specimens.

The medial gastralium was absent in hatchlings, whereas the lateral gastralium was present, but was incipient, already at this stage (Fig. 19E). In juveniles the medial gastralium had started to ossify, but the anterior median projection was short and poorly differentiated at this stage (Fig. 19F). The projection was pronounced in subadult and adults.

In one adult (i.e. UMZC R2605, Fig. 19A), the number of gastralia associated with each vertebra was higher than two. This condition seems to be pathological, as the medial gastralia display bifid arms in these specimens, forming additional lateral extensions.

Remarks on fossil taxa

Cartilaginous elements, such as the uncinate processes and intercostal and sternocostal ribs, were better preserved in specimens from Fossil-Lagerstätten, and sometimes only visible under UV-light (Tischlinger and Arratia 2013). Some rhynchocephalians from the Solnhofen Archipelago, i.e. *Homoeosaurus*, *Kallimodon*,

Sphenodraco Beccari *et al.*, 2025a and *Sphenofontis*, preserve cartilaginous elements (Cocude-Michel 1963, Fabre 1981, Villa *et al.* 2021, Beccari *et al.* 2025a). *Homoeosaurus maximiliani*, *Homoeosaurus parvipes*, *Kallimodon pulchellus*, and *Sphenofontis* have uncinate processes, similar in morphology to those of *Sphenodon*. These specimens also showed both intercostal and sternocostal ribs. *Pleurosaurus goldfussi* (SNSB-BSPG 1925 I 18) only preserves some intercostal ribs. The intercostal ribs of *Pleurosaurus goldfussi* and *Kallimodon pulchellus* were tubular and segmented (Figs 8C and 17B, respectively). The sternocostal ribs were poorly preserved in most specimens. In the holotypes of *Kallimodon pulchellus* (SNSB-BSPG 1887 VI 1) and *Homoeosaurus parvipes* (MB.R.1007), they showed an asymmetrical X shape, similar to that of *Sphenodon*, but were substantially slenderer and more elongated (Fig. 17). This could be an ontogeny related feature, given that juvenile *Sphenodon* specimens showed elongated sternocostal ribs. However, at least the holotype of *Kallimodon pulchellus* (SNSB-BSPG 1887 VI 1) pertains to a possibly adult specimen (Cocude-Michel 1963).

Gastralia were present in fossil rhynchocephalians, and the overall morphology was similar to that of *Sphenodon* (i.e. being composed of lateral and medial gastralia, the latter of which shows an anterior median projection). The contact between the lateral gastralia and the arms of the medial elements varied intragenerically, with *Pleurosaurus* showing lateral gastralia that extended almost to the level of the median projection (Fig. 8C), whereas the lateral gastralium extended only halfway through the medial gastralium in *Homoeosaurus* and *Kallimodon* (Fig. 17C, D). The anterior gastralia of *Palaeopleurosaurus* and *Pleurosaurus* showed an acute posterior angle between the arms of the medial element (ranging from 50° to 70°; Fig. 8C), which increased in the posterior gastralia to an obtuse angle (ranging from 120° to 135°). *Clevosaurus hudsoni* (NHMUK PV R36832) showed acute angles in both anterior- and posteriormost gastralia, and obtuse angles only in gastralia from the middle portion of the series (O'Brien *et al.* 2018). Most other rhynchocephalians consistently showed obtuse angles throughout the gastralia series, similar to *Sphenodon*. In some taxa, e.g. *Homoeosaurus*, *Kallimodon*, and *Sapheosaurus*, the angle between the arms of the medial gastralium were almost straight (the gastralia of *Kallimodon pulchellus* showed angles of up to 170°; Fig. 17A–B).

Sternum

General adult morphology

The sternum was a large, roughly pentagonal, calcified cartilaginous plate (Fig. 20). This plate was the presternum, and the mesosternum and xiphisternum were absent (Russell and Bauer 2008). The anterolateral margins of the sternum were dorsoventrally thickened (Fig. 20C), forming the articular facet for the coracoid (coracosternal groove *sensu* Russell and Bauer 2008). Medial to these grooves, two anteromedian processes flanked the median shaft of the interclavicle and covered the coracoid dorsally (Fig. 20A–B). Posterior to the coracosternal articulation, some specimens had transverse fontanelles. A longitudinal median fontanelle may also be present, but it was usually hidden ventrally by the median shaft of the interclavicle (Russell and Bauer 2008); in the specimens we studied, the presence of this fontanelle was a variable feature (e.g. present in four adult specimens, and absent in five, including I-MEHJ S1; Fig. 20B). The lateral margins of the sternum showed three short costal processes that articulated with the sternocostal ribs of PSV9 to 11 (Fig. 20B). These processes were separated by intercostal notches. The posterolateral corners of the sternum expanded further posteriorly than the posteromedial margin, forming two lateral trabeculae.

Ontogenetic and individual variation

The sternum was poorly calcified or unformed in hatchling specimens. The calcification developed in the juvenile stage. As mentioned above, the presence of fontanelles in the sternum was not consistent throughout our sample. However, this does not seem to be due to ontogeny or sexual dimorphism, as, for instance, the median fontanelle was present in some juveniles, subadults, and adults, and male and female specimens, but not all. The lateral trabeculae were less developed in some specimens.

Remarks on fossil taxa

As was the case for the cartilaginous rib elements, the preservation of the sternum in fossil rhynchocephalians was rare and understudied. No sternum has been recognized so far for early branching rhynchocephalians, or clevosaurids. Some specimens from the Solnhofen Archipelago, e.g. the holotypes of *Kallimodon pulchellus* (SNSB-BSPG 1887 VI 1; Fig. 17B) and *Sphenofontis velserae* (SNSB-BSPG 1993 XVIII 4) preserved remnants of the sternal plate (Cocude-Michel 1963, Fabre 1981, Villa *et al.* 2021). However, these can mainly be observed using UV-light and were usually poorly preserved. In *Kallimodon pulchellus* SNSB-BSPG 1887 VI 1, the preserved sternum was roughly diamond shaped, with laterally expanded anterolateral margins (Fig. 17B). No fontanelles were observed in this specimen.

Sacral vertebrae

General adult morphology

Centrum

The centrum was amphicoelous and slightly longer than wide (Fig. 21). In anterior and posterior views, the cotyles appeared circular with a similar height and width. In the centre of each cotyle, the notochordal canal was visible, but closed, as in the presacral vertebrae. It had a radius which was about half that of the centrum, and it was circular in outline.

The posterior centrosynapophyseal lamina (PCYL) was less pronounced in the sacral vertebrae than in the presacral vertebrae, and the post-synapophyseal groove, albeit present, was shallow and poorly marked in the lateral surface of these vertebrae. The ventral surface of the sacral vertebrae was smooth (Fig. 21E), with no ridges and grooves such as those present in the anteriormost presacral vertebrae.

Foramina

In most specimens (15 out of 16 adults), the ventral surface of sacral centra shows subcentral foramina (Fig. 21E), which can be either paired or single, limited to one side.

Intercentrum

The first sacral intercentrum was wedge shaped and lacked the rudimentary hypapophysis, being similar to that of the posterior presacral vertebrae. The second sacral intercentrum was fused to

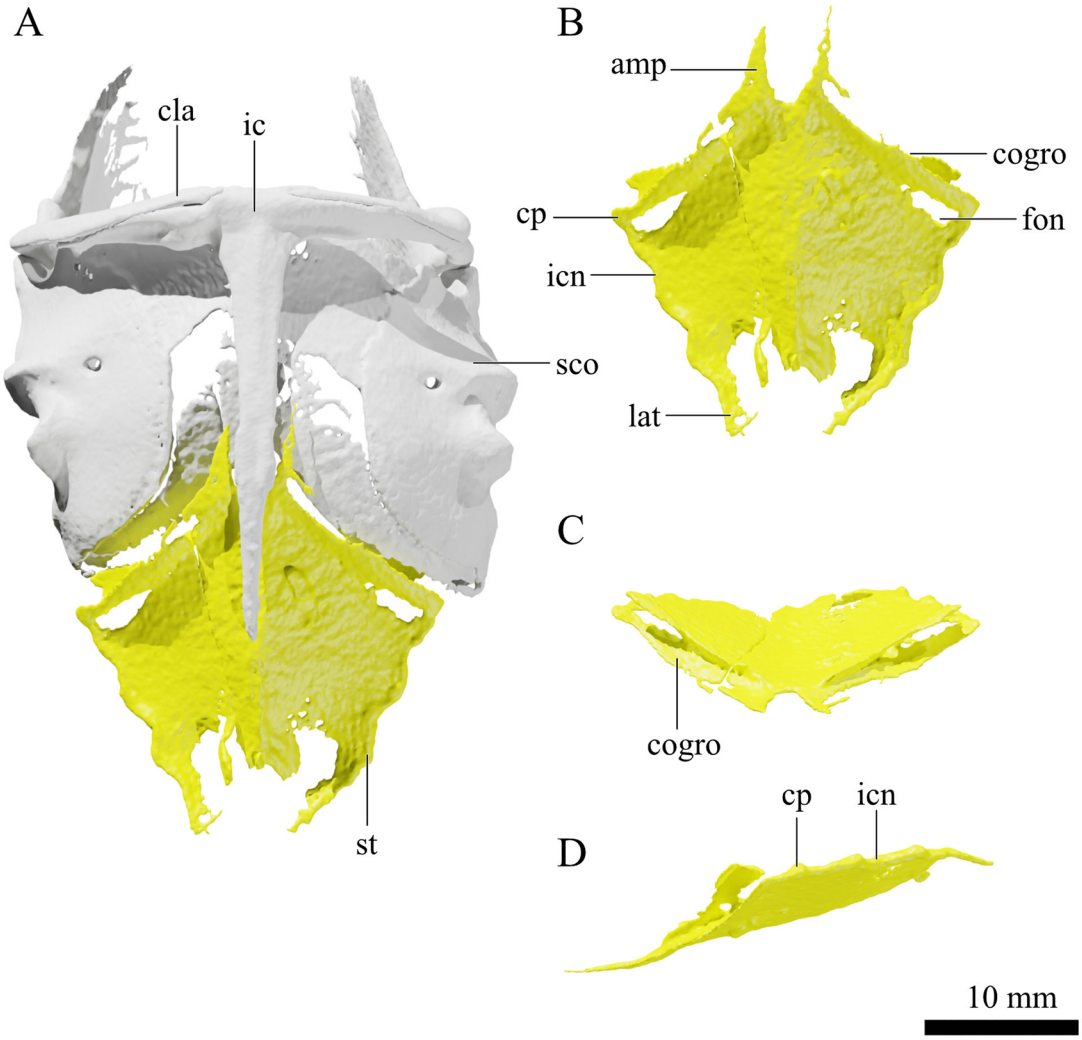

Figure 20. 3D representation of the pectoral girdle and sternum of *Sphenodon* (I-MEHJ S1). A, 3D renders of the articulated pectoral girdle and sternum in ventral view. B–D, 3D renders of the sternum: (B) ventral view; (C) anterior view; (D) left lateral view. Abbreviations: amp, anteromesial process; cla, clavicle; cogro, coracosternal groove; cp, costal process; fon, fontanelle; ic, interclavicle; icn, intercostal notch; lat, lateral trabecula; sco, scapulocoracoid; st, sternum.

the sacral vertebrae, connecting the posterior end of SV1 to the anterior end of SV2 (Fig. 21E).

Neural arch and canal

The neural arches in the sacral vertebrae were similar to that of the presacral. The arches were relatively robust and well ossified, such that, in anterior view, the neural canal was smaller in diameter than the centrum (Fig. 21B–C). The dorsal and lateral margins of the canal were part of a single curve, whereas the ventral margin was relatively horizontal to slightly convex (Fig. 21B–C). The synapophyses were well developed. This creates a distinct bulge on the lateral walls of the arch, to which the sacral ribs (pleurapophyses) articulate and fuse.

Zygapophyses

There were paired prezygapophyses and postzygapophyses. In dorsal view, these extended slightly laterally from the neural arch (Fig. 21D). In anterior or posterior view, the zygapophyses were located more laterally than the lateral margins of the respective cotyle and to a level more dorsal than the roof of the neural canal. The prezygapophyseal articulation was raised dorsolaterally at about 30 to 45°, having a slightly concave articular facet. The postzygapophyses created a distinct bulge on the lateral wall of the neural arch. They were narrower (measured from the lateral tip of the left to right postzygapophyses) in SV1 compared to the last PSV and SV2. In most presacral vertebrae, the postzygapophyses were wider than the prezygapophyses, but this was inverted in SV1.

Neural spine

The neural spine was represented by a tall midline crest. In lateral view, the anterior margin of the spine was posterodorsally inclined, whereas the posterior margin was vertical (Fig. 21A). The dorsal margin of the spine developed as a short crest. When articulated, the dorsal tips of SV1 and SV2 were separated by a distance similar to the length of each crest. Both a POSL and PRSL were present on the sacral neural spines (Fig. 21B–C). The PRSL was usually straight in SV1 and showed a low anterior 'bump' in SV2 (Fig. 21A).

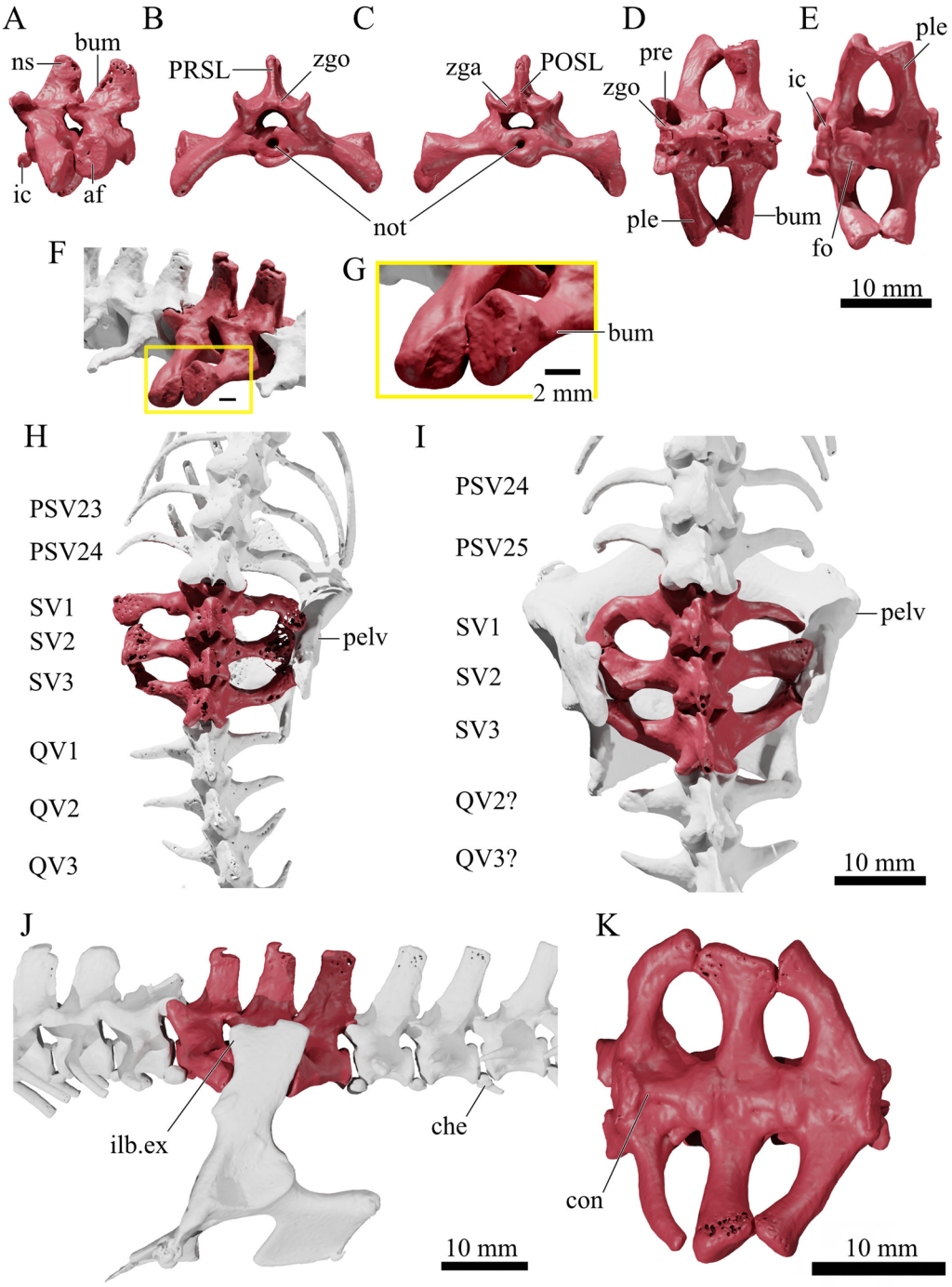

Figure 21. 3D representation of the sacral vertebrae of *Sphenodon*. A–E, 3D renders of sacral vertebrae of *Sphenodon* I-MEHJ S1: (A) left lateral view; (B) anterior view; (C) posterior view; (D) dorsal view; (E) ventral view. F–G, a 3D render of the sacral vertebrae of *Sphenodon* ZMB 13837 (adult), in posterolateral view, highlighting the posterior bump. H, a 3D render of the sacral region of *Sphenodon* ZMB 9804 (subadult) in dorsal view, focusing on the sacral vertebrae. I–K, 3D renders of *Sphenodon* UMZC R2616 (adult) in (I) dorsal view; (J) lateral view; (K) ventral view of the sacral vertebrae. Abbreviations: af, articular facet to the ilium; bum, bump; che, chevron; con, constriction; fo, subcentral foramen; ic, intercentrum; ilb.ex, iliac blade expansion; not, notochordal canal; ns, neural spine; pelv, pelvic girdle; ple, pleurapophysis; POSL, postspinal lamina; pre, prezygapophysis; PRSL, prespinal lamina; PSV, presacral vertebra; QV, caudal vertebra; SV, sacral vertebra; zga, zygantrum; zgo, zygosphene.

Sacral ribs (pleurapophyses)

The sacral ribs were fused to the massive synapophyses. These have been regarded as transverse processes (e.g. Villa *et al.* 2021, DeMar *et al.* 2022, Simões *et al.* 2022), but they were here regarded as pleurapophyses, because these were fused ribs, rather than expanded processes of the vertebral centra (*sensu* Hoffstetter and Gasc 1969). The sacral pleurapophyses were robust and short when compared to the presacral ribs. The first pair of pleurapophyses were slightly longer than the second pair (Fig. 21D–E). The dorsal surface of the ribs lies mainly on the horizontal plane. The

ventral surface, on the other hand, was oblique, because of the distal dorsoventral broadening of the ribs (Fig. 21A). The articular surface with the ilium was triangular in cross section (Fig. 21A, G).

The second pair of sacral pleurapophyses were constricted at midlength, expanding both dorsoventrally and anteroposteriorly at their distal end (Fig. 21A–E). In cross section, the distal end was ovoid (Fig. 21A). These pleurapophyses were usually anteroventrally oriented, expanding in the direction of the first pair of sacral pleurapophyses.

Sexual dimorphism, ontogeny, and individual variation

The PCA of sacral vertebrae in *Sphenodon* showed a similar trend to that of presacral vertebrae, with a separation between males and females, but also between SV1 and SV2 (Fig. 22A). The combination of the first two variation axes explained 61.7% of the variability, with 95% of the variability being explained by the combination of the initial 12 out of 26 axes. Both sacral vertebrae were significantly different from each other ($p = 0.0001$). Significant difference was also found between sacral vertebrae of males and females ($p = 0.0001$), albeit when comparing each vertebra and sex separately, female SV1 and SV2 were not significantly different from each other ($p = 0.10$).

Shape variation between sacral vertebrae of females and males was similar to that of presacral vertebrae, with females having slightly longer and wider centra and significantly lower neural spines than males.

Number

It was possible that only one sacral vertebra was in direct contact with the ilium in hatchlings (Howes and Swinnerton 1901), but this was hard to confirm due to the poor of ossification at the distal ends of the sacral ribs at this ontogenetic stage. The sacral vertebrae were even harder to distinguish from presacral vertebrae at this stage. Albeit rare, some individuals had sacralized lumbar or caudal vertebrae (see below).

Centrum

In juveniles, and particularly in hatchlings, the centra appeared more concave in anterior and posterior view. At the same ontogenetic stages, the two sacral centra were completely separated, but the intervertebral space was minimum. Contact between the centra appeared in subadults, but without fusion. Only adult specimens had fused sacral central (Fig. 21E).

Foramina

The sacral centrum displayed nutritive foramina on the dorsal, ventral (subcentral foramen), and lateral (lateral foramen) surfaces in hatchlings. The lateral foramina disappeared in early juveniles, and the dorsal foramina were fully closed in subadults and adults. Only the subcentral foramina lasted throughout the entire ontogeny. Three adult specimens had completely closed subcentral foramina (subcentral foramina were closed in SV1 of UMZC R2595, and in SV2 of IDHRN NH 84.19 and ZMB 10607).

Intercentrum

The sacral intercentra were paired in juvenile specimens, and single units (i.e. merged into wedge-shaped elements) in all subadult and adult specimens. The first sacral intercentrum remained unfused to the sacral pleurocentrum throughout life, whereas the second one fused to the posteroventral margin of SV1 and the anteroventral margin of SV2, in adults only. Therefore, both sacral vertebrae pleurocentra were continuous in ventral view at this ontogenetic stage, with no suture visible between them in ventral view (Fig. 21E).

Neural arch and canal

The neural arch was represented as separate left and right pedicels in hatchlings and some juveniles, so that the canal was dorsally open at the midline. In anterior view, the neural canal was much larger than the centrum at these ontogenetic stages. The pedicels were medially concave and angled, so that the neural canal was effectively hexagonal. In other juveniles, the canal was pentagonal.

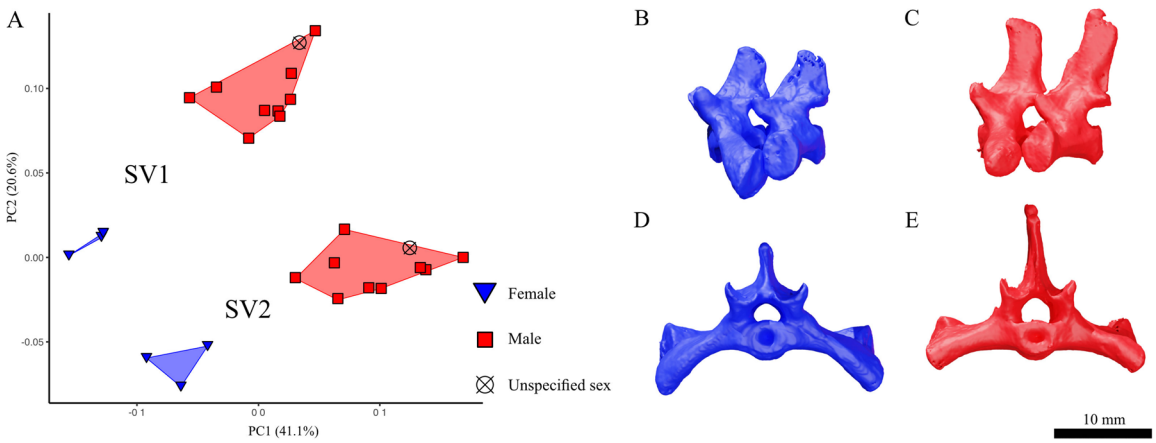

Figure 22. Combination of the main axes of the Principal Component Analysis (PCA) of the sacral vertebrae SV) of adult *Sphenodon*. A, combination of the two main axes of variation (PC1 and PC2) of SV1 and SV2 of adult males and females. B–E, 3D renders of sacral vertebrae of the adult specimens I-MEHJ S1 (in blue) and UMZC R2605 (in red) in (B–C) left lateral view; (D–E) anterior view.

Zygapophyses

The postzygapophyses were fully formed already at the hatchling ontogenetic stage, but the lateral torsion of the prezygapophyses fully develops during the juvenile stage.

Neural spine

The neural spine was absent in hatchlings, short in juveniles, but fully ossified by the subadult stage. The neural arch fused with the centrum during the juvenile stage, but suture lines were still visible until the subadult stage. The paired epiphyses developed in late juveniles and fused to the neural spines in subadults.

Sacral ribs (pleurapophyses)

The sacral ribs fused to the synapophysis in subadults (but our sample included a subadult with still unfused ribs: UMMZ.Herp 406.51). At this ontogenetic stage, the pleurapophyses started expanding at their distal end. In all but five subadult and adult specimens (i.e. subadult IDHNR NH 3-116, and adult I-MEHJ S1, UMZC R2604, UMZC R2608, and ZMB 10607), this expansion was so developed that the distal ends of the sacral pleurapophyses came into contact (Fig. 21F–G, I). However, the pleurapophyses were never fused to each other.

The morphology of the sacral pleurapophyses varied strongly across specimens. The pleurapophyses of SV1 were generally straight and perpendicular to the centrum, but in seven specimens (two juveniles, one subadult, and four adults), the distal end curved posteriorly. A small posterior bump was visible on the pleurapophyses of SV2 in two specimens (i.e. specimen I-MEHJ S1, adult; Fig. 21D–E, and specimen ZMB 13837; Fig. 21F–G). This bump might be homologous with the posterior process observed in extinct rhynchocephalians: it is, of course, not as developed as the process in the fossils, but it was located in the same area. In any case, a real posterior process of SV2 was absent in *Sphenodon*.

Other (third sacral vertebra)

Two specimens in this study showed three sacral vertebrae: these were ZMB 9804 (a subadult; Fig. 21H) and UMZC R2616 (an adult; Fig. 21I). The presence of three sacral vertebrae in *Sphenodon* was previously reported by Howes and Swinnerton (1901: page 30, fig. 6) for a specimen referred to as the 'Dublin Museum specimen' (another adult). In this latter specimen, the distal half of the left pleurapophysis of QV1 bent anteriorly, reaching the ilium and forming a trisegmental sacrum, whereas the right pleurapophysis showed the expected morphology to that of QV1.

Specimen UMZC R2616 showed an unusual morphology of the vertebral sequence, i.e. lumbar, sacral, and anterior caudal vertebrae. The last two presacral vertebrae anterior to the sacrum showed the typical lumbar morphology, bearing short ribs and no associated intercostal and sternocostal cartilage. However, the morphology of the caudal vertebra immediately posterior to the sacral was that of the expected QV2 (Fig. 23A). An incipient chevron was present in the third caudal in this series (Fig. 21J), different from most other specimens, where the first chevron was associated with QV4 (only three other specimens in this study showed the same condition as UMZC R2616). Additionally, the first autotomic septum was present in the sixth caudal vertebra posterior to the last sacral. Usually, the autotomic septum was present in QV8, with some specimens having the autotomic septum in QV7. No specimen in this study showed an autotomic septum in QV6, which was consistent with previous studies (e.g. Seligmann *et al.* 2008). Therefore, one interpretation would be that the third sacral vertebra pertained to the sacralized QV1, similar to the 'Dublin Museum specimen' (Howes and Swinnerton 1901). However, some arguments could be made for a sacralized dorsal instead. The morphology of the right pleurapophysis of SV1 was similar to that of the typical PSV25, i.e. short, slightly posteriorly bent, and tapering at the distal end (Fig. 21I). The left iliac blade of UMZC R2616 showed an abnormal anterior expansion (Fig. 21J), which contacted the left pleurapophysis of SV1 (Fig. 21I). The morphology of the ventral surface of the centra (Fig. 21K) also showed that the second sacral in this series had a condition typical to the SV1 (Fig. 21E), whereas the first sacral in UMZC R2616 showed a slightly constricted centrum, typical of the last lumbar vertebra (PSV 25; Fig. 12J). This mosaic of contrasting features in the lumbar, sacral, and caudal vertebrae of UMZC R2616 hampered the identification of the third sacral vertebra as either a sacralized dorsal or caudal.

In ZMB 9804 (Fig. 21H), by contrast, the sacralized vertebra was the last presacral (PSV25). Its morphology was that expected for SV1, with wider prezygapophyses than postzygapophyses and expanded synapophyses. The distal end of the ribs, now modified into pleurapophyses, contacted the distal end of the corresponding structures in SV2 (primordial SV1). The pleurapophyses of this SV2 were distally expanded both anteriorly and posteriorly, contacting both SV1 and SV3 (primordial SV2). The pleurapophyses of SV3 extended anterolaterally to reach those of SV2. However, only the right pleurapophysis of SV3 was dorsoventrally expanded. An argument could be made for the sacralization of QV1 concurrent with the loss of PSV25 in this specimen, given that a number of 24 presacral vertebrae was known in two other specimens in this study (i.e. UF.Herp 14110 and ZMB 55044). However, in the case of ZMB 9804, morphology of the fist caudal vertebrae was as expected (see 'Caudal vertebrae' section below): pleurapophyses were perpendicular to the centrum in QV1 and QV2 and bowed anteriorly from QV3 onwards, and QV8 was the first autotomic caudal vertebra. The presacral vertebral count and the overall morphology of the caudal vertebrae support the claim that SV1 was indeed a modified PSV25 in this specimen.

Remarks on fossil taxa

Many of the remarks made for the presacral vertebrae can be made for the sacral vertebrae of fossil rhynchocephalians as well. Across observed taxa, only *Gephyrosaurus* shows subcentral foramina in the sacral vertebra (Evans 1981). At least in *Gephyrosaurus*, *Kallimodon*, *Planocephalosaurus*, and *Vadasaurus*, the centra of SV1 and SV2 were unfused (Cocude-Michel 1963, Evans 1981, Fraser and Walkden 1984, Bever and Norell 2017). However, this could be related to the ontogenetic stage of the fossils attributed to these taxa, as only adult *Sphenodon* specimens showed fused sacral vertebrae.

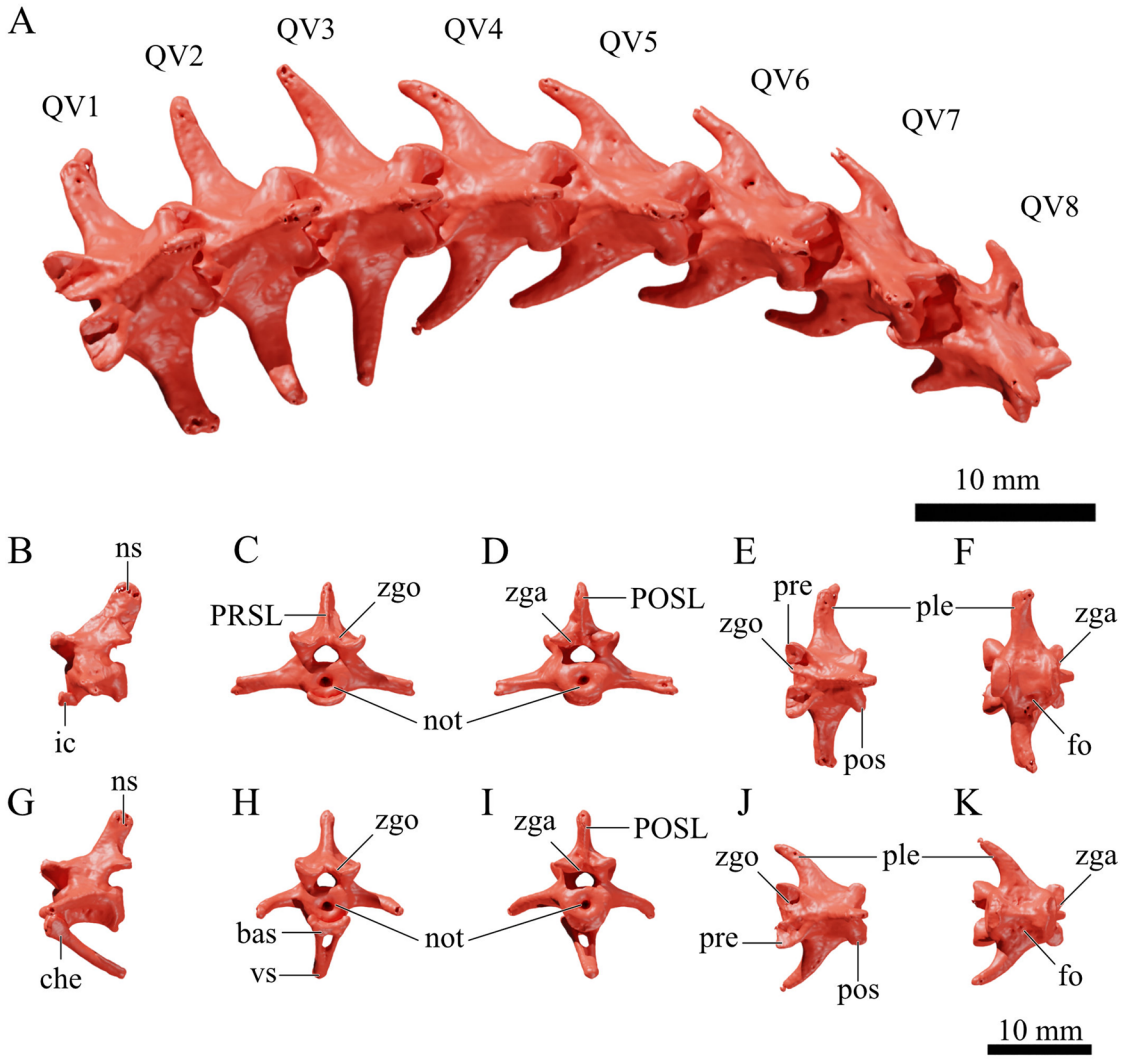

Figure 23. 3D representation of the anterior caudal vertebrae of *Sphenodon* (I-MEHJ S1). A, a 3D render of the articulated anterior caudal vertebrae (QV1–8) in dorsal view. B–F, 3D renders of caudal vertebra 1 (QV1). G–K, 3D renders of caudal vertebra 4 (QV4). B, G, left lateral view. C, H, anterior view. D, I, posterior view. E, J, dorsal view. F, K, ventral view. Abbreviations: bas, chevron base; che, chevron; fo, subcentral foramen; ic, intercentrum; not, notochordal canal; ns, neural spine; ple, pleurapophysis; pos, postzygapophysis; POSL, postspinal lamina; pre, prezygapophysis; PRSL, prespinal lamina; QV, caudal vertebra; vs, ventral spine of the chevron; zga, zygantrum; zgo, zygosphene.

The neural spines were much lower than those of *Sphenodon* in early branching rhynchocephalians (Evans 1981, Fraser and Walkden 1984), and they were squared in the Solnhofen Archipelago taxa (Cocude-Michel 1963, Fabre 1981, Dupret 2004).

Most fossil rhynchocephalians showed a well-developed, posterolaterally oriented posterior process of the second sacral pleurapophysis. This process can extend laterally up to the level of the distal margin of the second sacral pleurapophysis (e.g. *Kallimodon pulchellus* and *Sapheosaurus*; Cocude-Michel 1963, Fabre 1981) or be shorter (e.g. *Homoeosaurus*, *Kallimodon cerinensis*, *Planocephalosaurus*, *Pleurosaurus*, *Sphenodraco*, *Sphenofontis*, and *Vadasaurus*; Cocude-Michel 1963, Fabre 1974, 1981, Fraser and Walkden 1984, Barbera and Macuglia 1988, Cau *et al.* 2014, Bever and Norell 2017, O'Brien *et al.* 2018, Villa *et al.* 2021, Beccari *et al.* 2025a). In most taxa, the lateral margin of this posterior process was concave, but it formed a sharp lateral angle in *Palaeopleurosaurus*, *Sapheosaurus*, and *Vadasaurus*.

Caudal vertebrae

General adult morphology

Centrum

The centrum was amphicoelous and hourglass shaped in the caudals, as was the case for the other vertebrae (Figs 23–25). The absolute length of the centrum increased progressively in the posterior caudals (Fig. 4F), reaching a maximum around QV18 and then gradually decreasing again. Autotomic septa were present from QV8 on posteriorly. These transverse fracture planes were located at the end of the anterior third of the vertebrae (Fig. 24B, G). Two anteroposteriorly aligned ventral protuberances marked the ventral margin of the septum in lateral view (Fig. 24B, G).

These protuberances were less pronounced in the first autotomic septum. A longitudinal median sulcus was present on the ventral surface of the posterior caudals (Fig. 24F, K).

Foramina

Subcentral foramina may be present in the anterior caudals (Fig. 23F, K) but seemed to be absent in all posterior caudals.

Intercentra

The intercentra of the three anterior caudal vertebrae were wedge like, similar in morphology to those of the dorsal vertebrae (Fig. 23B). They lacked the rudimentary hypapophysis present in the cervical intercentra. Starting from the fourth caudal intercentrum, these bones were modified into chevrons. These were oriented obliquely to the caudal pleurocentrum, from anterodorsal to posteroventral in lateral view (Fig. 23G). The anterior chevrons (from QV4 up to 25) were Y shaped (Figs 23H, 24C), with the fused haemapophyses forming long ventral spines, whereas the posterior chevrons (from QV26 posteriorwards) had unfused haemapophyses (*sensu* Hoffstetter and Gasc 1969), being V shaped in anterior view. The haemal canal was triangular in anterior view.

In the anteriormost chevrons (QV4 to 9 in all but one specimen, up to QV10 in a single adult specimen, NHMUK LS 1969.2204), the haemal canal was closed dorsally at the chevron base (Figs 23H, 24C). The chevron articulated both anterodorsally with the previous vertebra, and posterodorsally with its corresponding vertebra. However, in many specimens, the chevrons were closely associated only with the anterior vertebrae (e.g. chevron of QV5 was in association with QV4 only). In all specimens, a marked, oblique articular facet was visible on the posteroventral margin of the caudal pleurocentra, whereas the anteroventral

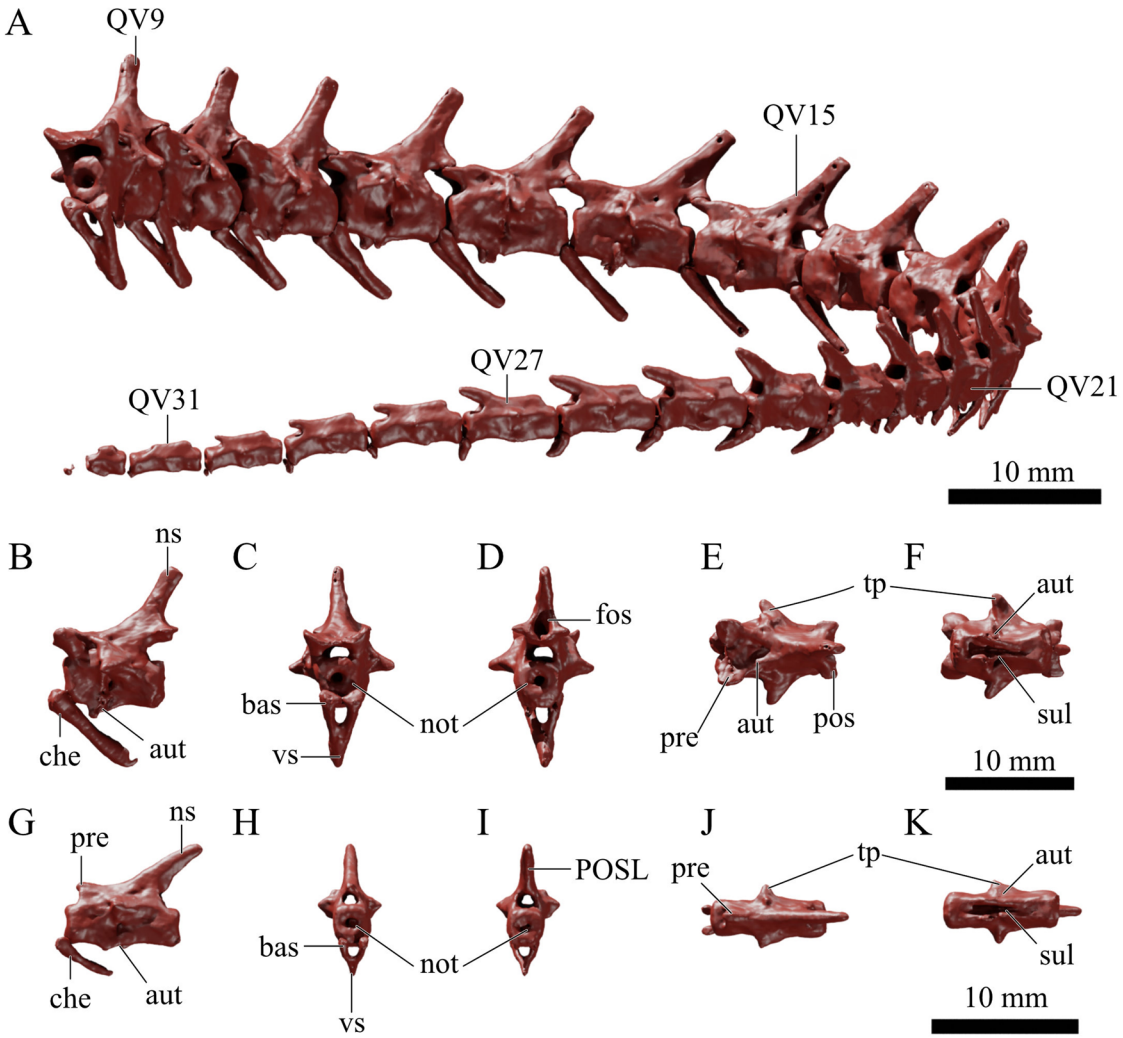

Figure 24. 3D representation of the posterior caudal vertebrae of *Sphenodon* (I-MEHJ S1). A, a 3D render of the articulated posterior caudal vertebrae (QV 9–31) in dorsal view. B–F, 3D renders of caudal vertebra 9 (QV 9). G–K, 3D renders of caudal vertebra 21 (QV 21). B, G, left lateral view. C, H, anterior view. D, I, posterior view. E, J, dorsal view. F, K, ventral view. Abbreviations: aut, autotomy septum; bas, chevron base; che, chevron; fos, fossa; not, notochordal canal; ns, neural spine; pos, postzygapophysis; POSL, postspinal lamina; pre, prezygapophysis; QV, caudal vertebra; sul, sulcus; tp, transverse process; vs, ventral spine of the chevron.

margin of the subsequent pleurocentra showed only a light depression for the articulation with the chevron.

Neural arch and canal

The neural arch of the caudals was lower than that of the presacral and sacral vertebrae and increased in length with the caudal centra (Fig. 23C–D, H–I). Both anterior and posterior margins of the arch were concave in lateral view. The autotomic septum was only marked in the lateral margins of the neural arch anterior to the transverse processes, so that in dorsal view, it was represented only as a faint ridge (Fig. 24E). In the anterior caudals, the neural arch was as wide as the centrum, but it became progressively lower and narrower in the posterior caudals, to the point of being reduced to almost a median ridge in the posteriormost vertebrae (Fig. 24H–J). The neural canal was circular and decreased in diameter in the posterior caudals, until almost closing in the posteriormost vertebrae.

Zygapophyses

The morphology of the zygapophyses in the anterior caudal vertebrae was similar to that of the posterior dorsal vertebrae, with the prezygapophysis extending slightly more laterally than the postzygapophysis in dorsal view (Fig. 23C–E, H–J). The zygosphene-zygantrum articulation was present only in the anterior caudals (Fig. 23C–D, H–I). In the posterior caudals, the zygapophyses gradually move towards the neural spine. In the posterior portion of the tail, the zygapophyses tended to merge medially (Fig. 24J), with the postzygapophyses doing so at a more anterior level (around QV18) than the prezygapophyses. At this point, the zygapophyses were not in articulation anymore. In some posterior caudals (between QV9 and 15), the zygantrum was replaced by a deep posterior fossa ventral to the neural spine (Fig. 24D), similar to the spinopostzygapophyseal fossa of sauropod dinosaurs (Wilson et al. 2011).

Neural spine

The neural spines of the caudal vertebrae were posterodorsally inclined (Figs 23B, G, 24B, G). These gradually decreased in anteroposterior length and became slender posteriorly, until around QV18, where the neural spines became progressively lower and more posteriorly inclined (Fig. 24G). Then, they almost disappeared in the posteriormost caudals. The anterior caudals showed both pre- and postspinal laminae, but the PRSL was absent in the posterior caudals.

Caudal ribs (pleurapophyses) and transverse processes

The anterior caudals (QV1–8) bore fused ribs, i.e. pleurapophyses (Fig. 25A, C). These pleurapophyses were shorter, i.e., not expanding lateraly as much as the sacral ones. Their morphology changed across the caudal series: the first pair was more robust and slightly expanded at the distal end, whereas the pairs of QV2–8 tapered to a point distally. In all studied specimens, the AQV pleurapophyses showed a consistent orientation pattern: they were laterally oriented in QV1 and 2, slightly anteriorly oriented in QV3, and strongly anteriorly bowed in QV4–8, forming a concave anterior margin in the latter (Fig. 23A). The last pair of caudal pleurapophyses (QV8) was much shorter than the preceding ones (QV1–QV7) and was crossed ventrally by the autotomic septum.

In the PQVs, the transverse processes were short lateral expansions of the neural arch. These were true vertebral processes, rather than fused ribs (Fig. 25B, D). Seen in anterior or posterior views, these processes were located at the same level as the floor of the neural canal. The ventral surface of the transverse processes was clearly marked by the autotomic septum, but the dorsal surface showed only a fine ridge indicating the fracture plane of the vertebrae.

Regrown tail

About half of the specimens in this study ($N = 16$) bore regrown tails. The regenerated portion was a straw-like calcified structure without vertebrae that formed from the autotomized vertebra. No specimen in this study showed intervertebral autotomy, but this condition has been previously reported in *Sphenodon* (Seligmann *et al.* 2008). In the specimens in this study, regrown tails were present from QV8 (LDKCL X 11, juvenile) to QV25 (UMZC R2596, subadult), with the most common being QV16 ($N = 4$). This was consistent with previous observations (from QV8 to QV27; Seligmann *et al.* 2008).

Ontogenetic and individual variation

In the specimens preserving the most caudal vertebrae (i.e. UMMZ.Herp.406.51, subadult, 37 QVs; and NHMUK LS 19.5.14.6.10.b, hatchling, 40 QVs), the caudal to presacral vertebrae length proportion (QVL/PSVL) ranged from 1.81 (NHMUK LS 19.5.14.6.10.b) to 1.85 (UMMZ.Herp.406.51). Nine specimens in this study preserved at least 24 QVs, and their QVL/PSVL (accounting only for the first 24 QVs) ranges from 1.25 to 1.38, showing no correlation between ontogeny and proportional caudal length (Supporting Information, Data S1).

The ossification timing of the caudal vertebrae was similar to that of the presacral and sacral vertebrae, fusing both pedicels to form the neural spine before fusing the neural arch to the centrum. The neural arches were fully separated as pedicels in hatchlings and one juvenile (NHMUK LS 1855.10.163). These pedicels fused earlier in the posterior caudals than in the anterior caudals (as can be observed in the juvenile QMUL QMBC 0614; Fig. 25), and all caudal neural arches fully fused to the centrum earlier than the presacral and sacral neural arches. The caudal pleurapophyses were ankylosed already in two juvenile specimens (LDKCL X 11 and NHMUK LS 1972.2050), but not in NHMUK LS 1855.10.163 and QMUL QMBC 0614 (Fig. 25A, C for the latter).

The first autotomic septum appeared usually on QV8, but three adult specimens (UMZC R2605, UMZC R2608, and UMZC R2616) had their first fracture plane in QV7 and one adult specimen (UMZC R2609) in QV9. The autotomic septum was never fully developed across the dorsal surface of the vertebrae. In hatchlings, only the centrum was divided by the septum. At the juvenile stage, the neural arches were already marked by the septum.

Dorsal fusion of the chevron (chevron base; Figs 23H, 24C) developed throughout ontogeny in the anteriormost caudals (from QV4 to 10), also following an anterior (QV4) to posterior (up to QV10) order. The ventral spine followed the same pattern, but these were usually fused up to QV25. Four specimens (i.e. UMZC R2605, UMZC R2615, UMZC R2616, and ZMB 13837)

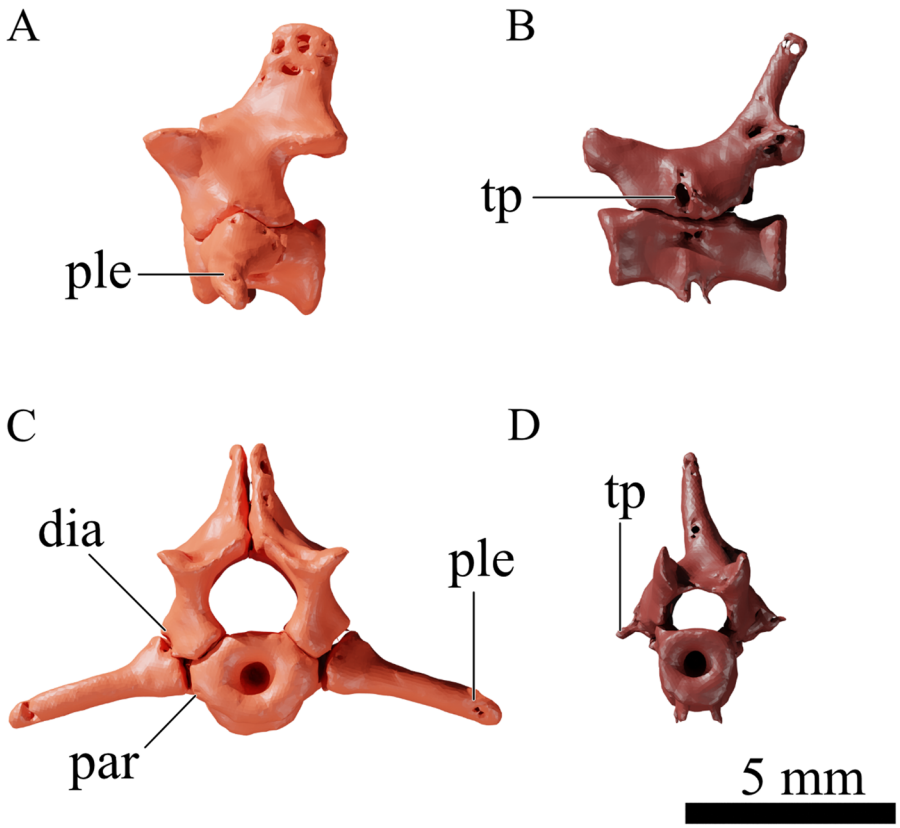

Figure 25. 3D representation of the caudal vertebrae of *Sphenodon* (QMUL QMBC 0614; juvenile), showing the differences between caudal ribs (pleurapophyses) and transverse processes. A, C, 3D renders of the first anterior caudal vertebra (QV1). B, D, 3D renders of the first posterior caudal vertebra (QV9). A–B, left lateral view. C–D, anterior view. Abbreviations: dia, diapophysis; par, parapophysis; ple, pleurapophysis; tp, transverse process.

presented incipient chevrons (i.e. fused base, but poorly developed ventral spines) already in QV3 (Fig. 21J).

Although the orientation of the caudal pleurapophyses was consistent among specimens, those of QV3 were slightly more anteriorly deflected, but never to the same degree as QV4–8.

Remarks on fossil taxa

Among the observed specimens that preserved seemingly complete presacral and caudal series, the holotype of *Homoeosaurus solnhofensis* Cocude-Michel, 1963 (SMF 4073) showed the lowest QVL/PSVL values (1.38, total of 35 QVs), followed by *Kallimodon pulchellus* (SNSB-BSPG 1887 VI 1; 1.58, preserved 28 QVs), *Piocormus laticeps* Wagner, 1852 (TM F03954; 2.0, counting all 25 QVs and regrown tail), *Acrosaurus frischmanni* (SNSB-BSPG AS I 564; 2.1, total of 112 QVs), *Pleurosaurus ginsburgi* (SNSB-BSPG 1977 X 40; 2.2, total 118 QVs), and *Sphenofontis* (SNSB-BSPG 1993 XVIII 4; 2.8, counting the regrown tail, and 2.3 counting only the 39 preserved QVs; Villa *et al.* 2021). Even when accounting only for the preserved QVs without the regrown tail, *Sphenofontis* shows the highest QVL/PSVL ratio, which is significantly higher than that of *Sphenodon* specimens with a similar QV count (i.e. the abovementioned UMMZ.Herp.406.51 and NHMUK LS 19.5.14.6.10.b).

As is the case for the presacral and sacral vertebrae, the ossification timing may vary among fossil taxa, even in adult specimens. In the subadult *Pleurosaurus ginsburgi* specimen SNSB-BSPG 1978 I 7, the neurocentral suture was still visible (Beccari *et al.* 2025b).

The autotomy septum was present in many fossil rhynchocephalians (e.g. *Gephyrosaurus*, *Homoeosaurus maximiliani*, *Navajosphenodon* Simões *et al.*, 2022, *Sapheosaurus*, *Sphenodraco*, *Sphenofontis*, and *Vadasaurus*; Cocude-Michel 1963, Evans 1981, Bever and Norell 2017, Villa *et al.* 2021, Simões *et al.* 2022, Beccari *et al.* 2025a) but not in pleurosaurids (i.e. *Acrosaurus*, *Palaeopleurosaurus*, and *Pleurosaurus*) and in *Kallimodon pulchellus*. Although being described as present in earlier works (Cocude-Michel 1963), later observations have found no autotomic septum in *Kallimodon pulchellus* specimens (e.g. the holotype SNSB-BSPG 1887 VI 1 and referred specimens MB.R.1008b and SNSB-BSPG 1887 VI 2; Beccari *et al.* 2025a).

Caudal pleurapophyses of fossil rhynchocephalians were present in most taxa, but the number of vertebrae with these fused ribs varied. In *Pleurosaurus*, only the anterior four caudals had pleurapophyses, and of these, QV3 and 4 were extremely reduced and unfused even in adult specimens (i.e. *Pleurosaurus goldfussi* SNSB-BSPG 1925 I 18 and *Pleurosaurus ginsburgi* SNSB-BSPG 1977 X 40). In other taxa, between seven and 10 caudal pleurapophyses were present, and this varied even among closely related taxa (e.g. seven in *Homoeosaurus parvipes*, eight in *Homoeosaurus maximiliani*, and 10 in *Homoeosaurus solnhofensis*; Cocude-Michel 1963, Fabre 1981). The orientation of the caudal pleurapophyses is also

variable among taxa but seems to be constant among conspecific specimens. For instance, the first caudal pleurapophysis was posterolaterally oriented in *Kallimodon pulchellus*, laterally oriented in *Homoeosaurus maximiliani*, and strongly anterolaterally oriented in *Sphenofontis*. Therefore, the orientation of these pleurapophyses has potential taxonomic and phylogenetic value for rhynchocephalians (Villa *et al.* 2021, Beccari *et al.* 2025a).

DISCUSSION

The present work adds new data on the morphology of the axial skeleton of *Sphenodon*, including a new proposed ontogenetic categorization, finer markers for vertebral regionalization, and new information on intraspecific variability, ontogeny, and sexual dimorphism. Consistent morphological differences among the extant *Sphenodon* and Mesozoic rhynchocephalians have also been observed throughout the osteological description herein. The discussion will follow the results, being divided into: (i) ontogenetic stages and ossification timing in *Sphenodon*; (ii) regionalization of the vertebral column in *Sphenodon*; (iii) shape differences in the axial skeleton of *Sphenodon*; (iv) implications of ossification timing for fossil rhynchocephalians; and (v) morphologic implications of the axial skeleton in fossil rhynchocephalians.

Ontogenetic stages and ossification timing in *Sphenodon*

Up to this point, different ontogenetic categories were used in rhynchocephalian studies, most dividing post-hatchling individuals into juveniles and adults (e.g. Evans 2008, Jones *et al.* 2011, DeMar *et al.* 2022, Simões *et al.* 2022), with some including subadults as a category (e.g. Jones *et al.* 2009a, Apesteguía and Carballido 2014, Villa *et al.* 2021, Beccari *et al.* 2025a, b). Here we provide a new definition for these ontogenetic categories. The ontogenetic analysis (ontogram; Fig. 3), aligned with linear measurements, suggests three post-hatchling categories: (i) juveniles, i.e. small specimens (presacral vertebrae total length less than 100 mm) with a low degree of bone fusion and ossification; (ii) subadults, i.e. all specimens similar in size (albeit slightly smaller) than adults, showing a higher degree of bone fusion and ossification; and (iii) adults, i.e. skeletally mature individuals with complete bone fusion and ossification.

The ossification pattern in *Sphenodon* is similar to that observed in squamates and early amniotes (Verrière *et al.* 2022). Most of the ossification and fusion of bones in *Sphenodon* occurs at the transition between the hatchling and juvenile stage, and within the latter. In the axial skeleton of *Sphenodon*, the ossification of neural arches, ribs, and gastralia, and the fusion between pedicels (forming the neural spine) and the neurocentral suture occurs in the juvenile stage. The fusion of pleurapophyses in the lumbar and sacral vertebrae occurs later, during the subadult stage. Fused SV 1 and 2 is observed only in adult specimens. In the appendicular skeleton, juveniles show an unfused scapulocoracoid, pelvic girdle, and astragalocalcaneum, and poorly ossified limb epiphyses and carpals. During the subadult stage, the scapulocoracoids fuse, and limb ossification progresses, with the ossification of the proximal epiphyses of the radius, tibia, and fibula. Adult specimens show the last few steps of ossification, i.e. fusion of the pelvic girdle, complete ossification of limb epiphyses, and ossification of carpal and tarsal elements, such as the pisiform in the former, and the lateral process of the astragalocalcaneum in the latter. These ossification patterns are consistent with previous studies (i.e. Evans 2008, Russell and Bauer 2008, Jones *et al.* 2009a, 2011, Villa *et al.* 2021, Beccari *et al.* 2025b). It is worth noting that skeletal maturity does not correspond to sexual maturity in *Sphenodon* (Castanet *et al.* 1988, Herrel *et al.* 2010), which is also the case for other reptiles (Griffin *et al.* 2020). In our study, eggs were found in one subadult individual (UF.Herp 14110).

The ontogram shows a framework of skeletal ontogeny that will be useful for evaluating ontogeny in fossil specimens. However, a greater sampling of small specimens (i.e. juveniles and hatchlings) will likely reduce the differences between their size categories because although there are many skeletal changes during ontogeny, these do not all occur in a consistent order between individuals for all bones, e.g. sesamoids may have different ossification timings (Regnault *et al.* 2016, 2017). Similarly, the greater sampling of subadults and adults includes greater individual variation.

Regionalization of the vertebral column in *Sphenodon*

Properly defining axial anatomy and regionalization is important for taxonomical studies, as the number of vertebrae, their overall morphology, and proportions can be used to diagnose taxa and define new phylogenetic characters (e.g. in dinosaurs, Wilson *et al.* 2011, Baiano *et al.* 2023; mammals, Sargis 2001; and even among lepidosaurs, Dupret 2004, Szyndlar and Georgalis 2023, Hillan *et al.* 2024, Beccari *et al.* 2025b, Węgrzyn *et al.* 2025). Although presacral and caudal regionalization for this reptile have been proposed in previous studies (e.g. Romer 1956, Hoffstetter and Gasc 1969, Jones *et al.* 2009a, Jones *et al.* 2018), the subdivisions are inconsistent. The general consensus divides the presacral vertebrae only into cervical and dorsal vertebrae (Romer 1956, Hoffstetter and Gasc 1969), with some authors dividing the dorsals into anterior and posterior dorsals (Jones *et al.* 2018), and some others recognizing a lumbar region in *Sphenodon* (e.g. von Wettstein 1931, 1937, Hoffstetter and Gasc 1969, but not Jones *et al.* 2018). Our geometric morphometric analysis shows a complex pattern of regionalization in the presacral series, which involves discrete morphological characteristics, and allometry and changes in proportion of elements (i.e. neural spine, synapophyses, and zygapophyses). Similar results have been observed in squamates (e.g. Hillan *et al.* 2024), which highlights the importance of morphometrics for morphological studies in amniotes (e.g. Böhmer *et al.* 2015, Jones *et al.* 2018). Although vertebral morphology does not vary drastically across the axial series of *Sphenodon*, as it is the case in other clades, such as birds and mammals (Fleming *et al.* 2015, Jones *et al.* 2018, 2020, Verrière *et al.* 2022), significant variation across the skeleton is indeed present, especially regarding rib morphology. The position of the synapophyses changes throughout the presacral series, with the diapophysis overpassing the contact between the neural arch and the pleurocentrum in cervical vertebrae, whereas this structure is restricted to the neural arch in dorsal vertebrae. The parapophysis also shifts dorsally towards the neural arch in all (anterior and posterior) dorsal vertebrae, but not in the lumbar vertebrae. Cervical ribs are shorter and more anteroposteriorly flattened

compared to the dorsal ribs. The anterior dorsal vertebrae have an intermediate morphology between cervicals and posterior dorsals, and this is reflected in the rib morphology. The cervical intercentra show rudimentary hypapophyses, which are absent in the dorsal and lumbar intercentra. The head of anterior dorsal ribs is bean shaped and more robust than the elliptical morphology of posterior dorsal ribs (Fig. 18). The caudal vertebrae may also be subdivided into anterior (QV1–8) and posterior caudals (QV9 and posterior). The anterior caudals have anteroposteriorly longer neural spines. Pleurapophyses are only present in the anterior caudals, whereas posterior caudals have short, laterally oriented transverse processes (Fig. 25). It is worth mentioning that the autotomic septum is already present in the last two caudals (QV7 and 8), and as such is not being a good character in defining regionalization.

Our observations on the axial skeleton of *Sphenodon* highlight that some traits maintain a consistent morphology whereas others show a significant degree of variation within this taxon. Traits that are generally consistent include: (i) the number of presacral and sacral vertebrae (Fig. 4); (ii) position and oblique orientation of the presacral synapophyses (Figs 10–11); (iii) rudimentary hypapophysis in cervical intercentra (Fig. 10); (iv) the presence of specific laminae on the vertebrae (i.e. PCYL, POSL, PRSL; Figs 10–12, 21); (v) the overall trapezoidal shape of the neural spines in lateral view (Figs 10–12, 21, 23–24); (vi) the changes in proportions across the presacral series, with anteroposteriorly shorter post-axial cervical vertebrae than dorsal and lumbar vertebrae (Fig. 4); (vii) the morphology of ribs and cartilaginous elements in the presacral series (Fig. 18); and (viii) the orientation of the pleurapophyses in the anterior caudal vertebrae (Fig. 23). This morphological consistency in *Sphenodon* suggests that these traits may bear some taxonomic value; therefore, the condition shown by fossils, if observable, can be of help for species descriptions and identifications. However, there are other traits which show significant variation, which include: (i) the presence or absence of foramina, ridges, or grooves on the ventral surface of the presacral vertebrae (Figs 10–12, 21, 23–24); (ii) size of neural spines (Figs 10–12); and (iii) orientation of the sacral pleurapophyses (Fig. 21). Some traits exhibit notably variation even in a single individual (e.g. presence of subcentral foramina in some, but not all vertebrae, and on different sides of the centra). These features should be taken with caution when used as diagnostic traits for extinct rhynchocephalians.

Shape differences related to ontogeny, size, sex, and population

Skeletal variation can be related to population, ontogeny, size, and sex (e.g. Castanet *et al.* 1988, Lamar *et al.* 2022). Sexual dimorphism is evident in *Sphenodon*, but it remains unclear as to whether males show different allometry (Grandal-d'Anglade and López-González 2005) or more likely that females terminate their growth earlier than conspecific males (e.g. Frýdlová and Frynta 2015). Differentiating between these two possibilities requires large sample sizes from known populations. Also, two shortcomings regarding the *Sphenodon* specimens used in our study should be taken into consideration for the GMM analysis. Many of the museum specimens were collected in the past two centuries, and their specimen labels lack: (i) precise provenance and (ii) information on sex. At this moment, little is known about morphological variability across the distinct *Sphenodon* populations. The consensus is that *Sphenodon* is monospecific, with the single species being *Sphenodon punctatus*; this has been tested and corroborated in recent genetic studies (e.g. Hay *et al.* 2010, Gemmell *et al.* 2020, Macey *et al.* 2021). These studies do highlight interpopulation genetic differences in *Sphenodon* (especially in those living on Lady Alice Island), and that these should be taken into consideration for conservational efforts (Gemmell *et al.* 2020, Macey *et al.* 2021). We cannot exclude that at least part of the variation we observed in our sample is related to the origin of the specimens, and future studies should test this. As stated in the methods section above, we established sex for the studied specimens with observations on their external morphology, i.e. based on the size and spacing of the dorsal spiny crest. Although this seems like a reliable feature to identify *Sphenodon* individuals in the field (e.g. Lamar *et al.* 2021), little is known about the actual variability of the crest of *Sphenodon*, and it is possible that some specimens may have been misidentified. Nevertheless, the few specimens for which sex is known (e.g. I-MEHJ S1, NHMUK LS 1935.5.14.3, SNSB-ZSM 1318-2006, and UF.Herp 14110) do show the expected crest morphology for their assigned sexes.

Size, and by correlation, ontogeny, are additional important factors. The morphometric analysis shows negative allometry for the vertebral shape, with smaller individuals, including juveniles, but also adult females, having stouter vertebrae than larger specimens, i.e. subadults and adults, especially males (Figs 14–15). In our sample, juvenile specimens are much smaller than subadult and adult specimens, which is reflected in the vertebral morphology (Fig. 14). Adult male *Sphenodon* are reportedly 10 to 20% larger than females, but this difference might vary between populations (e.g. Castanet *et al.* 1988, Herrel *et al.* 2010), which is consistent with our sample (Supporting Information, Data S1). We do find statistically significant differences between the vertebrae of male and female specimens. In the sample, female vertebrae are usually smaller and proportionally shallower and wider than those of males (Fig. 13). These results are similar to those observed in agamid lizards and inferred for other reptile clades (Tereshchenko 1991, 2020), and agree with the known sexual size dimorphism of *Sphenodon*, with adult males being significantly larger than adult females (e.g. Castanet *et al.* 1988, Herrel *et al.* 2010, Jones and Cree 2012, Lamar *et al.* 2021, 2022). Two subadult specimens are substantially smaller than adult specimens, i.e. MZH MS 1853, of which no sex data is available, and UMZC R2596, a male specimen, whose presacral vertebrae length are 109 and 117 mm, respectively. This is lower than our sample average of adult males and females (143.6 mm and 131.4 mm, respectively; Supporting Information, Data S1). These smaller subadults show similar vertebral morphology to adult female specimens. A larger sample is needed to understand the precise relationship between size and shape, meaning that the inclusion of larger female and smaller male specimens may obscure sexual dimorphism results in morphometric analyses.

Ossification timing in fossil rhynchocephalians

To test how ossification timing differs in some extinct rhynchocephalian clades compared to that of *Sphenodon*, a simplified ontogenetic analysis (ontogram) was made (Fig. 26). Four ontograms were created to visualize the ossification and fusion timing among (i) the pleurosaurids *Acrosaurus frischmanni*, *Pleurosaurus ginsburgi*, and *Pleurosaurus goldfussi* (Fig. 26A); (ii) specimens in the *Kallimodon–Leptosaurus* complex (*sensu* Rauhut and López-Arbarello 2016) (Fig. 26B); (iii) *Homoeosaurus maximiliani* (Fig. 26C); and (iv) the sphenodontine *Sphenofontis* (Fig. 26D). The results show that ossification timings can vary considerably among taxa (see Supporting Information, Data S2 for the complete list of character changes). Contrary to *Sphenodon*, pleurosaurids show a delayed axial fusion (i.e. fusion of the neural arches). One specimen of *Pleurosaurus ginsburgi* (SNSB-BSPG 1978 I 7) showed a marked neurocentral suture in the presacral vertebrae, but well ossified limb bones such as the radius, tibia, and fibula. Specimens in the *Kallimodon–Leptosaurus* complex and of *Homoeosaurus maximiliani* show a similar earlier ossification of limb bone epiphyses than that expected in *Sphenodon*, especially when compared to the scapulocoracoid. Even in seemingly adult specimens (i.e. the Brunn specimens SNSB-BSPG 1993 XVIII 3 and SNSB-BSPG 1993 XVIII P11), the scapula and coracoid are unfused, whereas the femur, fibula, humerus, radius, tibia, and ulna are well ossified, especially the ulna where the patella ulnaris (*sensu* Russell and Bauer 2008) is sutured to the proximal epiphysis of this bone. Albeit the fusion of the scapulocoracoid cannot be observed in the possibly adult *Homoeosaurus maximiliani* neotype (SNSB-BSPG 1887 VI 502), this specimen also shows a well ossified patella ulnaris. Among the observed specimens, only the holotype of *Sphenofontis velserae* (SNSB-BSPG 1993 XVIII 4) shows a clearly fused scapulocoracoid, but conversely, a yet unfused patella ulnaris (Villa *et al.* 2021). None of the observed fossil specimens show fused pelvic girdle elements, which could indicate that these may not pertain to fully skeletally mature (adult) individuals, as the fusion of the pelvic girdle occurs late in *Sphenodon*. However, the different ossification timing in the fossil taxa can have functional, taxonomic, and phylogenetic implications.

The late ossification and fusion of bones has been correlated with an aquatic lifestyle in lepidosaurs (e.g. Lee *et al.* 2016, Bever and Norell, 2017, Paparella *et al.* 2018, 2020, Caldwell *et al.* 2021, Beccari *et al.* 2025b). The pelvic girdle stays unfused in adults of aquatic and semi-aquatic squamates, such as dolichosaurids and mosasaurs (e.g. Lee and Caldwell 2000, Street and Caldwell 2017, Paparella

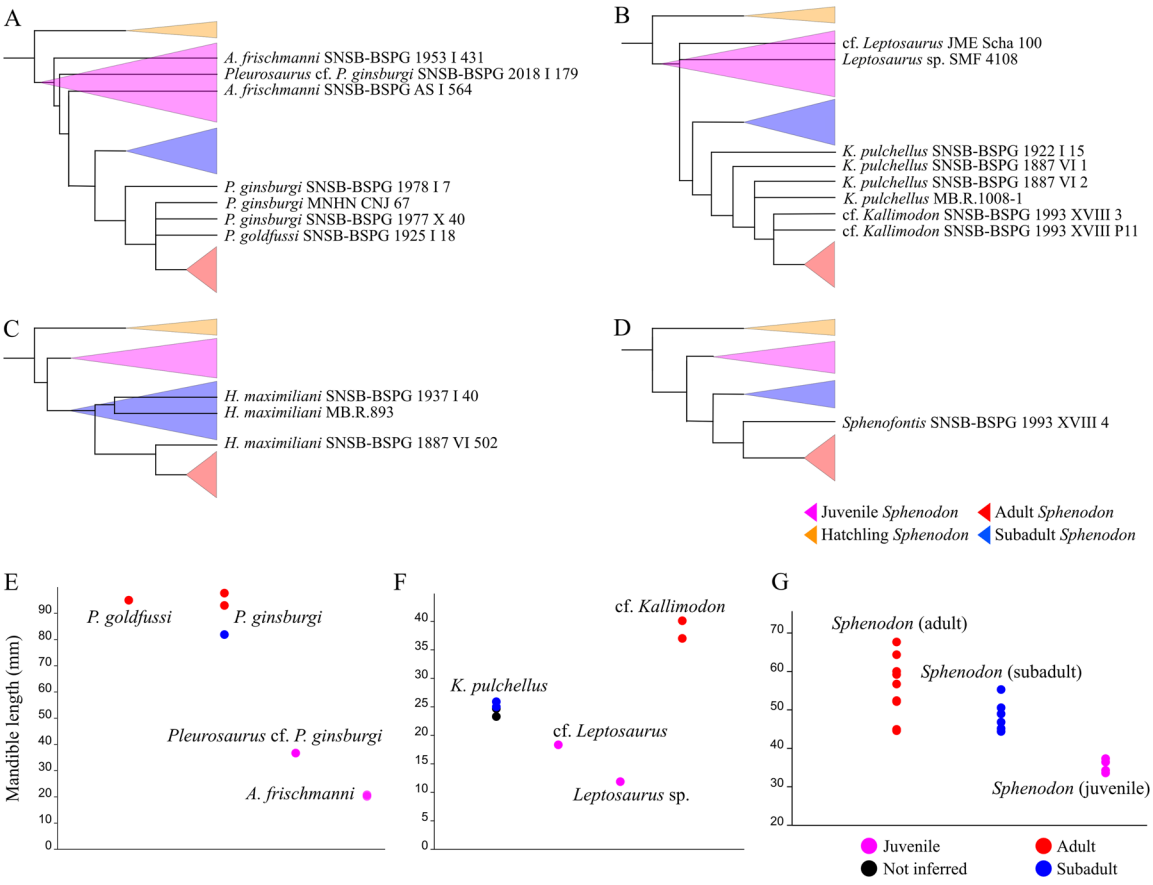

Figure 26. Ontogram showing the ossification sequence in the Solnhofen Archipelago rhynchocephalians. A, strict consensus tree of the pleurosaurids *Acrosaurus frischmanni* and *Pleurosaurus*. B, strict consensus tree of specimens in the *Kallimodon–Leptosaurus* complex. C, strict consensus tree of *Homoeosaurus maximiliani* (abbreviated as *H. maximiliani*) specimens. D, strict consensus tree of the sphenodontine *Sphenofontis velserae*. E, graph of the distribution of mandible length (in mm) of *Acrosaurus frischmanni* and *Pleurosaurus* specimens with inferred ontogenetic stages. F, graph of the distribution of mandible length (in mm) of specimens in the *Kallimodon–Leptosaurus* complex with inferred ontogenetic stages. G, graph of the distribution of mandible length (in mm) of post-hatchling *Sphenodon* specimens.

et al. 2018, 2020). Pleurosaurids, *Kallimodon*, and *Sapheosaurus* have previously been associated with an aquatic or semi-aquatic lifestyle (Carroll 1985, Carroll and Wild 1994, Bever and Norell 2017, Gutarra *et al.* 2023, Beccari *et al.* 2025a, b). The inferred adult *Pleurosaurus* specimens in this study (Fig. 26E) show this consistent delay in limb ossification (i.e. *Pleurosaurus ginsburgi* MNHN CNJ 67 and SNSB-BSPG 1977 X 40, *Pleurosaurus goldfussi* SNSB-BSPG 1925 I 18), consistent with the consensus of a marine lifestyle for *Pleurosaurus* (Fabre 1974, Carroll 1985, Carroll and Wild 1994, Dupret 2004, Bever and Norell 2017, Beccari *et al.* 2025b).

Ossification timing can also correlate to taxonomy. The Late Jurassic *Acrosaurus frischmanni* has been regarded as a possible junior synonym of the coeval *Pleurosaurus goldfussi* (Rothery 2002, 2005, Jones 2008, Beccari *et al.* 2025b). As a matter of fact, the holotype of *Acrosaurus frischmanni* (SNSB-BSPG AS I 564) is anatomically similar to *Pleurosaurus* specimens, but significantly smaller than even the smallest known juvenile *Pleurosaurus* described so far (SNSB-BSPG 2018 I 179; Beccari *et al.* 2025b). Yet, SNSB-BSPG AS I 564 shows a higher degree of axial and appendicular ossification than expected for an early juvenile specimen (Fig. 26A), i.e. the neural spines are fused and the humerus epiphyses are slightly more ossified in this specimen than that of the much larger SNSB-BSPG 2018 I 179, in which the neural arch pedicels are completely unfused to each other (Beccari *et al.* 2025b). For *Sphenodon*, our study shows that ossification timing patterns indicate an advanced level of bone fusion and ossification in larger specimens (i.e. subadults and adults). If a similar ontogenetic development can be inferred for fossil taxa, *Acrosaurus frischmanni* cannot reasonably be interpreted as an earlier juvenile of the described *Pleurosaurus* species and may indeed represent a valid species distinct from either *Pleurosaurus goldfussi* or *Pleurosaurus ginsburgi*, assuming that ossification wasn't more variable in Mesozoic forms than it is in *Sphenodon*.

As mentioned above, the scapula and coracoid remain unfused even in adult and subadult *Pleurosaurus* and *Kallimodon* specimens. From early branching fossil rhynchocephalians such as *Gephyrosaurus* and *Clevosaurus hudsoni*, to the extant *Sphenodon*, the scapulocoracoid is fused in subadult and adult specimens (Evans 1981, Russell and Bauer 2008, O'Brien *et al.* 2018). Additionally, most extant limbed squamates show fused a scapulocoracoid, with the main exceptions being monitor lizards (Conrad 2015, Kępa *et al.* 2023). It is currently unclear if the fusion of the scapulocoracoid in lepidosaurs has functional implications. However, this feature could have a phylogenetic signal, possibly being shared among non-sphenodontid Solnhofen rhynchocephalians, sometimes recovered in phylogenetic analyses as the clade Leptorhynchia DeMar *et al.*, 2022 (e.g. DeMar *et al.* 2022, Beccari *et al.* 2025a; 'Clade A' in Simões *et al.* 2022).

Morphologic implications of the axial skeleton in fossil rhynchocephalians

The structure and organisation of the axial skeleton is related to habitat use, locomotion, and even feeding strategies (Jones *et al.* 2009a, Montuelle *et al.* 2009, Lee *et al.* 2016, Caldwell *et al.* 2021, Gutarra *et al.* 2023, Molnar and Watanabe 2023, Beccari *et al.* 2025a, b). Functional studies of the vertebrae of fossil rhynchocephalians are still scarce, with the main exceptions being focused on vertebral ossification timing and increase in bone density and mass (e.g. osteosclerosis and pachyostosis; Reynoso 2000, Klein and Scheyer 2017) in pleurosaurids, both interpreted as markers for an aquatic lifestyle (Reynoso 2000, Lee *et al.* 2016, Bever and Norell 2017, Klein and Scheyer 2017, Beccari *et al.* 2025b), and at least two studies highlighting the correlation between axial proportions and lifestyle (Gutarra *et al.* 2023, Beccari *et al.* 2025a).

In addition to the ossification timing, the axial morphology of extinct rhynchocephalians can be used for ecomorphological inferences. In extant lizards, body vs. limb length proportions have been associated with substrate preferences (e.g. Zaaf and Van Damme 2001, Hagey *et al.* 2017, Foster *et al.* 2018, Ríos-Orjuela *et al.* 2020, Cordero *et al.* 2021, Feiner *et al.* 2021), and those between tail length and presacral length play an important role in speed and balance (e.g. Clemente *et al.* 2013, McElroy and Bergmann 2013). The Late Jurassic *Sphenofontis velserae* shows the highest tail-to-body ratio (see Villa *et al.* 2021) among the observed specimens in this study, even including pleurosaurids, whose elongated tails have been correlated with body undulation (Gutarra *et al.* 2023). Considering also the relatively long, well-ossified hind limbs, *Sphenofontis* could have displayed high running performances, using its long tail to move the centre of mass closer to the hindlimbs (McElroy and Bergmann 2013). The presence of caudal autotomy may negatively influence the performance in running and climbing taxa (e.g. Zani 1996, Seligmann *et al.* 2008, Marvin 2010, Domínguez-López *et al.* 2015), as well as underwater propulsion for aquatic and semi-aquatic lizards (Marvin 2010). All specimens assigned to *Kallimodon pulchellus* and pleurosaurids, e.g. *Acrosaurus frischmanni*, *Palaeopleurosaurus*, and *Pleurosaurus*, lack autotomic septa and were, thus, most likely unable to perform caudal autotomy. This loss of caudal autotomy may indicate that, as previously proposed, *Kallimodon pulchellus* was at least semi-aquatic (Carroll and Wild 1994, Goodman 2009, Marvin 2010, McElroy and Bergmann 2013). Further studies including morphometry of the axial skeleton may provide additional insights into the wider group's ecomorphology.

As discussed above, the morphology of the axial skeleton in *Sphenodon* shows consistent traits across the observed sample in this study. When comparing those to the axial skeleton of Mesozoic rhynchocephalians, new taxonomic and phylogenetic informative characters can be observed. The number of presacral and sacral vertebrae has been previously used to diagnose some pleurosaurids, i.e. *Palaeopleurosaurus* (37 PSVs), *Pleurosaurus ginsburgi* (57 PSVs), and *Pleurosaurus goldfussi* (50 PSVs) (Fabre 1974, Carroll 1985, Dupret 2004), albeit some specimens assigned to *Pleurosaurus* show different number of vertebrae (59 PSVs in SNSB-BSPG 1977 X 40; Beccari *et al.* 2025b). The position, shape, and orientation of the presacral synapophyses is variable among fossil rhynchocephalians. Although many taxa (e.g. *Gephyrosaurus*, *Planocephalosaurus*, *Clevosaurus*, and *Homoeosaurus*; Cocude-Michel 1963, Evans 1981, Fraser and Walkden 1984, Fraser 1988, O'Brien *et al.* 2018) show a similar morphology to that of *Sphenodon*, pleurosaurids show vertical, cylindrical synapophyses (Fig. 8E), whereas *Kallimodon pulchellus* shows slightly posteriorly oriented synapophyses (Fig. 17B). Rudimentary hypapophyses in cervical intercentra are also present in some fossil taxa, e.g. *Gephyrosaurus*, *Clevosaurus hudsoni*, and *Kallimodon pulchellus* (Cocude-Michel 1963, Evans 1981, O'Brien *et al.* 2018), but not in *Pleurosaurus* (Fig. 8B). Clevosaurids, early branching

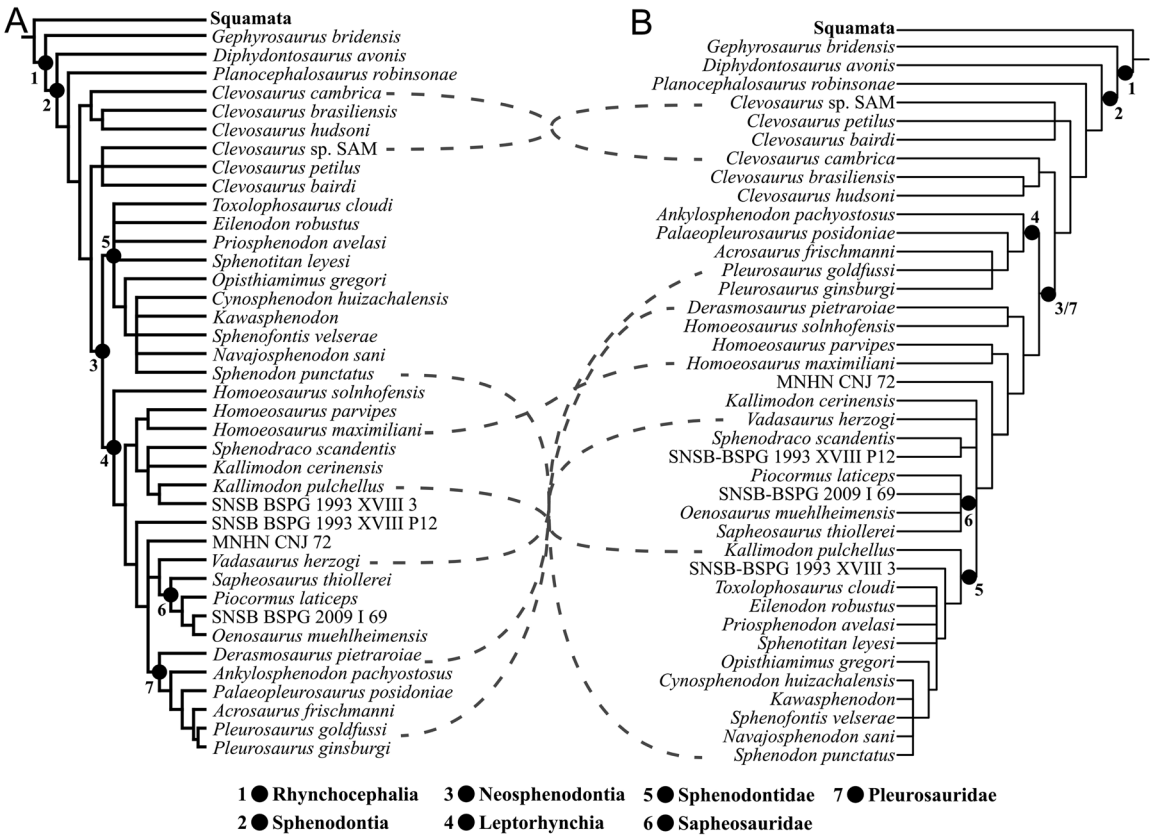

Figure 27. Phylogenetic analysis of fossil rhynchocephalians. A, most parsimonious tree of the first phylogenetic analysis (A1), following the dataset of Beccari *et al.* (2025a), which includes 16 additional morphological characters of the axial skeleton. B, most parsimonious tree of the second phylogenetic analysis (A2), without the additional morphological characters of the axial skeleton. The numbers on the nodes represent major rhynchocephalian clades (as per label). The dotted lines represent some of the major differences between the relationships of OTUs in A1 and A2.

rhynchocephalians, and sphenodontines show overall trapezoidal neural spines in the presacral vertebrae (Cocude-Michel 1963, Evans 1981, Fraser and Walkden 1984, Fraser 1988, O'Brien *et al.* 2018, DeMar *et al.* 2022, Simões *et al.* 2022), whereas *Homoeosaurus*, *Kallimodon*, and *Pleurosaurus* (Fig. 8E) show squared neural spines, about as long anteroposteriorly as dorsoventrally tall (see also Cocude-Michel 1963). Most fossil rhynchocephalians show a posterior process in the second sacral pleurapophysis (Cocude-Michel 1963, Evans 1981, Fabre 1981, Fraser and Walkden 1984, Villa *et al.* 2021), which is absent in *Sphenodon*. The orientation of the caudal pleurapophyses is consistent across the sample of *Sphenodon* specimens. Fossil taxa show diverse morphologies and orientation of these pleurapophyses, which have been used as one of the diagnostic features of *Sphenofontis* (Villa *et al.* 2021). These morphological features have been incorporated into the phylogenetic dataset of Beccari *et al.* (2025a; derived from Simões *et al.* 2022), which resulted in the creation of 16 new morphological characters for the axial skeleton (increasing the number of axial characters from 18 to 34, making up to 23% of all characters in this dataset). The inclusion of new axial characters has implications for the evolutionary history of neosphenodontians (Fig. 27), including synapomorphic characters, i.e. two new unambiguous synapomorphies for Sapheosauridae (lateral extension of the posterior process of the second sacral pleurapophysis, and posteriorly oriented pleurapophyses of caudal vertebra 4), one unambiguous synapomorphy for a clade containing *Homoeosaurus*, *Kallimodon*, and *Sphenodraco* (presacral intercentra present in the cervical series only), and one unambiguous synapomorphy (synapophyses oriented posterolaterally) for a clade containing *Kallimodon pulchellus*, *Kallimodon cerinensis*, *Sphenodraco*, and SNSB-BSPG 1993 XVIII 3 (undescribed Brunn specimen with affinities to *Kallimodon*; Rauhut *et al.* 2017). The resulting strict consensus tree of A1 (with additional axial characters; Fig. 27A) shows marked differences to the topology of A2 (without the 16 new axial characters; Fig. 27B). Among these, the most striking differences regard the relationships of neosphenodontians. In the analysis of Beccari *et al.* (2025a), the clade Leptorhynchia DeMar *et al.*, 2022 includes all European neosphenodontians, except for *Sphenofontis*. This clade has been defined as containing all taxa more closely related to *Pleurosaurus* than *Sphenodon* (DeMar *et al.* 2022). In A2, Leptorhynchia would include only *Acrosaurus*, *Ankylosphenodon*, *Palaeopleurosaurus*, and *Pleurosaurus*, but not *Derasmosaurus* (which is recovered as a sister taxon to these taxa in A1). The clade Pleurosauridae Lydekker, 1880 (*sensu* Simões *et al.* 2020) is recovered in A1 including *Acrosaurus*, *Ankylosphenodon*, *Derasmosaurus*, *Palaeopleurosaurus*, and *Pleurosaurus*, and is synonymous with Neosphenodontia Herrera-Flores *et al.*, 2018 (*sensu* Simões *et al.* 2020) in A2, as in this analysis, *Derasmosaurus*

is recovered as the sister taxon to *Homoeosaurus solnhofensis* (Fig. 27B). The clade-wide differences between A1 and A2 highlights the importance of the new axial characters, but also remarks possible taxonomic issues with current clade definitions, which should be explored at a later date.

Currently, the results of the new phylogenetic analysis are highly sensitive to the addition of new characters and operational taxonomic unities (OTUs), and A1 differs significantly from other studies, which have focused mainly on cranial characters (i.e. Chambi-Trowell *et al.* 2021, DeMar *et al.* 2022; axial characters comprising 3 and 8% of total dataset, respectively). The addition of new axial characters highlights the previously reported importance of postcranial characters in phylogenetic analyses of rhynchocephalians (DeMar *et al.* 2022, Beccari *et al.* 2025a), and follows a current trend in the phylogenetic analyses of different clades (e.g. eusuchian phylogeny in Blanco 2021, and pterosaurs in Pêgas 2025). Therefore, we suggest that new morphological characters, especially those of the appendicular skeleton, as well as additional OTUs, should be added in future analyses to solve some of the lingering issues in rhynchocephalian phylogeny.

CONCLUSION

The present work describes the axial skeletal morphology of the extant rhynchocephalian *Sphenodon punctatus* in detail. We used a comprehensive sample of 33 specimens of different ontogenetic stages and sexes to compare individual, sexual, and ontogenetic variation. Our ontogenetic analysis shows a clear pattern of ossification timing across the sample of *Sphenodon* specimens. Four ontogenetic stages have been identified, i.e. hatchlings, juveniles, subadults, and adults. During the juvenile stage, the axial skeleton ossifies and all elements (i.e. neural arch pedicels and centra) fuse, whereas the appendicular skeleton remains poorly ossified and the girdles unfused. The ossification of vertebral and limb bone epiphyses continues during the subadult stage, but only adult specimens show fully ossified epiphyses. The scapulocoracoid fuses in the subadult stage, but the pelvic girdle elements are only fused in adult individuals.

The vertebral column of *Sphenodon* can be subdivided into seven regions: (i) cervical vertebrae; (ii) and (iii) anterior and posterior dorsal vertebrae; (iv) lumbar vertebrae; (v) sacral vertebrae; and (vi) and (vii) anterior and posterior caudal vertebrae. The axial regionalization in *Sphenodon* can be established through a combination of geometric morphometrics and discrete morphological characters. The 3D geometric morphometric analysis shows that cervical, anterior dorsal, and lumbar vertebrae are anteroposteriorly shorter, but laterally wider, than posterior dorsal vertebrae. Discrete characters indicating vertebral regionalization are (i) position of synapophyses (being lower and more laterally position in cervical and lumbar vertebrae than in dorsal vertebrae); (ii) presence and development of cartilaginous elements associated with the vertebrae, i.e. uncinate processes and sternocostal ribs are present only in dorsal vertebrae; (iii) fusion of ribs (pleurapophyses) in the lumbar and anterior caudal vertebrae; (iv) presence of transverse processes in the posterior caudal vertebrae.

Many aspects of the axial anatomy of *Sphenodon* are consistent across our sample and may be of taxonomic importance: (i) number of presacral vertebrae being 25 (with minor individual variation); (ii) laterally oriented, oblique presacral synapophyses; (iii) rudimentary hypapophyses in the cervical vertebrae intercentra; (iv) presence of marked vertebral lamination, i.e. PCYL, POSL, PRSL; (v) trapezoidal neural spines, decreasing in anteroposterior length at their apexes; (vi) vertebral regionalization; (vii) presence of cartilaginous elements, i.e. uncinate processes, intercostal and sternocostal ribs associated with the presacral vertebrae ribs; and (viii) orientation of the pleurapophyses in the anterior caudal vertebrae, being lateral in QV1–2, to anterolaterally oriented in QV3–8. Some anatomical features show considerable variation within the axial skeleton of *Sphenodon*: (i) presence and number of nutrient foramina, which may be present in some, but not all vertebrae of the same individual; (ii) presence of longitudinal ridges in the ventral surface of the presacral vertebrae, with some individuals showing ridges only in the anteriormost cervicals, whereas others show ridges until the anterior dorsal vertebrae; and (iii) the overall morphology of the sacral pleurapophyses, with some individuals showing relatively straight pleurapophyses, whereas others show bowed sacral pleurapophyses.

The factor showing the greatest influence on the individual variability in *Sphenodon* axial skeleton is size. The presacral vertebrae show negative allometry, with larger specimens (which usually includes males, especially adults) characterized by relatively tall neural spines, but proportionally shorter and narrower vertebrae compared to smaller individuals (i.e. juveniles and adult females). However, due to a small sample of different ontogenetic stages (juveniles $N = 4$) and female specimens ($N = 4$), part of the variability may be underrepresented, and future studies should incorporate more specimens in these categories. The lack of specimen provenance may also impact our understanding of *Sphenodon* variability.

We also compared the axial morphology of *Sphenodon* to that of Mesozoic rhynchocephalians. Ossification timing and axial morphology can be of taxonomic and phylogenetic importance for extinct taxa, such as the synapophyseal morphology, shape of the neural spines, and presence or absence of laminae in the vertebrae. The late ossification of bones was previously considered to bear an ecomorphological signal in fossil taxa, more specifically being tied to aquatic or semi-aquatic animals. Here, we highlight that this may have been a more widespread characteristic among rhynchocephalians, even though still playing an important role in their lifestyle. In the case of *Acrosaurus frischmanni*, the significantly smaller holotype shows a higher degree of ossification than larger juvenile specimens of the potentially related *Pleurosaurus* species, which could support different taxonomic status instead of previous suggestions that this taxon simply represents an early juvenile of the latter. The proportional changes in vertebral sizes, as well as the lack of caudal autotomy in some fossil taxa, such as *Kallimodon*, pleurosaurids, and *Sphenofontis* may have important ecological roles in locomotion performance, both for terrestrial and aquatic taxa. Finally, we discuss the inclusion of additional morphological characters of the axial skeleton in phylogenetic analyses. The relationships of neosphenodontians change significantly with the addition of these characters, with many characters of the axial skeleton being synapomorphic. The new analyses shows marked differences in the relationships of neosphenodontians and more support to some clades (e.g., Pleurosauridae and

Sapheosauridae), highlighting the importance of postcranial in phylogenetic datasets.

ACKNOWLEDGEMENTS

V.B. thanks the following colleagues for access to specimens and scan data: Anne Schulp and Tim de Zeeuw (TM); Rainer Brocke and Gunnar Riedel (SMF); Karin Peyer and Nour-Eddine Jalil (MNHN); Michael O. Day, Susannah Maidment, and Zerina Johansen (NHMUK); Rebecca Hunt-Foster (DM); Maureen Walsh and Nathan Smith (NHMLA); Gillian Sales and Moya Meredith Smith (KCL); John Hutchinson (RVCUK); Mark N. Hutchinson (SAMA); and Daniel Brinkman and Vanessa Rhue (YB). We would like to thank the anonymous reviewers and the editors for their comments and time dedicated to the revision of this manuscript.

SUPPLEMENTARY DATA

Supplementary data is available at *Zoological Journal of the Linnean Society* online.

CONFLICT OF INTEREST

There are no conflict of interest regarding this manuscript.

FUNDING

This work is a contribution to the Deutsche Forschungsgemeinschaft (D.F.G) grant RA 1012/28 awarded to V.B. A.V. was supported by a Humboldt Research Fellowship from the Alexander von Humboldt Foundation during part of the development of this work; he is now funded by Secretaria d'Universitats i Recerca of the Departament de Recerca i Universitats, Generalitat de Catalunya, through a Beatriu de Pinós postdoctoral grant (2021 BP 00038). A.V. further acknowledges support from the CERCA Programme/Generalitat de Catalunya and the Agència de Gestió d'Ajuts Universitaris i de Recerca of the Generalitat de Catalunya (2021 SGR 00620).

DATA AVAILABILITY

All CT scans of *Sphenodon* specimens in this study are publicly available in online repositories (e.g. MorphoSource). The specific link to each specimen, as well as additional information, measurement, and the datasets for the ontogenetic analyses are found in the Supporting Information, Data S1–S4 herein.

REFERENCES

Adams DC, Otárola-Castillo E. geomorph: an R package for the collection and analysis of geometric morphometric shape data. *Methods in Ecology and Evolution* 2013;**4**:393–9. https://doi.org/10.1111/2041-210X.12035

Adams DC, Rohlf FJ, Slice DE. Geometric morphometrics: ten years of progress following the 'revolution'. *Italian Journal of Zoology* 2004;**71**:5–16.

Apesteguía S. Esfenodontes (Reptilia: Lepidosauria) del Cretácico Superior de Patagonia. Ph.D. Thesis, Universidad Nacional de La Plata, 2008. https://doi.org/10.35537/10915/4405

Apesteguía S, Carballido JL. A new eilenodontine (Lepidosauria, Sphenodontidae) from the Lower Cretaceous of central Patagonia. *Journal of Vertebrate Paleontology* 2014;**34**:303–17. https://doi.org/10.1080/02724634.2013.803974

Apesteguía S, Novas FE. Large Cretaceous sphenodontian from Patagonia provides insight into lepidosaur evolution in Gondwana. *Nature* 2003;**425**:609–12. https://doi.org/10.1038/nature01995

Baiano MA, Coria R, Chiappe LM *et al.* Osteology of the axial skeleton of *Aucasaurus garridoi*: phylogenetic and paleobiological inferences. *PeerJ* 2023;**11**:e16236. https://doi.org/10.7717/peerj.16236

Barbera C, Macuglia L. Revisione dei tetrapodi del Cretacico inferiore di Pietraroia (Matese orientale, Benevento) appartenenti alla collezione Costa del Museo di Paleontologia dell'Università di Napoli. *Memorie della Società Geologica Italiana* 1988;**41**:567–74.

Baur G. The proatlas, atlas and axis of the crocodilia. *The American Naturalist* 1886;**20**:288–99.

Beccari V, Guillaume ARD, Jones MEH *et al.* An arboreal rhynchocephalian (Lepidosauria: Rhynchocephalia) from the Late Jurassic of Germany, and the importance of the appendicular skeleton for ecomorphology in lepidosaurs. *Zoological Journal of the Linnean Society* 2025a;**204**:39. https://doi.org/10.1093/zoolinnean/zlaf073

Beccari V, Jones MEH, Villa A, Cooper N, Regnault S, Glaw F, Rauhut OWM. Ontogenetic and intraspecific variability in the postcranial skeleton of the tuatara (*Sphenodon punctatus*) and implications for fossil rhynchocephalians. In: *Book of Abstracts of the 10th World Congress of Herpetology, Kuching, Sarawak, 2024*. Abstract A-0461. International Herpetological Committee, 2024, 238–9.

Beccari V, Villa A, Jones MEH *et al.* A juvenile pleurosaurid (Lepidosauria: Rhynchocephalia) from the Tithonian of the Mörnsheim Formation, Germany. *Anatomical Record* 2025b;**308**:844–67. https://doi.org/10.1002/ar.25545

Bever GS, Norell MA. A new rhynchocephalian (Reptilia: Lepidosauria) from the Late Jurassic of Solnhofen (Germany) and the origin of the marine Pleurosauridae. *Royal Society Open Science* 2017;**4**:170570. https://doi.org/10.1098/rsos.170570

Blackburn DC, Boyer DM, Gray JA; oVert Project Team, *et al.* Increasing the impact of vertebrate scientific collections through 3D imaging: the openVertebrate (oVert) Thematic Collections Network. *BioScience* 2024;**74**:169–86. https://doi.org/10.1093/biosci/biad120

Blanco A. Importance of the postcranial skeleton in eusuchian phylogeny: reassessing the systematics of allodaposuchid crocodylians. *PLoS One* 2021;**16**:e0251900. https://doi.org/10.1371/journal.pone.0251900

Böhmer C, Rauhut OWM, Wörheide G. Correlation between Hox code and vertebral morphology in archosaurs. *Proceedings of the Royal Society B: Biological Sciences* 2015;**282**:20150077. https://doi.org/10.1098/rspb.2015.0077

Bookstein FL. *Morphometric Tools for Landmark Data*. New York, NY: Cambridge University Press, 1991.

Brochu CA. Ontogeny of the postcranium in crocodylomorph archosaurs. Ph.D. Thesis, The University of Texas at Austin, 1992. https://repositories.lib.utexas.edu/items/a0c8722b-0b86-4368-aba7-e8348c995d65

Brownstein CD, Meyer DL, Fabbri M *et al.* Evolutionary origins of the prolonged extant squamate radiation. *Nature Communications* 2022;**13**:7087. https://doi.org/10.1038/s41467-022-34217-5

Caldwell MW, Simões TR, Palci A *et al. Tetrapodophis amplectus* is not a snake: re-assessment of the osteology, phylogeny and functional morphology of an Early Cretaceous dolichosaurid lizard. *Journal of Systematic Palaeontology* 2021;**19**:893–952. https://doi.org/10.1080/14772019.2021.1983044

Carroll RL. A pleurosaur from the Lower Jurassic and the taxonomic position of the Sphenodontida. *Palaeontographica. Abteilung A, Paläozoologie, Stratigraphie* 1985;**189**:1–28.

Carroll RL, Wild R. Marine members of the Sphenodontia. In: Fraser NC, Sues H-D (eds), *In the Shadow of the Dinosaurs: Early Mesozoic Tetrapods*. Cambridge, UK: Cambridge University Press, 1994, 70–83.

Castanet J, Newman DG, Girons HS. Skeletochronological data on the growth, age, and population structure of the tuatara, *Sphenodon punctatus*, on Stephens and Lady Alice islands, New Zealand. *Herpetologica* 1988;**44**:25–37.

Cau A, Baiano MA, Raia P. A new sphenodontian (Reptilia, Lepidosauria) from the Lower Cretaceous of Southern Italy and the phylogenetic affinities of the Pietraroia Plattenkalk rhynchocephalians. *Cretaceous Research* 2014;**49**:172–80. https://doi.org/10.1016/j.cretres.2014.02.001

Čerňanský A, Stanley EL. The atlas–axis complex in Dibamidae (Reptilia: Squamata) and their potential relatives: the effect of a fossorial lifestyle on the morphology of this skeletal bridge. *Journal of Morphology* 2019;**280**:1777–97. https://doi.org/10.1002/jmor.21064

Chambi-Trowell SAV, Martinelli AG, Whiteside DI *et al.* The diversity of Triassic South American sphenodontians: a new basal form, clevosaurs, and a revision of rhynchocephalian phylogeny. *Journal of Systematic Palaeontology* 2021;**19**:787–820. https://doi.org/10.1080/14772019.2021.1976292

Chambi-Trowell SAV, Whiteside DI, Benton MJ. Diversity in rhynchocephalian *Clevosaurus* skulls based on CT reconstruction of two Late Triassic species from Great Britain. *Acta Palaeontologica Polonica* 2019;**64**:41–64. https://doi.org/10.4202/app.00569.2018

Chambi-Trowell SAV, Whiteside DI, Benton MJ *et al.* Biomechanical properties of the jaws of two species of *Clevosaurus* and a reanalysis of rhynchocephalian dentary morphospace. *Palaeontology* 2020;**63**:919–39. https://doi.org/10.1111/pala.12493

Clark EG, Jenkins KM, Brodersen CR. Back to life: techniques for developing high-quality 3D reconstructions of plants and animals from digitized specimens. *PLoS One* 2023;**18**:e0283027. https://doi.org/10.1371/journal.pone.0283027

Clemente CJ, Withers PC, Thompson GG *et al.* Lizard tricks: overcoming conflicting requirements of speed versus climbing ability by altering biomechanics of the lizard stride. *The Journal of Experimental Biology* 2013;**216**:3854–62. https://doi.org/10.1242/jeb.089060

Cocude-Michel M. Les rhynchocéphales et les sauriens des calcaires lithographiques (Jurassique supérieur) d'Europe occidentale. *Nouvelles archives du Muséum d'histoire naturelle de Lyon* 1963;**7**:3–224. https://doi.org/10.3406/mhnly.1963.992

Conrad JL. Skeletons of the little-known palawan monitor, *Varanus palawanensis* (Squamata: Varanidae). *Journal of Herpetology* 2015;**49**:485–90. https://doi.org/10.1670/13-117

Cordero GA, Maliuk A, Schlindwein X *et al.* Phylogenetic patterns and ontogenetic origins of limb length variation in ecologically diverse lacertine lizards. *Biological Journal of the Linnean Society* 2021;**132**:283–96. https://doi.org/10.1093/biolinnean/blaa183

Cree A. *Tuatara—Biology and Conservation of a Venerable Survivor*, Vol. **160**. Christchurch, New Zealand: Canterbury University Press, 2014.

DeMar DG, Jones MEH, Carrano MT. A nearly complete skeleton of a new eusphenodontian from the Upper Jurassic Morrison Formation, Wyoming, USA, provides insight into the evolution and diversity of Rhynchocephalia (Reptilia: Lepidosauria). *Journal of Systematic Palaeontology* 2022;**20**:1–64. https://doi.org/10.1080/14772019.2022.2093139

Domínguez-López ME, Ortega-León ÁM, Zamora-Abrego GJ. Tail autotomy effects on the escape behavior of the lizard *Gonatodes albogularis* (Squamata: Sphaerodactylidae), from Córdoba, Colombia. *Revista Chilena de Historia Natural* 2015;**88**:1. https://doi.org/10.1186/s40693-014-0010-6

Dupret V. The pleurosaurs: anatomy and phylogeny. *Revue de Paléobiologie, Genève* 2004;**9**:61–80.

Evans SE. The skull of a new eosuchian reptile from the Lower Jurassic of South Wales. *Zoological Journal of the Linnean Society* 1980;**70**:203–64. https://doi.org/10.1111/j.1096-3642.1980.tb00852.x

Evans SE. The postcranial skeleton of the Lower Jurassic eosuchian *Gephyrosaurus bridensis*. *Zoological Journal of the Linnean Society* 1981;**73**:81–116. https://doi.org/10.1111/j.1096-3642.1981.tb01580.x

Evans SE. The skull of lizards and tuatara. *Biology of Reptilia* 2008;**20**:1–347.

Ezcurra MD, Butler RJ. Post-hatchling cranial ontogeny in the Early Triassic diapsid reptile *Proterosuchus fergusi*. *Journal of Anatomy* 2015;**226**:387–402. https://doi.org/10.1111/joa.12300

Fabre J. Un squelette de *Pleurosaurus ginsburgi* nov. sp. (Rhynchocephalia) du Portlandien du Petit Plan de Canjuers (Var). *Comptes Rendus Hebdomadaires Des Seances De L Academie Des Sciences Serie D* 1974;**278**:2417–20.

Fabre J. *Les rhynchocéphales et les ptérosauriens à crête pariétale du Kiméridgien supérieur-Berriasien d'Europe occidentale: Le gisement de Canjuers (Var-France) et ses abords*. Paris, France: Éditions de la Fondation Singer-Polignac, 1981.

Feiner N, Jackson ISC, Stanley EL *et al.* Evolution of the locomotor skeleton in *Anolis* lizards reflects the interplay between ecological opportunity and phylogenetic inertia. *Nature Communications* 2021;**12**:1525. https://doi.org/10.1038/s41467-021-21757-5

Fleming A, Kishida MG, Kimmel CB *et al.* Building the backbone: the development and evolution of vertebral patterning. *Development* 2015;**142**:1733–44.

Foster KL, Garland T, Schmitz L *et al.* Skink ecomorphology: forelimb and hind limb lengths, but not static stability, correlate with habitat use and demonstrate multiple solutions. *Biological Journal of the Linnean Society* 2018;**125**:673–92. https://doi.org/10.1093/biolinnean/bly146

Fraser NC. The osteology and relationships of *Clevosaurus* (Reptilia: Sphenodontida). *Philosophical Transactions of the Royal Society of London. B, Biological Sciences* 1988;**321**:125–78. https://doi.org/10.1098/rstb.1988.0092

Fraser NC, Walkden GM. The postcranial skeleton of the Upper Triassic sphenodontid *Planocephalosaurus robinsonae*. *Palaeontology* 1984;**27**:575–95.

Frýdlová P, Frynta D. Strong support for Rensch's rule in an American clade of lizards (Teiidae and Gymnophtalmidae) and a paradox of the largest tejus. *The Science of Nature* 2015;**102**:1–11.

Fürbringer M. Zur vergleichenden Anatomie des Brustschulterapparates und der Schultermuskeln. *Jenaische Zeitschrift für Naturwissenschaft* 1900;**34**:215–718.

Gemmell NJ, Rutherford K, Prost S; Ngatiwai Trust Board, *et al.* The tuatara genome reveals ancient features of amniote evolution. *Nature* 2020;**584**:403–9.

Goloboff PA, Morales ME. TNT version 1.6, with a graphical interface for MacOS and Linux, including new routines in parallel. *Cladistics: The International Journal of the Willi Hennig Society* 2023;**39**:144–53. https://doi.org/10.1111/cla.12524

Goodman BA. Nowhere to run: the role of habitat openness and refuge use in defining patterns of morphological and performance evolution in tropical lizards. *Journal of Evolutionary Biology* 2009;**22**:1535–44. https://doi.org/10.1111/j.1420-9101.2009.01766.x

Grandal-d'Anglade A, López-González F. Sexual dimorphism and ontogenetic variation in the skull of the cave bear (*Ursus spelaeus* Rosenmüller) of the European Upper Pleistocene. *Geobios* 2005;**38**:325–37. https://doi.org/10.1016/j.geobios.2003.12.001

Gray JE. Note on a peculiar structure in the head of an *Agama*. *Zoological Miscellany* 1831;**1**:13–4.

Gray JE. *Description of Two Hitherto Unrecorded Species of Reptiles from New Zealand; Presented to the British Museum by Dr Dieffenbach*. London: Zoological Miscellany, 1842, 1–72.

Griffin CT, Stocker MR, Colleary C *et al.* Assessing ontogenetic maturity in extinct saurian reptiles. *Biological Reviews of the Cambridge Philosophical Society* 2020;**96**:470–525. https://doi.org/10.1111/brv.12666

Günther A. Contribution to the anatomy of *Hatteria* (Rhynchocephalus, Owen). *Philosophical Transactions of the Royal Society of London* 1867;**157**:595–629.

Gutarra S, Stubbs TL, Moon BC *et al.* The locomotor ecomorphology of Mesozoic marine reptiles. *Palaeontology* 2023;**66**:e12645. https://doi.org/10.1111/pala.12645

Hagey TJ, Harte S, Vickers M *et al.* There's more than one way to climb a tree: limb length and microhabitat use in lizards with toe pads. *PLoS One* 2017;**12**:e0184641. https://doi.org/10.1371/journal.pone.0184641

Harrell Jr. Jr, Harrell Jr. Jr. Package 'hmisc'. CRAN2018, 2019, 235–6. https://doi.org/10.32614/CRAN.package.Hmisc

Hay JM, Sarre SD, Lambert DM *et al.* Genetic diversity and taxonomy: a reassessment of species designation in tuatara (Sphenodon: Reptilia). *Conservation Genetics* 2010;**11**:1063–81.

Herrel A, Moore JA, Bredeweg EM *et al.* Sexual dimorphism, body size, bite force and male mating success in tuatara. *Biological Journal of the Linnean Society* 2010;**100**:287–92. https://doi.org/10.1111/j.1095-8312.2010.01433.x

Herrera-Flores JA, Stubbs TL, Benton MJ. Macroevolutionary patterns in Rhynchocephalia: is the tuatara (*Sphenodon punctatus*) a living fossil? *Palaeontology* 2017;**60**:319–28. https://doi.org/10.1111/pala.12284

Herrera-Flores JA, Stubbs TL, Elsler A *et al.* Taxonomic reassessment of *Clevosaurus latidens* Fraser, 1993 (Lepidosauria, Rhynchocephalia) and rhynchocephalian phylogeny based on parsimony and Bayesian inference. *Journal of Paleontology* 2018;**92**:734–42. https://doi.org/10.1017/jpa.2017.136

Herrera-Flores JA, Stubbs TL, Sour-Tovar F. Redescription of the type specimens for the Late Jurassic rhynchocephalian *Opisthias rarus* and a new specimen of *Theretairus antiquus* from Quarry 9, Morrison Formation, Wyoming, USA. *Acta Palaeontologica Polonica* 2022;**67**:623–30. https://doi.org/10.4202/app.00929.2021

Hillan EJ, Roberts LE, Criswell KE *et al.* Conservation of rib skeleton regionalization in the homoplastic evolution of the snake-like body form in squamates. *Proceedings of the Royal Society B: Biological Sciences* 2024;**291**:20241160. https://doi.org/10.1098/rspb.2024.1160

Hoffstetter R, Gasc J-P. Vertebrae and ribs of modern reptiles. *Biology of the Reptilia* 1969;**1**:201–310.

Houssaye A. "Pachyostosis" in aquatic amniotes: a review. *Integrative Zoology* 2009;**4**:325–40. https://doi.org/10.1111/j.1749-4877.2009.00146.x

Howes GB, Swinnerton HH. On the development of the skeleton of the tuatara, *Sphenodon punctatus*; with remarks on the egg, on the hatching, and on the hatched young. *The Transactions of the Zoological Society of London* 1901;**16**:1–84.

Jones KE, Angielczyk KD, Polly PD *et al.* Fossils reveal the complex evolutionary history of the mammalian regionalized spine. *Science* 2018;**361**:1249–52. https://doi.org/10.1126/science.aar3126

Jones KE, Gonzalez S, Angielczyk KD *et al.* Regionalization of the axial skeleton predates functional adaptation in the forerunners of mammals. *Nature Ecology & Evolution* 2020;**4**:470–8.

Jones MEH. Skull shape and feeding strategy in *Sphenodon* and other Rhynchocephalia (Diapsida: Lepidosauria). *Journal of Morphology* 2008;**269**:945–66. https://doi.org/10.1002/jmor.10634

Jones MEH. Dentary tooth shape in *Sphenodon* and its fossil relatives (Diapsida: Lepidosauria: Rhynchocephalia). In: Koppe T, Meyer G, Alt KW (eds), *Comparative Dental Morphology*, Vol. **13**. Greifswald, Germany: Karger Publishers, 2009, 9–15.

Jones MEH, Cree A. Tuatara. *Current Biology* 2012;**22**:R986–7. https://doi.org/10.1016/j.cub.2012.10.049

Jones MEH, Curtis N, Fagan MJ *et al.* Hard tissue anatomy of the cranial joints in *Sphenodon* (Rhynchocephalia): sutures, kinesis, and skull mechanics. *Palaeontologia Electronica* 2011;**14**:92.

Jones MEH, Curtis N, O'Higgins P *et al.* The head and neck muscles associated with feeding in *Sphenodon* (Reptilia: Lepidosauria: Rhynchocephalia). *Palaeontologia Electronica* 2009a;**12**:56.

Jones MEH, Lappin AK. Bite-force performance of the last rhynchocephalian (Lepidosauria: *Sphenodon*). *Journal of the Royal Society of New Zealand* 2009;**39**:71–83. https://doi.org/10.1080/03014220909510565

Jones MEH, Tennyson AJD, Worthy JP *et al.* A sphenodontine (Rhynchocephalia) from the Miocene of New Zealand and palaeobiogeography of the tuatara (*Sphenodon*). *Proceedings of the Royal Society B: Biological Sciences* 2009b;**276**:1385–90. https://doi.org/10.1098/rspb.2008.1785

Keeble E, Whiteside DI, Benton MJ. The terrestrial fauna of the Late Triassic Pant-y-ffynnon Quarry fissures, South Wales, UK and a new species of *Clevosaurus* (Lepidosauria: Rhynchocephalia). *Proceedings of the Geologists' Association* 2018;**129**:99–119. https://doi.org/10.1016/j.pgeola.2017.11.001

Kępa M, Tomańska A, Staszewska J *et al.* Functional anatomy of the thoracic limb of the komodo dragon (*Varanus komodoensis*). *Animals* 2023;**13**:2895. https://doi.org/10.3390/ani13182895

Kikinis R, Pieper SD, Vosburgh KG. 3D Slicer: a platform for subject-specific image analysis, visualization, and clinical support. In: FA Jolesz (ed.), *Intraoperative Imaging and Image-Guided Therapy*. New York, NY: Springer, 2014, 277–89. https://doi.org/10.1007/978-1-4614-7657-3_19

Klein N, Scheyer TM. Microanatomy and life history in Palaeopleurosaurus (Rhynchocephalia: Pleurosauridae) from the Early Jurassic of Germany. *Die Naturwissenschaften* 2017;**104**:4. https://doi.org/10.1007/s00114-016-1427-3

Lamar SK, Altobelli JT, Nelson NJ *et al.* Investigating the link between morphological characteristics and diet in an island population of omnivorous reptiles (*Sphenodon punctatus*). *Biology Open* 2022;**11**:bio059393. https://doi.org/10.1242/bio.059393

Lamar SK, Nelson NJ, Moore JA *et al.* Initial collection, characterization, and storage of tuatara (*Sphenodon punctatus*) sperm offers insight into their unique reproductive system. *PLoS One* 2021;**16**:e0253628. https://doi.org/10.1371/journal.pone.0253628

Lawing AM, Polly PD. Geometric morphometrics: recent applications to the study of evolution and development. *Journal of Zoology* 2010;**280**:1–7. https://doi.org/10.1111/j.1469-7998.2009.00620.x

Lee MS, Caldwell MW. *Adriosaurus* and the affinities of mosasaurs, dolichosaurs, and snakes. *Journal of Paleontology* 2000;**74**:915–37.

Lee MSY, Palci A, Jones MEH *et al.* Aquatic adaptations in the four limbs of the snake-like reptile *Tetrapodophis* from the Lower Cretaceous of Brazil. *Cretaceous Research* 2016;**66**:194–9. https://doi.org/10.1016/j.cretres.2016.06.004

Lydekker R. *Catalogue of the Fossil Reptilia and Amphibia in the British Museum: Vol. Part 1*. London, UK: British Museum, 1880.

Macey JR, Pabinger S, Barbieri CG *et al.* Evidence of two deeply divergent co-existing mitochondrial genomes in the tuatara reveals an extremely complex genomic organization. *Communications Biology* 2021;**4**:116–0. https://doi.org/10.1038/s42003-020-01639-0

Martinez Arbizu P. pairwiseAdonis: pairwise multilevel comparison using adonis. R Package Version 0.4, 2020, 1.

Marvin GA. Effect of caudal autotomy on aquatic and terrestrial locomotor performance in two desmognathine salamander species. *Copeia* 2010;**2010**:468–74. https://doi.org/10.1643/CP-09-188

McElroy EJ, Bergmann PJ. Tail autotomy, tail size, and locomotor performance in lizards. *Physiological and Biochemical Zoology* 2013;**86**:669–79. https://doi.org/10.1086/673890

Molnar J, Watanabe A. Morphological and functional regionalization of trunk vertebrae as an adaptation for arboreal locomotion in chameleons. *Royal Society Open Science* 2023;**10**:221509. https://doi.org/10.1098/rsos.221509

Montuelle SJ, Herrel A, Schaerlaeken V *et al.* Inertial feeding in the teiid lizard *Tupinambis merianae*: the effect of prey size on the movements of hyolingual apparatus and the cranio-cervical system. *The Journal of Experimental Biology* 2009;**212**:2501–10. https://doi.org/10.1242/jeb.026336

Munnecke A, Westphal H, Kölbl-Ebert M. Diagenesis of plattenkalk: examples from the Solnhofen area (Upper Jurassic, southern Germany). *Sedimentology* 2008;**55**:1931–46. https://doi.org/10.1111/j.1365-3091.2008.00975.x

O'Brien A, Whiteside DI, Marshall JEA. Anatomical study of two previously undescribed specimens of *Clevosaurus hudsoni* (Lepidosauria: Rhynchocephalia) from Cromhall Quarry, UK, aided by computed tomography, yields additional information on the skeleton and hitherto undescribed bones. *Zoological Journal of the Linnean Society* 2018;**183**:163–95. https://doi.org/10.1093/zoolinnean/zlx087

Oksanen J, Blanchet FG, Kindt R *et al.* Package 'vegan'. *Community Ecology Package, Version 2*. 2013;**2**:1–295.

Osborn HF. Intercentra and hypapophyses in the cervical region of mosasaurs, lizards, and *Sphenodon*. *The American Naturalist* 1900;**34**:1–7. https://doi.org/10.1086/277528

Paparella I, LeBlanc ARH, Doschak MR *et al.* The iliosacral joint in lizards: an osteological and histological analysis. *Journal of Anatomy* 2020;**236**:668–87. https://doi.org/10.1111/joa.13132

Paparella I, Palci A, Nicosia U *et al.* A new fossil marine lizard with soft tissues from the Late Cretaceous of southern Italy. *Royal Society Open Science* 2018;**5**:172411. https://doi.org/10.1098/rsos.172411

Pardo JD, Anderson JS. Cranial morphology of the Carboniferous-Permian tetrapod *Brachydectes newberryi* (Lepospondyli, Lysorophia): new data from μCT. *PLoS One* 2016;**11**:e0161823. https://doi.org/10.1371/journal.pone.0161823

Pêgas RV. A taxonomic note on the tapejarid pterosaurs from the Pterosaur Graveyard site (Caiuá Group, ?Early Cretaceous of Southern Brazil): evidence for the presence of two species. *Historical Biology* 2025;**37**:1277–98. https://doi.org/10.1080/08912963.2024.2355664

R Core Team. *R: a Language and Environment for Statistical Computing*. Vienna, Austria: R Foundation for Statistical Computing, 2020.

Rauhut OWM, Heyng AM, López-Arbarello A *et al.* A new rhynchocephalian from the Late Jurassic of Germany with a dentition that is unique amongst tetrapods. *PLoS One* 2012;**7**:e46839. https://doi.org/10.1371/journal.pone.0046839

Rauhut OWM, López-Arbarello A. Zur Taxonomie der Brückenechse aus dem oberen Jura von Schamhaupten. *Archaeopteryx* 2016;**33**:1–11.

Rauhut OWM, López-Arbarello A, Röper M *et al.* Vertebrate fossils from the Kimmeridgian of Brunn: the oldest fauna from the Solnhofen Archipelago (Late Jurassic, Bavaria, Germany). *Zitteliana* 2017;**89**:305–29.

Rauhut OWM, Röper M. Brückenechsen aus dem oberen Jura von Brunn (Oberpfalz). Freunde der Bayerischen Staatssammlung für Paläontologie und Historische Geologie eV. *Jahresbericht und Mitteilungen* 2013;**41**:55–72.

Regnault S, Hutchinson JR, Jones MEH. Sesamoid bones in tuatara (*Sphenodon punctatus*) investigated with X-ray microtomography, and implications for sesamoid evolution in Lepidosauria. *Journal of Morphology* 2017;**278**:62–72. https://doi.org/10.1002/jmor.20619

Regnault S, Jones MEH, Pitsillides AA *et al.* Anatomy, morphology and evolution of the patella in squamate lizards and tuatara (*Sphenodon punctatus*). *Journal of Anatomy* 2016;**228**:864–76. https://doi.org/10.1111/joa.12435

Reynoso V-H. An unusual aquatic sphenodontian (Reptilia: Diapsida) from the Tlayua Formation (Albian), Central Mexico. *Journal of Paleontology* 2000;**74**:133–48. https://doi.org/10.1666/0022-3360(2000)074<0133: AUASRD>2.0.CO; 2

Ríos-Orjuela JC, Camacho-Bastidas JS, Jerez A. Appendicular morphology and locomotor performance of two morphotypes of continental anoles: *Anolis heterodermus* and *Anolis tolimensis*. *Journal of Anatomy* 2020;**236**:252–73.

Robb J. *The Tuatara*, Vol. **6**. Durham, UK: Meadowfield Press, 1977.

Rohlf FJ, Slice D. Extensions of the Procrustes method for the optimal superimposition of landmarks. *Systematic Zoology* 1990;**39**:40–59.

Rolfe S, Pieper S, Porto A *et al.* SlicerMorph: an open and extensible platform to retrieve, visualize and analyse 3D morphology. *Methods in Ecology and Evolution* 2021;**12**:1816–25. https://doi.org/10.1111/2041-210X.13669

Romer AS. *Osteology of the Reptiles (3rd imprint)*. Chicago, IL: University of Chicago Press, 1956.

Rothery T. Are there juvenile specimens of the aquatic sphenodontid Pleurosaurus, and if so, what can they tell us about growth in this group. *Journal of Vertebrate Paleontology* 2002;**22S**:100A.

Rothery T. Juvenile pleurosaurs. Ph.D. Thesis, University of McGill, 2005.

Russell AP, Bauer AM. The appendicular locomotor apparatus of *Sphenodon* and normal-limbed squamates. In: Gans C, Gaunt A, Adler K (eds), *Biology of the Reptilia. Vol. 21, Morphology I: The Skull and Appendicular Locomotor Apparatus of Lepidosauria*. Ithaca, New York, USA: Society for the Study of Amphibians and Reptiles, 2008, 1–468.

Sargis EJ. A preliminary qualitative analysis of the axial skeleton of tupaiids (Mammalia, Scandentia): functional morphology and phylogenetic implications. *Journal of Zoology* 2001;**253**:473–83. https://doi.org/10.1017/S0952836901000437

Schauinsland H. Weitere Beiträge zur Entwicklungsgeschichte der Hatteria Skelettsystem, schallleitender Apparat, Hirnnerven etc. *Archiv für Mikroskopische Anatomie* 1900;**56**:747–867.

Schlager S. Morpho and Rvcg–Shape Analysis in R: R-Packages for geometric morphometrics, shape analysis and surface manipulations. In: Zheng G, Li S, Székely G (eds), *Statistical Shape and Deformation Analysis*. Amsterdam, Netherlands: Elsevier, 2017, 217–56.

Seligmann H, Moravec J, Werner YL. Morphological, functional and evolutionary aspects of tail autotomy and regeneration in the 'living fossil' *Sphenodon* (Reptilia: Rhynchocephalia). *Biological Journal of the Linnean Society* 2008;**93**:721–43. https://doi.org/10.1111/j.1095-8312.2008.00975.x

Simões TR, Caldwell MW, Pierce SE. Sphenodontian phylogeny and the impact of model choice in Bayesian morphological clock estimates of divergence times and evolutionary rates. *BMC Biology* 2020;**18**:191. https://doi.org/10.1186/s12915-020-00901-5

Simões TR, Kinney-Broderick G, Pierce SE. An exceptionally preserved *Sphenodon*-like sphenodontian reveals deep time conservation of the tuatara skeleton and ontogeny. *Communications Biology* 2022;**5**:195–19. https://doi.org/10.1038/s42003-022-03144-y

Street HP, Caldwell MW. Rediagnosis and redescription of *Mosasaurus hoffmannii* (Squamata: Mosasauridae) and an assessment of species assigned to the genus *Mosasaurus*. *Geological Magazine* 2017;**154**:521–57.

Sues H, Schoch RR. The oldest known rhynchocephalian reptile from the Middle Triassic (Ladinian) of Germany and its phylogenetic position among Lepidosauromorpha. *Anatomical Record* 2024;**307**:776–90. https://doi.org/10.1002/ar.25339

Sues H-D, Schoch RR. A new early-diverging sphenodontian (Lepidosauria, Rhynchocephalia) from the Upper Triassic of Virginia, U.S.A. *Journal of Paleontology* 2021;**95**:344–50. https://doi.org/10.1017/jpa.2020.87

Swinton WE. A new Triassic Rhynchocephalian from Gloucestershire. *Annals and Magazine of Natural History* 1939;**4**:591–4. https://doi.org/10.1080/00222933908655407

Szyndlar Z, Georgalis GL. An illustrated atlas of the vertebral morphology of extant non-caenophidian snakes, with special emphasis on the cloacal and caudal portions of the column. *Vertebrate Zoology* 2023;**73**:717–886. https://doi.org/10.3897/vz.73.e101372

Tereshchenko VS. Sexual dimorphism of the postcranial skeleton in lizards of family Agamidae (Lacertilia). *Zoologičeskij Žurnal* 1991;**70**:91–103.

Tereshchenko VS. Sexual dimorphism in the postcranial skeleton of dinosaurs. *Paleontological Journal* 2020;**54**:1410–33. https://doi.org/10.1134/S0031030120120047

Tischlinger H, Arratia G. Ultraviolet light as a tool for investigating Mesozoic fishes, with a focus on the ichthyofauna of the Solnhofen archipelago. In: Arratia G, Schultze H-P, Wilson MVH (eds), *Mesozoic Fishes 5—Global Diversity and Evolution*. Munich, Germany: Verlag Dr Friedrich Pfeil, 2013, 549–60.

Tschopp E. Nomenclature of vertebral laminae in lizards, with comments on ontogenetic and serial variation in Lacertini (Squamata, Lacertidae). *PLoS One* 2016;**11**:e0149445. https://doi.org/10.1371/journal.pone.0149445

Verrière A, Fröbisch NB, Fröbisch J. Regionalization, constraints, and the ancestral ossification patterns in the vertebral column of amniotes. *Scientific Reports* 2022;**12**:22257. https://doi.org/10.1038/s41598-022-24983-z

Villa A, Montie R, Röper M *et al. Sphenofontis velserae* gen. et sp. nov., a new rhynchocephalian from the Late Jurassic of Brunn (Solnhofen Archipelago, southern Germany). *PeerJ* 2021;**9**:e11363. https://doi.org/10.7717/peerj.11363

von Meyer H. Neue fossile Reptilien, aus der Ordnung der Saurier. *Nova Acta Academiae Caesareae Leopoldino-Carolinae Germanicae Naturae Curiosorum* 1831;**15**:194–5.

von Meyer H. *Homoeosaurus maximiliani und Rhamphorhynchus (Pterodactylus) longicaudus: Zwei Fossile Reptilien aus dem Kalkschiefer von Solenhofen*. Frankfurt am Main, Germany: S. Schmerber'schen Buchhandlung, 1847.

von Meyer H. Description de l'Atoposaurus jourdani et du Sapheosaurus thiollierei, reptiles fossiles des calcaires lithographiques du Bugey. *Annales des sciences physiques et naturelles, d'Agriculture et d'industrie, 2e série* 1850;**3**:113–27.

von Meyer H. *Acrosaurus frischmanni*. Neues Jahrbuch für Mineralogie. *Geologie und Paläontologie* 1854;**22**:47–58.

von Wettstein O. Ordnung der Klasse Reptilia: Rhynchocephalia. *Kükenthal und Krumbach's Handbuch der Zoologie* 1931;**7**:1–128.

von Wettstein O. Ordnung der Klasse Reptilia: Rhynchocephalia. *Kükenthal und Krumbach's Handbuch der Zoologie* 1937;**7**:225–35.

Wagner A. Neu-aufgefundene Saurier-Ueberreste aus den lithographischen Schiefern und dem obern Jurakalke. *Abhandlungen der Bayerischen Akademie der Wissenschaften—Mathematisch-naturwissenschaftliche Klasse* 1852;**6**:661–710.

Wainwright T, Trevena M, Alewijnse SR *et al.* Sex biases and the scarcity of sex metadata in global herpetology collections. *Biological Journal of the Linnean Society* 2024;**142**:308–18.

Węgrzyn K, Pauwels OSG, Brecko J *et al.* Vertebral morphology and intracolumnar variation of the iconic African viperid snake Atheris (Serpentes, Viperidae). *Anatomical Record* 2025;**308**:2076–112. https://doi.org/10.1002/ar.25579

Wickham H, Chang W, Wickham MH. Package 'ggplot2'. Create elegant data visualisations using the grammar of graphics. Version 2. 2016;**2**:1–189.

Wickham H, Hester J, Chang W, Bryan J. devtools: tools to make developing r packages easier, 2022. https://devtools.r-lib.org/, https://github.com/r-lib/devtools

Wilson JA, D'Emic MD, Ikejiri T *et al.* A nomenclature for vertebral fossae in sauropods and other saurischian dinosaurs. *PLoS One* 2011;**6**:e17114. https://doi.org/10.1371/journal.pone.0017114

Zaaf A, Van Damme R. Limb proportions in climbing and ground-dwelling geckos (Lepidosauria, Gekkonidae): a phylogenetically informed analysis. *Zoomorphology* 2001;**121**:45–53. https://doi.org/10.1007/s004350100044

Zani PA. Patterns of caudal-autotomy evolution in lizards. *Journal of Zoology* 1996;**240**:201–20. https://doi.org/10.1111/j.1469-7998.1996.tb05280.x

Zittel KAv. Handbuch der Paläontologie. Abteilung 1. Paläozoologie Band III, Munich, Germany: 1887–1890.